



THE UNIVERSITY *of* EDINBURGH

Edinburgh Research Explorer

Cemdata18: A chemical thermodynamic database for hydrated Portland cements and alkali-activated materials

Citation for published version:

Lothenbach, B, Kulik, D, Matschei, T, Balonis, M, Baquerizo, L, Dilnesa, B, Miron, G & Myers, RJ 2019, 'Cemdata18: A chemical thermodynamic database for hydrated Portland cements and alkali-activated materials', *Cement and Concrete Research*, vol. 115, pp. 472-506.
<https://doi.org/10.1016/j.cemconres.2018.04.018>

Digital Object Identifier (DOI):

[10.1016/j.cemconres.2018.04.018](https://doi.org/10.1016/j.cemconres.2018.04.018)

Link:

[Link to publication record in Edinburgh Research Explorer](#)

Document Version:

Peer reviewed version

Published In:

Cement and Concrete Research

General rights

Copyright for the publications made accessible via the Edinburgh Research Explorer is retained by the author(s) and / or other copyright owners and it is a condition of accessing these publications that users recognise and abide by the legal requirements associated with these rights.

Take down policy

The University of Edinburgh has made every reasonable effort to ensure that Edinburgh Research Explorer content complies with UK legislation. If you believe that the public display of this file breaches copyright please contact openaccess@ed.ac.uk providing details, and we will remove access to the work immediately and investigate your claim.



1 **Cemdata18: A chemical thermodynamic database for hydrated Portland cements and alkali-**
2 **activated materials**

3
4 Barbara Lothenbach^{1*}, Dmitrii A. Kulik², Thomas Matschei³, Magdalena Balonis⁴, Luis Baquerizo⁵, Belay
5 Dilnesa⁶, George D. Miron², Rupert J. Myers^{7,8}

6
7 ¹Empa, Laboratory for Concrete & Construction Chemistry, CH-8600 Dübendorf, Switzerland

8 ²Paul Scherrer Institut, Laboratory for Waste Management, 5232 Villigen PSI, Switzerland

9 ³HTW Dresden University of Applied Sciences, Department of Civil Engineering, 01069 Dresden, Ger-
10 many

11 ⁴Department of Materials Science and Engineering, University of California Los Angeles, Los Angeles,
12 CA, USA

13 ⁵Lafarge Centre de Recherche, 38291 Saint-Quentin Fallavier, France

14 ⁶BASF Schweiz AG, 5082 Kaisten, Switzerland

15 ⁷University of Sheffield, Department of Materials Science and Engineering, Sheffield, S1 3JD, UK

16 ⁸Current address: University of Edinburgh, School of Engineering, Edinburgh, EH9 3FB, UK

17
18 * Corresponding author. Tel: +41 58 765 47 88; barbara.lothenbach@empa.ch

19 Keywords: thermodynamic modelling, cement, database, solubility, C-S-H

20
21 *For submission to Cement and Concrete Research, version 31.10.2017*

22
23 **Abstract**

24 Thermodynamic modelling can reliably predict hydrated cement phase assemblages and chemical
25 compositions, including their interactions with prevailing service environments, provided an accurate
26 and complete thermodynamic database is used. Here, we summarise the Cemdata18 database, which
27 has been developed specifically for hydrated Portland, calcium aluminate, calcium sulfoaluminate and
28 blended cements, as well as for alkali-activated materials. It is available in GEMS and PHREEQC com-
29 puter program formats, and includes thermodynamic properties determined from various experimental
30 data published in recent years. Cemdata18 contains thermodynamic data for common cement hy-
31 drates such as C-S-H, AFm and AFt phases, hydrogarnet, hydrotoalcite, zeolites, and M-S-H that are val-

32 id over temperatures ranging from 0 to at least 100°C. Solid solution models for AFm, AFt, C-S-H, and
33 M-S-H are also included in the Cemdata18 database.

34

35 **1 Introduction**

36 Numerous studies have shown that chemical thermodynamic modelling, coupled with accurate and
37 complete thermodynamic databases, can reliably predict hydrated cement phase assemblages and
38 chemical compositions. One of the most interesting aspects of applying thermodynamics to hydrated
39 cements has been the discovery that the chemical compositions of $\text{Al}_2\text{O}_3\text{-Fe}_2\text{O}_3$ mono (AFm) and
40 $\text{Al}_2\text{O}_3\text{-Fe}_2\text{O}_3$ tri (AFt) phases are very sensitive to the presence of carbonate [1-3] and temperature [4-
41 6], thus demonstrating that these factors may significantly modify hydrated cement phase assemblag-
42 es. Experiments have shown that compositions of hydrate cement phase assemblages can alter rapidly,
43 often within weeks or months, reflecting changing system compositions and temperatures. Thus,
44 thermodynamic calculations and experiments support each other: on the one hand, calculations enable
45 more complete interpretations of limited experimental datasets and help to identify key experiments
46 to perform; and on the other hand, experiments provide the data that are needed to validate calcula-
47 tion results and model parameters.

48 The quality of thermodynamic modelling results depends directly on the accuracy and completeness of
49 the input thermodynamic properties of substances and phases, which are usually supplied from a
50 thermodynamic database. Relevant thermodynamic data for solid cementitious substances, such as the
51 solubility products of ettringite or hydrogarnet, have been compiled in several specific "cement data-
52 bases" such as (1) the Cemdata07 and Cemdata14 databases [1, 7-12] (<http://www.empa.ch/cemdata>),
53 which are available for GEMS [13, 14], (2) the Thermoddem (<http://thermoddem.brgm.fr/>) database
54 [15, 16] available for the Geochemists Workbench® [17](<https://www.gwb.com/>) and PHREEQC [18] or
55 (3) HATCHES database [19] available for PHREEQC [18]. Data in the first two databases are generally
56 comparable, although some differences exist, as discussed in more detail in Damidot et al. [20]. Our
57 experience applying Cemdata in thermodynamic modelling applications underlines the importance of
58 a careful data selection and evaluation process, and of including sensitivity analyses into the analysis
59 and discussion of results.

60 Additional experimental data, and thermodynamic properties derived from these data, have become
61 available since the first compilation of Cemdata07 in 2007/2008 and subsequent compilation of
62 Cemdata14 in 2013/2014 [1, 7, 21]. Cemdata18 provides a significant update to both Cemdata07 and
63 Cemdata14. Cemdata18 is written into a format supporting the GEM-Selektor code [13, 14] and is fully
64 compatible with the freely available GEMS-Selektor version of the PSI-Nagra 12/07 TDB [22, 23]
65 (<http://gems.web.psi.ch/>). PSI/Nagra 12/07 TDB [22] contains the same entries for aqueous spe-
66 cies/complexes relevant to cement systems as the PSI/Nagra 01/01 [24], with only slight changes: the
67 thermodynamic properties of $\text{Si}_4\text{O}_8(\text{OH})_4^{4-}$ and $\text{AlSiO}_3(\text{OH})_4^{3-}$ were added, while the complex Al-
68 $\text{SiO}(\text{OH})_6^-$ was removed. The GEMS version of the PSI/Nagra 12/07 TDB includes further changes to the
69 thermodynamic properties of Al bearing species/complexes and the addition of Helgeson-Kirkham-
70 Flowers equation of state parameters to account for changes in temperature and pressure [25, 26].

71 Cemdata18 includes a comprehensive selection of cement hydrates commonly encountered in Port-
72 land cement (PC) systems in the temperature range of 0 to 100°C, including calcium silicate hydrate (C-
73 S-H), magnesium silicate hydrate (M-S-H), hydrogarnet, hydrotalcite-like phases, some zeolites, AFm
74 and AFt phases, and various solid solutions used to describe the solubility of these phases. Solubility
75 constants have generally been calculated based on critical reviews of all available experimental data
76 and from additional experiments made either to obtain missing data or to verify existing data. Addi-
77 tional solubility data were measured and compiled using temperatures ranging from 0 to 100°C in
78 many instances, as documented in [9, 12, 27, 28]. Numerous solid solutions among AFm and AFt
79 phases, siliceous hydrogarnets, hydrotalcite-like phases, C-S-H, and M-S-H have been observed and
80 are included in Cemdata18.

81 Several C-S-H solid solution models, as well as two models for hydroxide-hydrotalcite are available in
82 Cemdata18. The CSHQ model from [11] and the OH-hydrotalcite end member with Mg/Al = 2 are well
83 adapted for PC. Although the CSHQ model is able to describe the entire range of Ca/Si ratios encoun-
84 tered, it is best used for high Ca/Si C-S-H, as it still lacks the ability to predict aluminium uptake, which
85 is of less importance for Portland cements than for blended cements. For alkali activated binders, the
86 calcium (alkali) aluminosilicate hydrate (C-(N-)A-S-H) gel model, with lower calcium but higher alu-
87 minium and alkali content than in the C-S-H type phase which exists in hydrated PC, and a Mg-Al lay-
88 ered double hydroxide with variable Mg/Al ratio, are available.

89 This paper summarises Cemdata18, which includes the most important additions to the Cemdata07
90 and Cemdata14 databases in recent years. It also discusses the relevance and implications of these ad-
91 ditions, and compares Cemdata07 and Cemdata18, accounting for their main differences. Summaries
92 of the thermodynamic data compiled in the Cemdata18 database are available in formats supported
93 (readable) by the computer programs GEM-Selektor [13, 14] and PHREEQC [18]. Both of these Cemda-
94 ta18 variants can be freely downloaded from <http://www.empa.ch/cemdata>.

95

96 **2 Thermodynamic data for cements**

97 Recent experimental data has enabled the Cemdata07 and Cemdata14 databases to be extended and
98 refined [1, 7, 21]. We report this more comprehensive and refined dataset here as Cemdata18, com-
99 piled in several tables. Cemdata18 has been developed to predict changes in chemistry that occur dur-
100 ing the hydration of Portland, blended and alkali activated cements, and also their interactions with
101 service environments during use.

102 Table 1 reports the thermodynamic properties of minerals important for cementitious systems, while
103 Table 2 reports their solubility products referring to the dominate species present at the high pH val-
104 ues of cementitious systems. The data for hydrotalcite-like phases and detailed discussions of the dif-
105 ferent models for C-S-H are given in sections 2.6 and 2.7. Standard thermodynamic data for minerals
106 such as calcite, brucite and aqueous and gaseous species already documented in the PSI-Nagra chem-
107 ical thermodynamic database [22] are not repeated in these tables, but given only in summary tables in
108 Appendix B and D. To enable users to model cementitious systems using the Cemdata18 dataset with

109 the law of mass action (LMA) geochemical modelling package PHREEQC [18], a variant of the Cemda-
 110 ta18 dataset has been generated as documented in Appendix B.

111

112 Table 1: Cemdata18 database: Standard thermodynamic properties at 25°C and 1 bar. Update of
 113 Cemdata07 [1, 7, 29]. The data are compatible with the GEMS version of the PSI/Nagra 12/07 TDB [22,
 114 23]. Standard properties of master species and properties of reactions of forming product species out
 115 of master species, commonly used in LMA programs such as PHREEQC, are compiled in the Appendix
 116 B.

117	$\Delta_f G^\circ$	$\Delta_f H^\circ$	S°	a_0	a_1	a_2	a_3	V°	Ref	
118	[kJ/mol]	[kJ/mol]	[J/K/mol]	[J/K/mol]	[J/mol/K ²]	[J K/mol]	[J/K ^{0.5} /mol]	[cm ³ /mol]		
119	Solids									
120	<u>Aft-phases</u>									
121	(Al-)ettringite ^{a,b,c}	-15205.94	-17535	1900	1939	0.789	-	-	707	[1, 7]
122	C ₆ As ₃ H ₃₀ ^c	-14728.1	-16950.2	1792.4	1452	2.156	-	-	708	[30]
123	C ₆ As ₃ H ₁₃	-10540.6	-11530.3	1960.4	970.7	1.483	-	-	411	[30]
124	C ₆ As ₃ H ₉	-9540.4	-10643.7	646.6	764.3	1.638	-	-	361	[30]
125	tricarboaluminate ^a	-14565.64	-16792	1858	2042	0.559	-7.78·10 ⁶	-	650	[1, 7]
126	Fe-ettringite ^b	-14282.36	-16600	1937	1922	0.855	2.02·10 ⁶	-	717	[1, 21]
127	Thaumasite	-7564.52	-8700	897.1	1031	0.263	-3.40·10 ⁶	-	330	[28]
128										
129	<u>Hydrogarnet</u>									
130	C ₃ AH ₆ ^d	-5008.2	-5537.3	422	290	0.644	-3.25·10 ⁶	-	150	[9, 12]
131	C ₃ AS _{0.41} H _{5.18} ^{*d}	-5192.9	-5699	399	310	0.566	-4.37·10 ⁶	-	146	[9]
132	C ₃ AS _{0.84} H _{4.32} ^{*e}	-5365.2	-5847	375	331	0.484	-5.55·10 ⁶	-	142	[9]
133	C ₃ FH ₆ ^{***f}	-4122.8	-4518	870	330	1.237	-4.74·10 ⁶	-	155	[9]
134										
135	<u>Al-Fe siliceous hydrogarnet (solid solution)</u>									
136	C ₃ FS _{0.84} H _{4.32} ^{e,f}	-4479.9	-4823	840	371	0.478	-7.03·10 ⁶	-	149	[9]
137	C ₃ A _{0.5} F _{0.5} S _{0.84} H _{4.32} ^e	-4926.0	-5335	619	367	0.471	-8.10·10 ⁶	-	146	[9]
138										
139	C ₃ FS _{1.34} H _{3.32}	-4681.1	-4994	820	395	0.383	-8.39·10 ⁶	-	145	[9]
140										
141	<u>AFm-phases</u>									
142	C ₄ AH ₁₉	-8749.9	-10017.9	1120	1163	1.047	-	-1600	369	[12, 31]
143	C ₄ AH ₁₃ ^g	-7325.7	-8262.4	831.5	208.3	3.13	-	-	274	[31]
144	C ₄ AH ₁₁	-6841.4	-7656.6	772.7	0.0119	3.56	1.34·10 ⁻⁷	-	257	[31]
145	C ₂ AH _{7.5}	-4695.5	-5277.5	450	323	0.728	-	-	180	[12]
146	CAH ₁₀	-4623.0	-5288.2	610	151	1.113	-	3200	193	[12]
147	C ₄ AC _{0.5} H ₁₂	-7335.97	-8270	713	664	1.014	-1.30·10 ⁶	-800	285	[1, 7]
148	C ₄ AC _{0.5} H _{10.5}	-6970.3	-7813.3	668.3	0.0095	2.836	1.07·10 ⁻⁷	-	261	[31]
149	C ₄ AC _{0.5} H ₉	-6597.4	-7349.7	622.5	0.0088	2.635	9.94·10 ⁻⁸	-	249	[31]
150	C ₄ ACH ₁₁	-7337.46	-8250	657	618	0.982	-2.59·10 ⁶	-	262	[1, 7]
151	C ₄ ACH ₉	-6840.3	-7618.6	640.6	192.4	2.042	-	-	234	[31]
152	C ₄ AsH ₁₆	-8726.8	-9930.5	975.0	636	1.606	-	-	351	[31, 32]
153	C ₄ AsH ₁₄	-8252.9	-9321.8	960.9	1028.5	-	-	-	332	[31, 32]
154	C ₄ AsH ₁₂ ^{g, h}	-7778.4	-8758.6	791.6	175	2.594	-	-	310	[31, 32]
155	C ₄ AsH _{10.5}	-7414.9	-8311.9	721	172	2.402	-	-	282	[31, 32]
156	C ₄ AsH ₉	-7047.6	-7845.5	703.6	169	2.211	-	-	275	[31, 32]
157	C ₂ ASH ₈ ⁱ	-5705.15	-6360	546	438	0.749	-1.13·10 ⁶	-800	216	[1, 7]
158	C ₂ ASH ₇ ^j	-5464.0	-6066.8	487.6	0.0063	1.887	7.12·10 ⁻⁸	-	215	[31]
159	C ₂ ASH _{5.5}	-5095.2	-5603.4	454.8	0.0057	1.685	6.36·10 ⁻⁸	-	213	[31]
160	C ₄ AS _{0.5} ClH ₁₂	-7533.4	-8472 ^j	820	557	1.141	-1.02·10 ⁶	751	289	[27, 33]

161	$C_4AlCl_2H_{10}^k$	-6810.9	-7604	731	498	0.895	$-2.04 \cdot 10^6$	1503	272	[33, 34]
162	$C_4A(NO_3)_2H_{10}$	-6778.1	-7719.3	821	580	1.02	$-2.77 \cdot 10^6$	872	296	[34, 35]
163	$C_4A(NO_2)_2H_{10}$	-6606.8	-7493.1	799	565	0.99	$-2.24 \cdot 10^6$	703	275	[34-36]
164										
165	$C_4FH_{13}^{**}$	-6438.6	-7435	630	694	1.113	$2.02 \cdot 10^6$	1600	286	[9]
166	$C_4Fc_{0.5}H_{10}$	-5952.9	-6581	1270	308	1.201	$-9.08 \cdot 10^5$	3200	273	[8]
167	C_4FcH_{12}	-6674.0	-7485	1230	612	1.157	$-5.73 \cdot 10^5$	-	292	[8]
168	$C_4FsH_{12}^h$	-6873.2	-7663	1430	577	1.234	$2.02 \cdot 10^6$	-	321	[10]
169	C_2FSH_8				not stable					[37]
170	$C_4FCl_2H_{10}^k$	-5900.1	-6528 ^l	1286	481	0.961	$-1.61 \cdot 10^4$	1503	278 ^l	[37]
171										
172	<u>Sulfates</u>									
173	Cs (anhydrite)	-1322.12	-1434.60	106.7	70.2	-0.099	-	-	46	[22, 23]
174	CsH ₂ (gypsum)	-1797.76	-2023.36	193.8	91.4	-0.318	-	-	75	[22, 23]
175	CsH _{0.5} (hemihyd)	-1436.34 ^m	-1575.3 ^m	134.3	124.1	-	-	-	62	[38]
176	syngenite	-2884.91	-3172	326	201	0.308	$-1.78 \cdot 10^6$	-	128 ⁿ	[29]
177										
178	<u>(Hydr)oxides</u>									
179	Al(OH) ₃ (am)	-1143.2	-	not defined					32	[1]
180	Al(OH) ₃ (mic)	-1148.4	-1265.3 ^o	140 ^o	36	0.191	-	-	32	[12]
181	Al(OH) ₃ (gibbsite)*	-1151.0	-1288.7	70.1	36.2	0.191	-	-	32	[22, 23]
182										
183	Fe(OH) ₃ (am)	-700.1	-	not defined						[22, 23]
184	Fe(OH) ₃ (mic)	-711.6	-	not defined						[22, 23]
185	FeOOH(mic)	-480.14	-551.1	60	1.25	-0.233	$-3.14 \cdot 10^5$	-	21	[9, 22]
186	FeOOH(goethite)*	-497.26	-568.2	60	1.25	-0.233	$-3.14 \cdot 10^5$	-	21	[22, 23]
187										
188	CH (portlandite)	-897.01	-985	83	187	-0.022	-	-1600	33	[22, 23]
189	SiO ₂ (am)	-848.90	-903	41	47	0.034	$-1.13 \cdot 10^6$	-	29	[1, 7]
190	SiO ₂ (quartz)*	-854.79	-909	41	47	0.034	$-1.13 \cdot 10^6$	-	29	[22, 23]
191										
192	<u>Hydrotalcite-pyroaurite (solid solution)</u>									
193	$\frac{1}{2}M_6AcH_{13}^p$	-4339.85	-4875.9	411	512.6	-	-	-	115	[39]
194	$\frac{1}{2}M_6FCH_{13}^p$	-3882.60	-4415.1	423	521.7	-	-	-	119	[39]
195										
196	<u>M-S-H (solid solution)</u>									
197	Mg/Si=0.75									
198	$M_{1.5}S_2H_{2.5}^q$	-3218.43	-3507.52	270 ^r	318 ^r	-	-	-	95	[40]
199	Mg/Si =1.5									
200	$M_{1.5}SH_{2.5}^q$	-2355.66	-2594.22	216 ^r	250 ^r	-	-	-	74	[40]
201										
202	<u>Zeolites</u>									
203	Zeolite P(Ca)*	-5057.8	-5423	779	753	-	-	-	153 ^s	[41]
204	Natrolite*	-5325.7	-5728	360	359	-	-	-	169 ^s	[41]
205	Chabazite	-7111.8	-7774	581	617	-	-	-	251 ^s	[41]
206	Zeolite X(Na)	-5847.5	-6447	566	586	-	-	-	214 ^t	[41]
207	Zeolite Y(Na)	-7552.5	-8327	734	739	-	-	-	283 ^u	[41]
208										
209	<u>Clinkers</u>									
210	C ₃ S	-2784.33	-2931	169	209	0.036	$-4.25 \cdot 10^6$	-	73	[1, 7, 42]
211	C ₂ S	-2193.21	-2308	128	152	0.037	$-3.03 \cdot 10^6$	-	52	[1, 7, 42]
212	C ₃ A	-3382.35	-3561	205	261	0.019	$-5.06 \cdot 10^6$	-	89	[1, 7, 42]
213	C ₁₂ A ₇	-18451.44	-19414	1045	1263	0.274	$-2.31 \cdot 10^7$	-	518 ^v	[42]
214	CA	-2207.90	-2327	114	151	0.042	$-3.33 \cdot 10^6$	-	54 ^w	[42]
215	CA ₂	-3795.31	-4004	178	277	0.023	$-7.45 \cdot 10^6$	-	89 ^x	[42]
216	C ₄ AF	-4786.50	-5080	326	374	0.073	-	-	130	[1, 7, 42]
217	C (lime)	-604.03	-635	39.7	48.8	0.0045	$-6.53 \cdot 10^5$	-	17	[43]
218										
219	Ks (K ₂ SO ₄ arcanite)	-1319.60	-1438	176	120	0.100	$-1.78 \cdot 10^6$	-	66	[44]

220	K (K ₂ O)	-322.40	-363	94	77	0.036	-3.68·10 ⁵	-	40	[43]
221	Ns (Na ₂ SO ₄ thenardite)	-1269.80	-1387	150	58	0.023	-	-	53	[44]
222	N (Na ₂ O)	-376.07	-415	75	76	0.020	-1.21·10 ⁶	-	25	[43]

223 a_0, a_1, a_2, a_3 are the empirical coefficients of the heat capacity function: $C_p^\circ = a_0 + a_1T + a_2T^{-2} + a_3T^{-0.5}$; heat capacity functions for
224 cement hydrates are typically valid up to 100°C only; “-” = 0. Cement shorthand notation is used: A = Al₂O₃; C = CaO; F = Fe₂O₃;
225 H = H₂O; M = MgO; S = SiO₂; c = CO₂; s = SO₃;

226 * precipitates very slowly at 20°C, generally not included in calculations; ** tentative value.

227 ^a non-ideal solid solutions; miscibility gap: $X_{\text{SO}_4, \text{solid}} = 0.1-0.55$ reproduced with the dimensionless Guggenheim interaction param-
228 eters $\alpha_0 = 1.67$ and $\alpha_1 = 0.946$; downscaled in this paper to 1CO₂ : 1SO₃ replacement, instead of the 3CO₂ : 3SO₃ used in [4, 7].^b
229 non-ideal solid solution; miscibility gap: $X_{\text{Al}, \text{solid}} = 0.25-0.65$ reproduced with the dimensionless Guggenheim interaction param-
230 eters $\alpha_0 = 2.1$ and $\alpha_1 = -0.169$ [45].^{c,d,e,f,i,k,p,q} ideal solid solutions c.f. [9, 11, 30, 39].^g non-ideal solid solutions; miscibility gap:
231 $X_{\text{OH}, \text{solid}} = 0.50-0.97$ reproduced with the dimensionless Guggenheim interaction parameters $\alpha_0 = 0.188$ and $\alpha_1 = 2.49$ [7].^h non-
232 ideal solid solutions; miscibility gap: $X_{\text{Al}, \text{solid}} = 0.45-0.95$ reproduced with the dimensionless Guggenheim interaction parameters α_0
233 = 1.26 and $\alpha_1 = 1.57$ [10].^j typing error in [27], recalculated from G_f° and S from [27].^l typing error in [37], recalculated from G_f°
234 and S from [37]. Volume calculated from XRD data [37].^m recalculated from ΔG_f° of -20500 J/mol [38].ⁿ calculated from density
235 data from [33, 46].^o valid up to 60°C only, estimated to describe solubility of microcrystalline Al(OH)₃ aged for 19 months be-
236 tween 5 to 60°C [12].^r Estimated from C_p and S of talc, chrysotile and H₂O using data from [43].^s volume from [47].^t calculated
237 from XRD data: pdf 00-038-0237 [48];^u calculated from XRD data; pdf 00-039-1380 [49];^v [50];^w [51];^x [52]

238

239

240 Table 2: Equilibrium solubility products of solids and formation constants for calcium-silica complexes

241 at 1 bar, 25°C in Cemdata18 (as given in Table 1).

242	Mineral	log K ₅₀	Dissolution reactions used to calculate solubility products.		
243	Solids				
244	(Al-)ettringite	-44.9	Ca ₆ Al ₂ (SO ₄) ₃ (OH) ₁₂ ·26H ₂ O	→ 6Ca ²⁺ + 2Al(OH) ₄ ⁻ + 3SO ₄ ²⁻ + 4OH ⁻ + 26H ₂ O	
245	tricarboaluminate	-46.5	Ca ₆ Al ₂ (CO ₃) ₃ (OH) ₁₂ ·26H ₂ O	→ 6Ca ²⁺ + 2Al(OH) ₄ ⁻ + 3CO ₃ ²⁻ + 4OH ⁻ + 26H ₂ O	
246	Fe-ettringite	-44.0	Ca ₆ Fe ₂ (SO ₄) ₃ (OH) ₁₂ ·26H ₂ O	→ 6Ca ²⁺ + 2Fe(OH) ₄ ⁻ + 3SO ₄ ²⁻ + 4OH ⁻ + 26H ₂ O	
247	thaumasite	-24.75	Ca ₃ (SiO ₃)(SO ₄)(CO ₃)·15H ₂ O	→ 3Ca ²⁺ + H ₃ SiO ₄ ⁻ + SO ₄ ²⁻ + CO ₃ ²⁻ + OH ⁻ + 13H ₂ O	
248					
249	C ₃ AH ₆	-20.50	Ca ₃ Al ₂ (OH) ₁₂	→ 3Ca ²⁺ + 2Al(OH) ₄ ⁻ + 4OH ⁻	
250	C ₃ AS _{0.41} H _{5.18} [*]	-25.35	Ca ₃ Al ₂ (SiO ₄) _{0.41} (OH) _{10.36}	→ 3Ca ²⁺ + 2Al(OH) ₄ ⁻ + 0.41 SiO(OH) ₃ ⁻ + 3.59OH ⁻ - 1.23H ₂ O	
251	C ₃ AS _{0.84} H _{4.32} [*]	-26.70	Ca ₃ Al ₂ (SiO ₄) _{0.84} (OH) _{8.64}	→ 3Ca ²⁺ + 2Al(OH) ₄ ⁻ + 0.84 SiO(OH) ₃ ⁻ + 3.16OH ⁻ - 2.52H ₂ O	
252	C ₃ FH ₆	-26.30 ^{**}	Ca ₃ Fe ₂ (OH) ₁₂	→ 3Ca ²⁺ + 2Fe(OH) ₄ ⁻ + 4OH ⁻	
253	C ₃ FS _{0.84} H _{4.32}	-32.50	Ca ₃ Fe ₂ (SiO ₄) _{0.84} (OH) _{8.64}	→ 3Ca ²⁺ + 2Fe(OH) ₄ ⁻ + 0.84 SiO(OH) ₃ ⁻ + 3.16OH ⁻ - 2.52H ₂ O	
254	C ₃ (F,A)S _{0.84} H _{4.32}	-30.20	Ca ₃ FeAl(SiO ₄) _{0.84} (OH) _{8.64}	→ 3Ca ²⁺ + Al(OH) ₄ ⁻ + Fe(OH) ₄ ⁻ + 0.84 SiO(OH) ₃ ⁻ + 3.16OH ⁻ - 2.52H ₂ O	
255	C ₃ FS _{1.34} H _{3.32}	-34.20	Ca ₃ Fe ₂ (SiO ₄) _{1.34} (OH) _{6.64}	→ 3Ca ²⁺ + 2Fe(OH) ₄ ⁻ + 1.34 SiO(OH) ₃ ⁻ + 2.66OH ⁻ - 4.02H ₂ O	
256					
257	C ₄ AH ₁₉	-25.45	Ca ₄ Al ₂ (OH) ₁₄ ·12H ₂ O	→ 4Ca ²⁺ + 2Al(OH) ₄ ⁻ + 6OH ⁻ + 12H ₂ O	
258	C ₄ AH ₁₃	-25.25 ^{***}	Ca ₄ Al ₂ (OH) ₁₄ ·6H ₂ O	→ 4Ca ²⁺ + 2Al(OH) ₄ ⁻ + 6OH ⁻ + 6H ₂ O	
259	C ₂ AH _{7.5}	-13.80	Ca ₂ Al ₂ (OH) ₁₀ ·2.5H ₂ O	→ 2Ca ²⁺ + 2Al(OH) ₄ ⁻ + 2OH ⁻ + 2.5H ₂ O	
260	CAH ₁₀	-7.60	CaAl ₂ (OH) ₈ ·6H ₂ O	→ Ca ²⁺ + 2Al(OH) ₄ ⁻ + 6H ₂ O	
261	C ₄ AC _{0.5} H ₁₂	-29.13	Ca ₄ Al ₂ (CO ₃) _{0.5} (OH) ₁₃ ·7H ₂ O	→ 4Ca ²⁺ + 2Al(OH) ₄ ⁻ + 0.5CO ₃ ²⁻ + 5OH ⁻ + 7H ₂ O	
262	C ₄ ACH ₁₁	-31.47	Ca ₄ Al ₂ (CO ₃)(OH) ₁₂ ·5H ₂ O	→ 4Ca ²⁺ + 2Al(OH) ₄ ⁻ + CO ₃ ²⁻ + 4OH ⁻ + 5H ₂ O	
263	C ₄ ASH ₁₄	-29.26	Ca ₄ Al ₂ (SO ₄)(OH) ₁₂ ·6H ₂ O	→ 4Ca ²⁺ + 2Al(OH) ₄ ⁻ + SO ₄ ²⁻ + 4OH ⁻ + 6H ₂ O	
264	C ₄ ASH ₁₂	-29.23 ^{***}	Ca ₄ Al ₂ (SO ₄)(OH) ₁₂ ·6H ₂ O	→ 4Ca ²⁺ + 2Al(OH) ₄ ⁻ + SO ₄ ²⁻ + 4OH ⁻ + 6H ₂ O	
265	C ₂ ASH ₈	-19.70	Ca ₂ Al ₂ SiO ₂ (OH) ₁₀ ·3H ₂ O	→ 2Ca ²⁺ + 2Al(OH) ₄ ⁻ + 1SiO(OH) ₃ ⁻ + OH ⁻ + 2H ₂ O	
266	Friedel's salt	-27.27	Ca ₄ Al ₂ Cl ₂ (OH) ₁₂ ·4H ₂ O	→ 4Ca ²⁺ + 2Al(OH) ₄ ⁻ + 2Cl ⁻ + 4OH ⁻ + 4H ₂ O	
267	Kuzel's salt	-28.53	Ca ₄ Al ₂ Cl(SO ₄) _{0.5} (OH) ₁₂ ·6H ₂ O	→ 4Ca ²⁺ + 2Al(OH) ₄ ⁻ + Cl ⁻ + 0.5SO ₄ ²⁻ + 4OH ⁻ + 6H ₂ O	
268	Nitrate-AFm	-28.67	Ca ₄ Al ₂ (OH) ₁₂ (NO ₃) ₂ ·4H ₂ O	→ 4Ca ²⁺ + 2Al(OH) ₄ ⁻ + 2NO ₃ ⁻ + 4OH ⁻ + 4H ₂ O	
269	Nitrite-AFm	-26.24	Ca ₄ Al ₂ (OH) ₁₂ (NO ₂) ₂ ·4H ₂ O	→ 4Ca ²⁺ + 2Al(OH) ₄ ⁻ + 2NO ₂ ⁻ + 4OH ⁻ + 4H ₂ O	
270					
271	C ₄ FH ₁₃	-30.75 ^{**}	Ca ₄ Fe ₂ (OH) ₁₄ ·6H ₂ O	→ 4Ca ²⁺ + 2Fe(OH) ₄ ⁻ + 6OH ⁻ + 6H ₂ O	

272	Fe-hemicarbonate	-30.83	$\text{Ca}_4\text{Fe}_2(\text{CO}_3)_{0.5}(\text{OH})_{13} \cdot 3.5\text{H}_2\text{O}$	$\rightarrow 4\text{Ca}^{2+} + 2\text{Fe}(\text{OH})_4^- + 0.5\text{CO}_3^{2-} + 5\text{OH}^- + 3.5\text{H}_2\text{O}$
273	Fe-monocarbonate	-34.59	$\text{Ca}_4\text{Fe}_2(\text{CO}_3)(\text{OH})_{12} \cdot 6\text{H}_2\text{O}$	$\rightarrow 4\text{Ca}^{2+} + 2\text{Fe}(\text{OH})_4^- + \text{CO}_3^{2-} + 4\text{OH}^- + 6\text{H}_2\text{O}$
274	Fe-monosulfate	-31.57	$\text{Ca}_4\text{Fe}_2(\text{SO}_4)(\text{OH})_{12} \cdot 6\text{H}_2\text{O}$	$\rightarrow 4\text{Ca}^{2+} + 2\text{Fe}(\text{OH})_4^- + \text{SO}_4^{2-} + 4\text{OH}^- + 6\text{H}_2\text{O}$
275	Fe-Friedel's salt	-28.62	$\text{Ca}_4\text{Fe}_2\text{Cl}_2(\text{OH})_{12} \cdot 4\text{H}_2\text{O}$	$\rightarrow 4\text{Ca}^{2+} + 2\text{Fe}(\text{OH})_4^- + 2\text{Cl}^- + 4\text{OH}^- + 4\text{H}_2\text{O}$
276				
277	Cs (anhydrite)	-4.357	CaSO_4	$\rightarrow \text{Ca}^{2+} + \text{SO}_4^{2-}$
278	CsH ₂ (gypsum)	-4.581	$\text{CaSO}_4 \cdot 2\text{H}_2\text{O}$	$\rightarrow \text{Ca}^{2+} + \text{SO}_4^{2-} + 2\text{H}_2\text{O}$
279	CsH _{0.5} (hemihydrate)	-3.59	$\text{CaSO}_4 \cdot 0.5\text{H}_2\text{O}$	$\rightarrow \text{Ca}^{2+} + \text{SO}_4^{2-} + 0.5\text{H}_2\text{O}$
280	syngenite	-7.20	$\text{K}_2\text{Ca}(\text{SO}_4)_2 \cdot \text{H}_2\text{O}$	$\rightarrow 2\text{K}^+ + \text{Ca}^{2+} + 2\text{SO}_4^{2-} + \text{H}_2\text{O}$
281				
282	Al(OH) ₃ (am)	0.24	Al(OH) ₃ (am)	$\rightarrow \text{Al}(\text{OH})_4^- - \text{OH}^- - \text{H}_2\text{O}$
283	Al(OH) ₃ (mic)	-0.67	Al(OH) ₃ (mic)	$\rightarrow \text{Al}(\text{OH})_4^- - \text{OH}^- - \text{H}_2\text{O}$
284	Al(OH) ₃ (gibbsite) [*]	-1.12	Al(OH) ₃ (gibbsite)	$\rightarrow \text{Al}(\text{OH})_4^- - \text{OH}^- - \text{H}_2\text{O}$
285				
286	Fe(OH) ₃ (am)	-2.6	Fe(OH) ₃ (am)	$\rightarrow \text{Fe}(\text{OH})_4^- - \text{OH}^- - \text{H}_2\text{O}$
287	Fe(OH) ₃ (mic)	-4.6	Fe(OH) ₃ (mic)	$\rightarrow \text{Fe}(\text{OH})_4^- - \text{OH}^- - \text{H}_2\text{O}$
288	FeOOH(mic)	-5.6	FeOOH(mic)	$\rightarrow \text{Fe}(\text{OH})_4^- - \text{OH}^- - 2\text{H}_2\text{O}$
289	FeOOH(goethite) [*]	-8.6	FeOOH(goethite)	$\rightarrow \text{Fe}(\text{OH})_4^- - \text{OH}^- - 2\text{H}_2\text{O}$
290				
291	CH	-5.2	Ca(OH) ₂	$\rightarrow \text{Ca}^{2+} + 2\text{OH}^-$
292	SiO ₂ (am)	-2.714	SiO ₂ (am)	$\rightarrow \text{SiO}_2^0$
293	SiO ₂ (quartz) [*]	-3.746	SiO ₂ (quartz)	$\rightarrow \text{SiO}_2^0$
294				
295	¹ / ₂ Mg ₆ AcH ₁₃	-33.29 ^{***}	$\text{Mg}_3\text{Al}(\text{OH})_8(\text{CO}_3)_{0.5} \cdot 2.5\text{H}_2\text{O}$	$\rightarrow 3\text{Mg}^{2+} + \text{Al}(\text{OH})_4^- + 0.5\text{CO}_3^{2-} + 4\text{OH}^- + 2.5\text{H}_2\text{O}$
296	¹ / ₂ Mg ₆ FcH ₁₃	-33.64 ^{***}	$\text{Mg}_3\text{Fe}(\text{OH})_8(\text{CO}_3)_{0.5} \cdot 2.5\text{H}_2\text{O}$	$\rightarrow 3\text{Mg}^{2+} + \text{Fe}(\text{OH})_4^- + 0.5\text{CO}_3^{2-} + 4\text{OH}^- + 2.5\text{H}_2\text{O}$
297				
298	M _{1.5} S ₂ H _{2.5}	-28.80	$(\text{MgO})_{1.5}(\text{SiO}_2)_2(\text{H}_2\text{O})_{2.5}$	$\rightarrow 1.5\text{Mg}^{2+} + 2\text{SiO}_2^0 + 3\text{OH}^- + \text{H}_2\text{O}$
299	M _{1.5} SH _{2.5}	-23.57	$(\text{MgO})_{1.5}\text{SiO}_2(\text{H}_2\text{O})_{2.5}$	$\rightarrow 1.5\text{Mg}^{2+} + \text{SiO}_2^0 + 3\text{OH}^- + \text{H}_2\text{O}$
300				
301	Zeolite P(Ca) [*]	-20.3	$\text{CaAl}_2\text{Si}_2\text{O}_8 \cdot 4.5\text{H}_2\text{O}$	$\rightarrow \text{Ca}^{2+} + 2\text{Al}(\text{OH})_4^- + 2\text{SiO}_2^0 + 0.5\text{H}_2\text{O}$
302	Natrolite [*]	-30.2	$\text{Na}_2\text{Al}_2\text{Si}_3\text{O}_{10} \cdot 2\text{H}_2\text{O}$	$\rightarrow 2\text{Na}^+ + 2\text{Al}(\text{OH})_4^- + 3\text{SiO}_2^0 - 2\text{H}_2\text{O}$
303	Chabazite	-25.8	$\text{CaAl}_2\text{Si}_4\text{O}_{12} \cdot 6\text{H}_2\text{O}$	$\rightarrow \text{Ca}^{2+} + 2\text{Al}(\text{OH})_4^- + 4\text{SiO}_2^0 + 2\text{H}_2\text{O}$
304	Zeolite X(Na)	-20.1	$\text{Na}_2\text{Al}_2\text{Si}_2.5\text{O}_9 \cdot 6.2\text{H}_2\text{O}$	$\rightarrow 2\text{Na}^+ + 2\text{Al}(\text{OH})_4^- + 2.5\text{SiO}_2^0 + 2.2\text{H}_2\text{O}$
305	Zeolite Y(Na)	-25.0	$\text{Na}_2\text{Al}_2\text{Si}_4\text{O}_{12} \cdot 8\text{H}_2\text{O}$	$\rightarrow 2\text{Na}^+ + 2\text{Al}(\text{OH})_4^- + 4\text{SiO}_2^0 + 4\text{H}_2\text{O}$
306				
307	Calcium silicate complexes			
308	CaHSiO ₃ ⁺	1.2 ^{xy}	$\text{Ca}^{2+} + \text{HSiO}_3^{2-}$	$\rightarrow \text{CaHSiO}_3^+$
309	CaSiO ₃ ⁰	4.6 ^{xy}	$\text{Ca}^{2+} + \text{SiO}_3^{2-}$	$\rightarrow \text{CaSiO}_3^0$

310 ^{*} precipitates very slowly at 20°C, generally not included in calculations; ^{**} tentative value; ^{***} recalculated in this pa-
311 per from ΔG_f^o values. ^{xy} The formation of less strong calcium silicate complexes have been recently suggested (log
312 K(CaHSiO₃⁺) = 0.5 and log K(CaSiO₃⁰) = 2.9. Within Cemdata18, however, the listed values for calcium silicate
313 complexes have to be used to maintain compatibility with the C-S-H models.

314

315

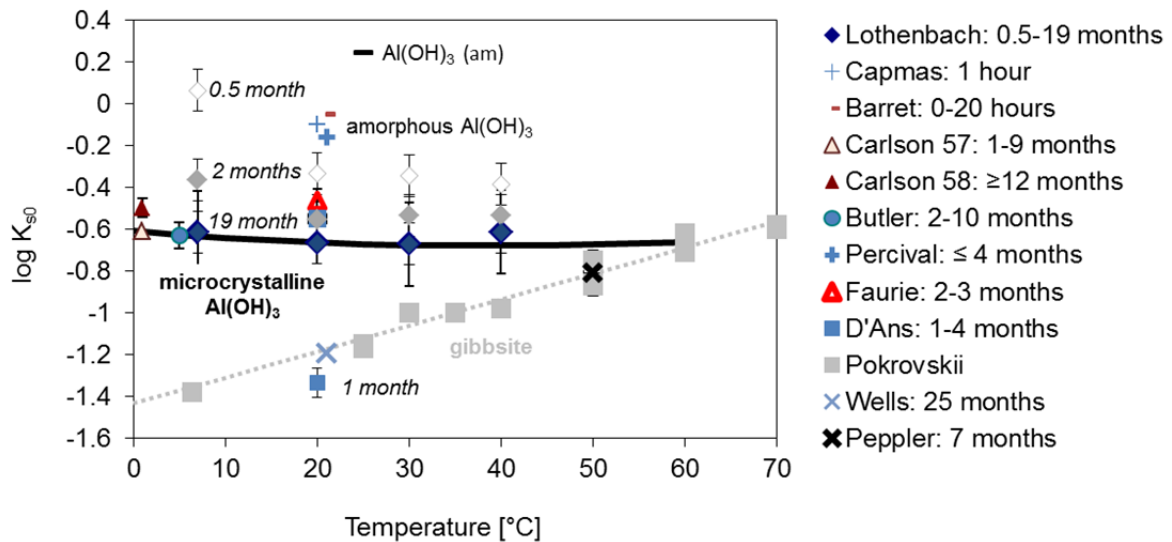
316 2.1 Solubility of Al(OH)₃ and its effect on calcium aluminate and calcium sul- 317 foaluminate cements

318 The solubility of precipitated Al(OH)₃ decreases with time. Initially "amorphous" or poorly ordered
319 Al(OH)₃ precipitates with a solubility product of approximately 0±0.2. With time, the degree of order-
320 ing increases, and microcrystalline Al(OH)₃ forms, while the solubility product decreases to -0.7 after 2
321 years. The solubility of hydrothermally prepared gibbsite is with -1.1 lower as illustrated in Figure 1,
322 however its formation is not expected within the timeframe of months to years generally considered
323 for hydrating cements. At 60°C and above, it is expected that microcrystalline Al(OH)₃ does not persist,
324 but that gibbsite forms relatively fast (Figure 1). The solubility of Al(OH)₃ determines whether CAH₁₀ (as

325 in the presence of $\text{Al}(\text{OH})_3$ with $\log K_{s0} \geq -0.6$ at 25°C) is formed initially in calcium aluminate cements
 326 or whether it converts to C_3AH_6 and microcrystalline $\text{Al}(\text{OH})_3$ [12]. The decrease of the solubility of
 327 $\text{Al}(\text{OH})_3$ with time is also responsible for the initial occurrence of CAH_{10} and ettringite instead of mono-
 328 sulfate plus microcrystalline $\text{Al}(\text{OH})_3$ in some calcium sulfoaluminate cements, as discussed in more de-
 329 tail in [53].

330 Which $\text{Al}(\text{OH})_3$ modification (see Table 1) should be taken into account depends mainly on the
 331 timeframe and the temperature considered. While gibbsite should be allowed to form at temperatures
 332 above 60°C , its precipitation should be suppressed for calculations at ambient temperatures, where
 333 microcrystalline $\text{Al}(\text{OH})_3$ will form instead. Within very short timeframes (minutes to hour), possibly on-
 334 ly amorphous $\text{Al}(\text{OH})_3$ should be allowed to precipitate. Similarly, also the formation of some other
 335 stable phases such as goethite (FeOOH), hematite (Fe_2O_3) and quartz (SiO_2) should be suppressed in
 336 calculations of hydrated cements in favour of their more disperse counterparts: microcrystalline
 337 FeOOH (or microcrystalline or amorphous $\text{Fe}(\text{OH})_3$, depending on the timeframe considered), and
 338 amorphous SiO_2 .

339



340

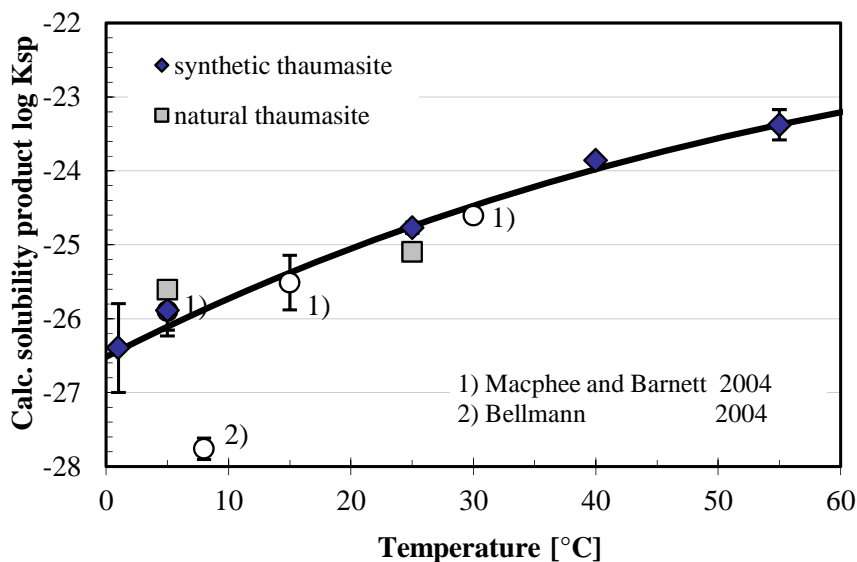
341 Figure 1: Logarithm of the solubility product of $\text{Al}(\text{OH})_3$ (referring to $\text{Al}(\text{OH})_4^-$ and OH^-) as a function of
 342 time and temperature calculated from the literature, adapted from [12]. Gibbsite solubility (dotted line)
 343 was calculated using data from the GEMS version of the PSI/Nagra 12/07 TDB [22, 23], whereas the
 344 solubility of microcrystalline $\text{Al}(\text{OH})_3$ (black line) and amorphous $\text{Al}(\text{OH})_3$ (black hyphen) was calculated
 345 based on the data given in Table 1.

346

347 2.2 Thaumasite

348 Damidot et al. [54] obtained solubility data to derive a solubility constant for thaumasite at 25°C , at
 349 which temperature thaumasite was considered to be stable. Invariant points were calculated for phase

350 assemblages including thaumasite in the system $\text{CaO-Al}_2\text{O}_3\text{-SiO}_2\text{-CaSO}_4\text{-CaCO}_3\text{-H}_2\text{O}$. Schmidt et al.
 351 [55] used the solubility data of Macphee and Barnett [56] to derive thermodynamic data for
 352 thaumasite over the temperature range 1 to 30°C to confirm experimental data showing formation of
 353 thaumasite in mortars at 8 and 20°C. Another set of solubility data at 8°C for natural thaumasite was
 354 reported by Bellmann [57] who also highlighted the potential pathways of formation of thaumasite at
 355 this temperature. Macphee and Barnett [56] obtained the solubility data of ettringite-thaumasite solid
 356 solutions in the temperature range between 5°C and 30°C; no apparent decomposition of thaumasite
 357 and related solid solutions occurred after 6 months storage at 30°C, which suggests the persistence of
 358 thaumasite at temperatures at least up to ~30°C. A complete solubility dataset representative for the
 359 stability range of thaumasite was missing, as [56] reported the solubility data for thaumasite-ettringite
 360 solid-solutions but not for pure thaumasite. Hence, due to a lack of experimental data, no thermody-
 361 namic data for thaumasite were included in the Cemdata07 database, but were added in a first update
 362 using the data derived in Schmidt et al. [55] based on the solubility data given by Macphee and Bar-
 363 nett [49]. In 2015, Matschei and Glasser [28] published a new dataset obtained on apparently pure-
 364 phase synthetic thaumasite. It was shown that pure thaumasite was thermally stable up to $68\pm 5^\circ\text{C}$. The
 365 obtained new data agreed well, within limits of error, with those obtained by Macphee and Barnett
 366 [56], but differs significantly from the data for natural thaumasite reported by Bellmann [57] at 8°C. Ex-
 367 periments done by [28, 56] excluded atmospheric carbon dioxide, whereas the solubility determina-
 368 tions reported in [57] were made in the presence of air containing carbon dioxide. The contact with the
 369 air may lead to the decomposition of thaumasite, which would make the interpretation of the solubility
 370 data invalid.



371
 372 Figure 2: Calculated solubility products referring to Ca^{2+} , $\text{SiO}(\text{OH})_3^-$, SO_4^{2-} , CO_3^{2-} , OH^- and H_2O of syn-
 373 thetic and natural thaumasite samples from solubility experiments. The curve shows the calculated
 374 best fit using a three-term temperature extrapolation. Reproduced from [28].

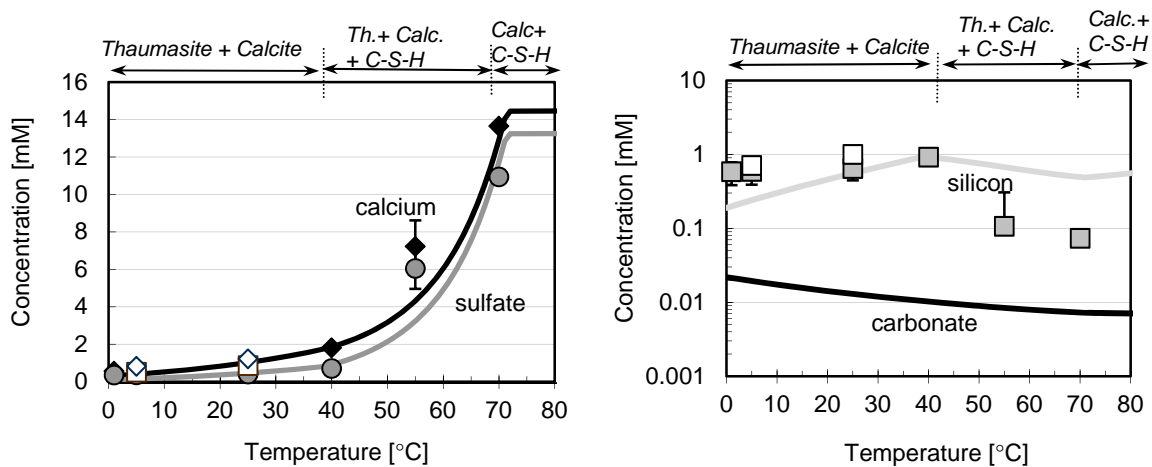
375

376 The heat capacities were estimated using a reference reaction with a solid having a known heat capaci-
 377 ty and similar structure, as discussed in more detail in [55] and [28]. As shown by Helgeson et al. [43],
 378 this principle can be successfully applied to estimate the heat capacity of silicate minerals by formulat-
 379 ing a reaction involving a structurally-related mineral of known heat capacity.

380

381 Finally, it is possible to do an internal consistency check and recalculate solubilities under the chosen
 382 experimental conditions with the thermodynamic data of the Cemdata18 dataset. As illustrated in Fig-
 383 ure 3, the calculated solubility data for thaumasite show generally good agreement with the experi-
 384 mentally-derived dataset. Despite an underestimation of the calculated silicon concentrations at 1°C
 385 and 5°C, both datasets, experimental and calculated, generally agree, proving the internal consistency
 386 of the data. Especially in the temperature range from 1 to ~40°C, where the solid phase assemblage
 387 consists mainly of thaumasite and traces of calcite, differences between experimental calcium and sul-
 388 fate concentrations are within analytical errors. In the temperature range 1°C to ~ 40°C, concentrations
 389 of calcium, sulfate and silicon increase with rising temperature, whereas calculated carbonate concen-
 390 trations show a continuous decrease. At temperatures > ~40°C, calcium and sulfate concentrations in-
 391 crease significantly, whereas silicon concentrations decrease due to the formation of C-S-H.
 392 Thaumasite is absent at temperatures above 70°C.

393



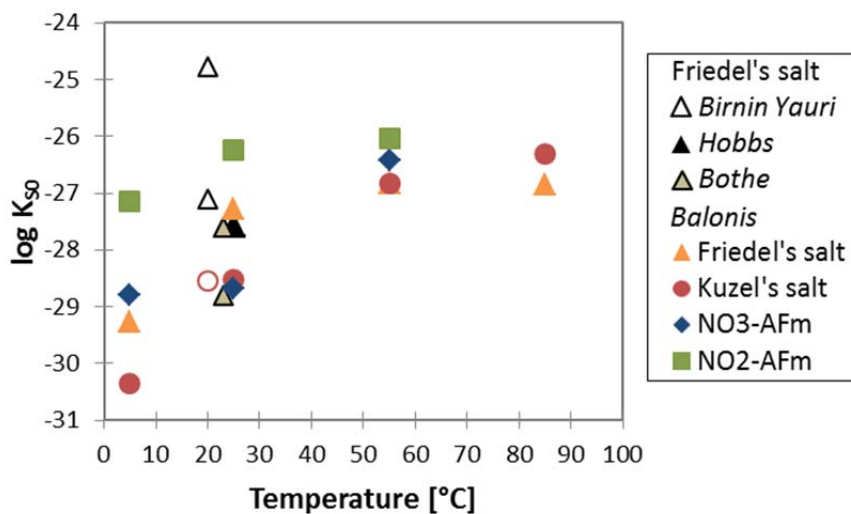
394 Figure 3: Experimentally measured (markers) and re-calculated (lines) solubility data for thaumasite;
 395 (filled markers represent the experimental data for synthetic thaumasite, open markers – the data for
 396 natural thaumasite from [28]). Calculations are based on the new thermodynamic data for thaumasite
 397 complemented with the CSHQ data from Cemdata18 [1, 7]. Predicted solid phases/ phase assemblages
 398 are shown along the top.

399

400 2.3 Chloride-, nitrate-, and nitrite-AFm phases

401 Binding of chloride and the formation of chloride bearing cement hydrates has been widely studied
 402 due to its impact on the corrosion of steel in reinforced concrete. The first comprehensive solubility
 403 data for Friedel's salt ($\text{Ca}_4\text{Al}_2\text{Cl}_2(\text{OH})_{12}\cdot 4\text{H}_2\text{O}$) and Kuzel's salt ($\text{Ca}_4\text{Al}_2\text{Cl}(\text{SO}_4)_{0.5}(\text{OH})_{12}\cdot 6\text{H}_2\text{O}$) were provid-
 404 ed in the late nineties. Birnin-Yauri [58] has described the dissolution of Friedel's salt as congruent and
 405 provided values of $\log K_{S0} = -27.1$ and -24.8 ($K_{S0} = \{\text{Ca}^{2+}\}^4\{\text{Al}(\text{OH})_4\}^2\{\text{Cl}^-\}^2\{\text{OH}^-\}^4\{\text{H}_2\text{O}\}^4$). Hobbs [59] esti-
 406 mated $\log K_{S0}$ as -27.6 ± 0.9 and Bothe [60] has estimated via geochemical modeling that the solubility
 407 product of Friedel's salt should fall within the range $-28.8 < \log K_{S0} < -27.6$. Balonis et al. [27] provid-
 408 ed solubility data for Friedel's salt as a function of time and temperature with an estimated value of
 409 solubility product for an ideal composition and at room temperature to be -27.27 [34, 36]. Compilation
 410 of the available solubility data is shown by triangles on Figure 4.

411 The estimated thermodynamic data [36] ($\Delta_f G^0 \sim -6810.9$ kJ/mol, $\Delta_f H^0 \sim -7604$ kJ/mol, S^0 731 J/mol K)
 412 have similar values (except the entropy) to the dataset published by Blanc et al. [16]
 413 ($\Delta_f G^0 \sim -6815.44$ kJ/mol, $\Delta_f H^0 \sim -7670.04$ kJ/mol, S^0 527.70 J/mol K), and agree reasonably well with
 414 the data obtained by Grishchenko et al. [61] ($\Delta_f G^0$ estimated in a range between 6800 and 6860 kJ/mol,
 415 $S^0 \sim 680$ J/mol K), though it should be kept in mind that Grishchenko's composition is reported to be
 416 slightly contaminated with carbonate ions. Attempts to synthesize Cl-AFm at temperatures above 0°C
 417 were unsuccessful [34], hence no thermodynamic data are available that can be used.



418
 419 Figure 4: Solubility products of Friedel's salt, Kuzel's salt, NO_3 -AFm and NO_2 -AFm (referring to reac-
 420 tions using Ca^{2+} , Cl^- , SO_4^{2-} , NO_3^- , NO_2^- , OH^- and H_2O as indicated in Table 2) as a function of tempera-
 421 ture. Data for Friedel's salt from [27, 58-60, 62], data for other AFm are from Balonis and co-workers
 422 [27, 34-36].

423
 424 Glasser et al. [62] first measured the solubility of Kuzel's salt and noted that its dissolution is strongly
 425 incongruent, with ettringite precipitating as a secondary phase. From the solubility data given by
 426 Glasser et al. a $\log K_{S0}$ of Kuzel's salt -28.54 ($K_{S0} = \{\text{Ca}^{2+}\}^4\{\text{Al}(\text{OH})_4\}^2\{\text{Cl}^-\}\{\text{SO}_4^{2-}\}^{0.5}\{\text{OH}^-\}^4\{\text{H}_2\text{O}\}^6$) was esti-
 427 mated [27]. Balonis et al. [27] has also experimentally derived the solubility data and calculated solubil-

428 ity products for Kuzel's salt at different temperatures ranging from 5 to 85°C for the period between 1-
429 12 months, with the solubility product at room temperature determined to be $\log K_{50} = -28.53$. Data for
430 12 months are shown by the filled circles in Figure 4.

431 In recent years, the impact of soluble nitrate and nitrite corrosion inhibitors on the mineralogy of ce-
432 ment pastes has been studied [34, 36, 63], and it has been demonstrated that the AFm phase has the
433 ability to accommodate NO_3^- and NO_2^- ions in the interlayer position. Solubility data along with ther-
434 modynamic parameters for the nitrate AFm ($\text{NO}_3\text{-AFm}$) and nitrite AFm ($\text{NO}_2\text{-AFm}$) published by Balo-
435 nis et al. [34, 35] are shown in Figure 4. Similarly, as in the case of Cl-AFt, an attempted synthesis of
436 $\text{NO}_3\text{-}$ or $\text{NO}_2\text{-AFt}$ at room temperature was not successful [34].

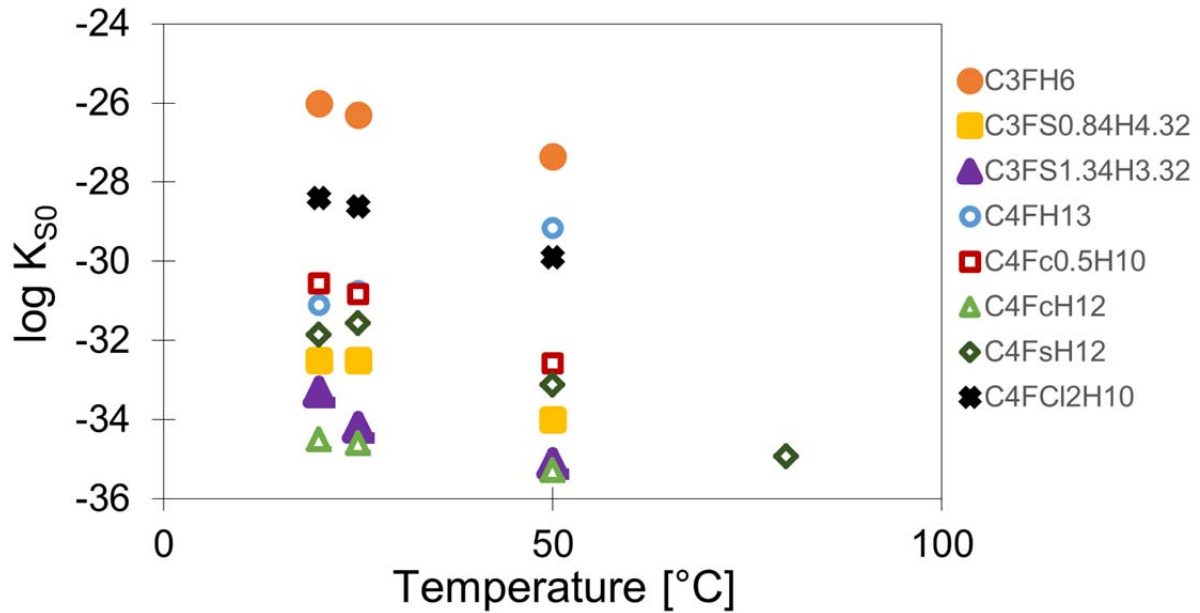
437

438 **2.4 Iron containing hydrates**

439 The main source of iron in cements is 5-15% ferrite clinker in Portland cements and slag in blended
440 cements. In synthetic systems containing only water, C_2F , calcium sulfate, calcium carbonate or silica,
441 different Fe-containing phases like ettringite, monosulfate, monocarbonate, siliceous hydrogarnet can
442 precipitate, as well as form solid solutions with their Al-containing analogues [8-10, 21].

443 The stability of Fe-containing phases generally is only moderately affected by temperature, as shown
444 in Figure 5. At ambient temperature, Fe-ettringite ($\text{C}_6\text{Fs}_3\text{H}_{32}$), Fe-monosulfate ($\text{C}_4\text{FsH}_{12}$), Fe-
445 monocarbonate ($\text{C}_4\text{FCH}_{12}$), Fe-Friedel's salt ($\text{C}_4\text{FCl}_2\text{H}_{10}$), and Fe-siliceous hydrogarnet ($\text{C}_3\text{FS}_{0.95}\text{H}_{4.1}$,
446 $\text{C}_3\text{FS}_{1.52}\text{H}_{2.96}$) are stable, while Fe-katoite (C_3FH_6) and Fe-hemicarbonate ($\text{C}_4\text{Fc}_{0.5}\text{H}_{10}$) are metastable [8-
447 10, 21, 37]. Attempts to synthesize Fe-strätlingite (C_2FSH_8) failed, as only portlandite, C-S-H and iron
448 hydroxide formed, indicating the instability of Fe-strätlingite at ambient conditions. $\text{C}_4\text{FsH}_{12}$, $\text{C}_4\text{FCH}_{12}$,
449 and $\text{C}_4\text{FC}_{12}\text{H}_{10}$ are also stable at 50° but not at 80°C, while Fe-siliceous hydrogarnet is stable at up to
450 110°C. The limited stability field of the Fe-containing AFm and AFt hydrates is related to the very high
451 stability of goethite (FeOOH) and hematite (Fe_2O_3), which form at 50°C within several months and at
452 80°C within days [9]. Although hematite and portlandite would be more stable than the Fe-katoite, AFt
453 and AFm phases between 0 and 100°C, the formation of goethite and hematite at ambient tempera-
454 tures is very slow, such that Fe-containing siliceous hydrogarnet, AFt and AFm phases can be synthe-
455 sized instead. Figure 3 shows the solubility products of Fe-containing phases calculated based on the
456 measured composition of the liquid phase at 20, 50 and 80°C; those data were used to derive the
457 thermodynamic data for standard conditions (25°C, 1 atm) given in Table 1. The formation of solid so-
458 lutions between Al and Fe-containing endmembers has been observed for ettringite, siliceous hy-
459 drogarnet, monosulfate, and Friedel's salt, while no solid solution formed between the rhombohedral
460 Fe-monocarbonate with the triclinic Al-monocarbonate due to the structural differences [8-10, 21, 37].

461



462

463 Figure 5: Solubility product (K_{S0}) of Fe-containing hydrogarnet and AFm-phases at different tempera-
 464 tures, referring to reactions using Ca^{2+} , $\text{Fe}(\text{OH})_4^-$, $\text{SiO}(\text{OH})_3^-$, SO_4^{2-} , CO_3^{2-} , Cl^- , OH^- and H_2O as indicated
 465 in Table 2. Data from Dilnesa and co-workers [8-10, 37].

466

467 While different Fe-containing hydrates could be synthesized, only Fe-siliceous hydrogarnet is expected
 468 to occur in hydrated cements. The solubility product of Fe-siliceous hydrogarnet (given in Table 1) is 5
 469 to 7 log units lower than that of Al-siliceous hydrogarnet indicating a high stabilization of Fe-siliceous
 470 hydrogarnet, while the solubility products of the Fe-containing hydrates are comparable or only
 471 somewhat more stable than their Al-containing analogues. In fact, in hydrated PC, Fe(III) precipitates as
 472 iron hydroxide during the first hours and as siliceous hydrogarnet ($\text{C}_3(\text{A},\text{F})\text{S}_{0.84}\text{H}_{4.32}$) after 1 day and
 473 longer [64-66]. The data for the $\text{C}_3\text{FS}_{0.84}\text{H}_{4.32}$ and for the mixed Al- and Fe-containing $\text{C}_3\text{A}_{0.5}\text{F}_{0.5}\text{S}_{0.84}\text{H}_{4.32}$
 474 determined by Dilnesa et al. [9] are included in Cemdata18, but not the data for the Al-based
 475 $\text{C}_3\text{AS}_{0.84}\text{H}_{4.32}$ due to its formation being kinetically hindered at ambient conditions [9].

476

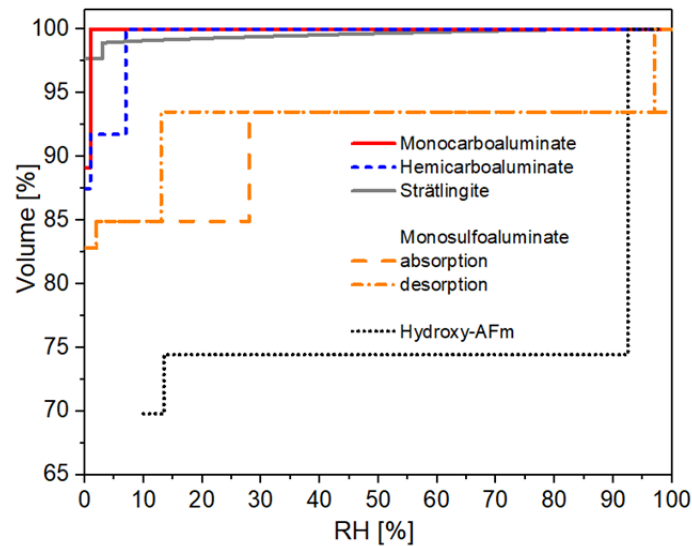
477 2.5 Effect of relative humidity

478 Cement hydrates are known to show varying water content as functions of temperature and relative
 479 humidity (RH). Some of these hydrates are crystalline phases with layered structure such as the AFm-
 480 phases or ettringite-type structures. The AFm and AFt phases have different hydration states (i.e. vary-
 481 ing molar water content) depending on the exposure conditions, which can impact the volume stabil-
 482 ity, porosity and density of cement paste. The molar volume of some AFm phases can decrease by as
 483 much as 20% during drying [31], which may strongly influence the porosity and performance of some
 484 cementitious systems.

485 In gel-like phases such as C-S-H, water can be present within the intrinsic gel porosity, as well as in its
486 interlayer. Unfortunately, until now there was no thermodynamic model capable of assessing this vary-
487 ing water content.

488 The crystalline AFm phases have a layered structure and are known for their varying water content in
489 the interlayer, which can be of two types. Firstly, the “space filling”, loosely integrated zeolitic water
490 molecules, which are easily removed from the structure upon increase of temperature or at an initial
491 small decrease of RH and have thermodynamic properties close to liquid water. Secondly, the “struc-
492 tural water” molecules, which are strongly bound to calcium cations of the main layer and can only be
493 removed at low water activities and/or high temperatures, typically accompanied by high enthalpies
494 values. Recently, the thermodynamic properties of the different hydration states of the most important
495 AFm phases were determined by Baquerizo et al. [31, 32] and are listed in Table 1. A summary of the
496 volume stability of AFm phases at 25°C is shown in Figure 6.

497



498

499 Figure 6: Volume changes of the AFm phases studied as function of RH at 25°C. 100% volume corre-
500 sponds to the higher hydration state of each phase.

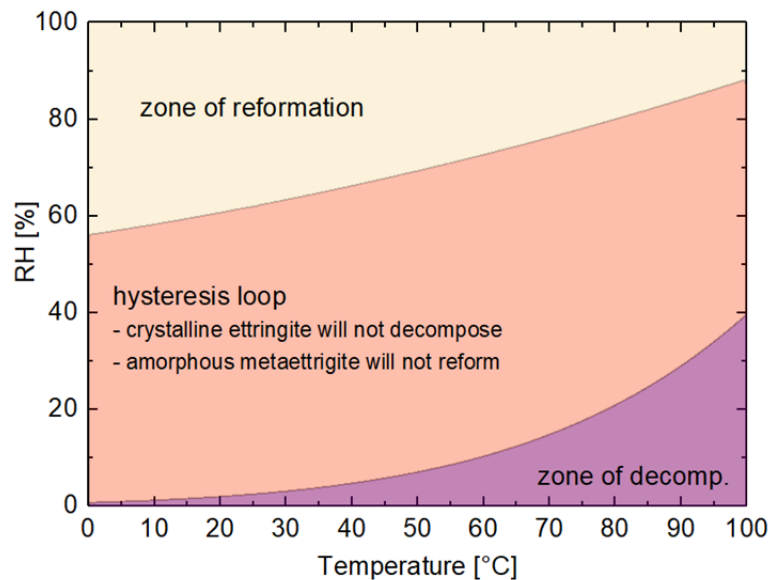
501

502 Ettringite, $C_6As_3H_{32}$, is also known to have varying water content. This hydrate is a common phase oc-
503 ccurring during the hydration of PC. It is also the main hydration product in calcium sulfoaluminate ce-
504 ments and calcium aluminate cement blended with gypsum. Understanding the stability of ettringite
505 during hydration and under different drying conditions is of great importance to assess the perfor-
506 mance of systems containing large amounts of this phase. In general, ettringite contains 32 H_2O mole-
507 cules per formula unit: 30 fixed in the columns and 2 H_2O of zeolitic water loosely bound in the chan-
508 nels. Removal of the two inter-channel water molecules takes place with decreasing relative humidity
509 (RH) without any significant change of the structure. Nevertheless, a series of structural changes are
510 observed when the water content is below 30 H_2O , resulting in an amorphous phase commonly known
511 as metaettringite. The thermodynamic properties of crystalline ettringite, having 32 and 30 H_2O , and
512 amorphous ettringite (or metaettringite) having 13 H_2O and 9 H_2O were recently derived by Baquerizo
513 et al. [30] and are listed in Table 1. Something interesting to notice is that decomposition and refor-

514 mation of ettringite takes place reversibly but with a marked hysteresis, which makes the estimation of
515 thermodynamic properties difficult. The values presented in Table 1 corresponds to those derived us-
516 ing the desorption equilibrium properties. Figure 7 shows the stability of ettringite at 25°, presenting
517 three different zones:

- 518 - The zone of decomposition, which has to be reached in order to decompose ettringite into
- 519 metaettringite.
- 520 - The hysteresis loop, where crystalline ettringite will not undergo decomposition unless the zone of
- 521 decomposition is reached and amorphous metaettringite will not reform unless the zone of refor-
- 522 mation is reached.
- 523 - The zone of reformation, which has to be reached in order to be convert metaettringite back to
- 524 crystalline ettringite.

525



526

527 Figure 7: Stability of ettringite as a function of relative humidity and temperature.

528

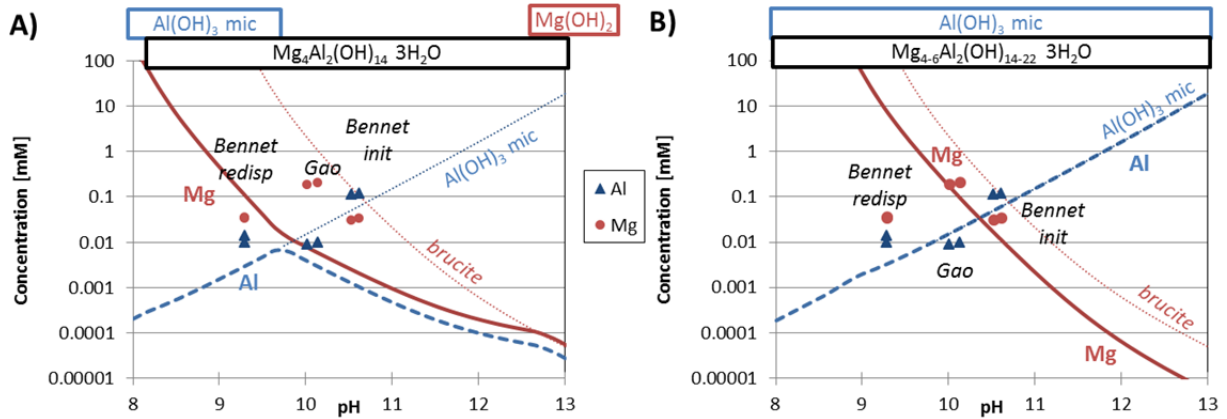
529 2.6 Mg-Al layered double hydroxide (hydrotalcite-like phase)

530 Mg-Al layered double hydroxide (LDH) type phases are structurally similar to hydrotalcite and typically
531 occur as secondary reaction products in hydrated Portland cements [67] and in alkali-activated granu-
532 lated blast furnace slag (GBFS) [68, 69]. In hydrated or alkali-activated cementitious materials free from
533 carbonation, Mg-Al LDH phases normally exhibit poor long-range structural order and are thought to
534 significantly occur along the solid solution series $Mg_{(1-x)}Al_x(OH)_{(2+x)}(H_2O)_4$, where $0.2 \leq x \leq 0.33$ [70, 71]
535 due to the deficiency of CO_2 in the system. Mg-Al LDH formation is thus often difficult to observe by
536 conventional X-ray diffraction, particularly at low MgO content.

537 Few solubility data for hydroxide containing hydrotalcite like Mg-Al LDH phases have been measured;
538 the data at 25°C are summarised in Figure 8A and B. The samples studied by Bennet et al. [72] were
539 synthesised for 2 days at 80°C, dried, and then re-dispersed in water for 4 weeks at 25°C. This proce-

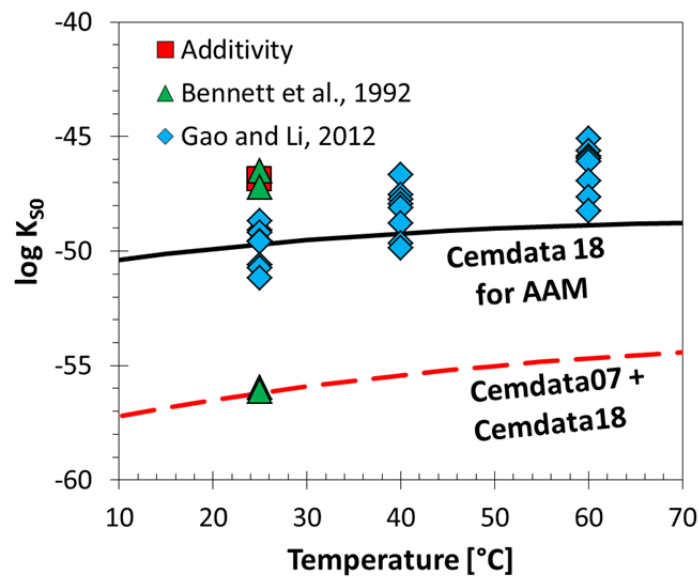
540 dure resulted in a solubility product of 10^{-47} for M_4AH_{10} . Further re-dispersion steps lowered the solu-
 541 bility product of M_4AH_{10} to 10^{-56} . This lower solubility product of 10^{-56} for M_4AH_{10} was selected for use
 542 in Cemdata07 [1, 29] (see Figure 8A and Figure 9), and by Bennet et al. [72].

543



544

545 Figure 8: Solubility of A) M_4AH_{10} (from Cemdata07+18) and B) of the MgAl-OH-LDH solid solution
 546 compared to the solubility of microcrystalline $Al(OH)_3$ and brucite (dotted lines) and to the experi-
 547 mental data (Mg: circles, Al: triangles) determined by Bennet et al. [72] and Gao and Li [73].



548

549 Figure 9: Measured and calculated solubility products of M_4AH_{10} (reactions refer to Mg^{2+} , $Al(OH)_4^-$, OH^-
 550 and H_2O as indicated in Table 3) at different temperatures. Adapted from Myers et al. [74].

551

552 Based on the solubility data of Gao and Li [73] for samples precipitated from oversaturated solutions
 553 (equilibration time 2 days), solubility data for hydrotalcite like Mg-Al LDH phases intercalated with OH^-
 554 (MgAl-OH-LDH) were recently recompiled and recalculated [74], as shown in Figure 8B) and Figure 9.
 555 Solubility products for the end members of MgAl-OH-LDH solid solution model were defined using
 556 the available data [72, 73] and guided using experimental observations in alkali activated slag cements
 557 with the high stability of MgAl-OH-LDH and absence of brucite in uncarbonated alkali-activated slag
 558 cements is widely documented and provides a reliable proxy for this task. An ideal (simple mixing) sol-

559 id solution thermodynamic model (MA-OH-LDH_ss) was provisionally defined using these data for
 560 Mg/Al molar ratios between 2 and 4. The use of independent experimental observations to derive the
 561 solid solution model is important because solubility products derived from the available solubility data
 562 are scattered by up to $\sim 10 \log_{10}$ units at 25°C, possibly due to the varied equilibration times used (2
 563 days [73] to 1 month [72]). We recommend using MgAl-OH-LDH_ss for alkali activated materials.

564
 565 Usage of the MgAl-OH-LDH_ss model (describing hydrotalcite-like phases with variable Mg/Al ratio,
 566 and recommended for use in alkali activated material systems) does not lead to hydrotalcite formation
 567 under typical PC conditions due to the low aluminium concentrations in the pore solution [29] of PCs,
 568 for which brucite would be calculated to precipitate instead. As the formation of hydrotalcite like
 569 phases is reported in well hydrated PCs with dolomite [75], the use of a single phase, M_4AH_{10} , with a
 570 lower solubility product (see Table 3, Figure 9) derived from the long-term experiments in [72] only, is
 571 recommended for hydrated PC. The necessity to use presently two different datasets and the large dif-
 572 ferences in the available data indicates that the solubility data selected for M_4AH_{10} and for MgAl-OH-
 573 LDH_ss are tentative and may require updating as more data become available. Therefore, we believe
 574 that additional solubility measurements for Mg-Al LDH phases are needed.

575
 576 Table 3: Standard thermodynamic properties at 25°C and 1 atm for hydrotalcite-like phases (provided
 577 in separate modules of Cemdata18 database). The data are consistent with the GEMS version of the
 578 PSI/Nagra 12/07 TDB [22, 23] and the data detailed in Table 1 and Table 4.

579	$\Delta_f G^\circ$	$\Delta_f H^\circ$	S°	a_0	a_1	a_2	a_3	V°	Ref
580	[kJ/mol]	[kJ/mol]	[J/K/mol]	[J/K/mol]	[J/mol/K ²]	[J K/mol]	[J/K ^{0.5} /mol]	[cm ³ /mol]	
581									
582	$M_4AH_{10}^*$	-6394.6	-7196	549	-364	4.21	$3.75 \cdot 10^6$	629	220 [1, 29]
583									
584	<u>MgAl-OH-LDH (ideal ternary solid solution)**</u>								
585	M_4AH_{10}	-6358.5	-7160.2	548.9	547.6	-	-	-	219.1 [74]
586	M_6AH_{12}	-8022.9	-9006.7	675.2	803.1	-	-	-	305.4 [74]
587	M_8AH_{14}	-9687.4	-10853.3	801.5	957.7	-	-	-	392.4 [74]
588	Mineral	log K_{50}	Dissolution reactions used to calculate solubility products.						
589	$M_4AH_{10}^*$	-56.02*	$Mg_4Al_2(OH)_{14} \cdot 3H_2O$	$\rightarrow 4Mg^{2+} + 2Al(OH)_4^- + 6OH^- + 3H_2O$					
590									
591	$M_4AH_{10}^{**}$	-49.7	$Mg_4Al_2(OH)_{14} \cdot 3H_2O$	$\rightarrow 4Mg^{2+} + 2Al(OH)_4^- + 6OH^- + 3H_2O$					
592	$M_6AH_{12}^{**}$	-72.0	$Mg_6Al_2(OH)_{18} \cdot 3H_2O$	$\rightarrow 6Mg^{2+} + 2Al(OH)_4^- + 10OH^- + 3H_2O$					
593	$M_8AH_{14}^{**}$	-94.3	$Mg_8Al_2(OH)_{22} \cdot 3H_2O$	$\rightarrow 8Mg^{2+} + 2Al(OH)_4^- + 14OH^- + 3H_2O$					

594 a_0, a_1, a_2, a_3 are the empirical coefficients of the heat capacity function: $C_p^\circ = a_0 + a_1T + a_2T^{-2} + a_3T^{-0.5}$; * tentative value; recom-
 595 mended for PC based systems. ** tentative values; recommended for alkali activated materials.

596

597 2.7 C-S-H solid solution models

598 The C-S-H gel-like phase is the major hydrate in PC and blended PC pastes. C-S-H is also the main
 599 "sorbent" of alkali, alkali-earth, and hazardous cations (Sr^{2+} , UO_2^{2+} , Zn^{2+} , etc.) in hydrated cements used
 600 as waste matrices, including engineered barriers in nuclear waste repositories.

601 C-S-H phases have a variable composition that depends on the prevailing Ca/Si ratio in the system
 602 that can change by pozzolanic reaction, leaching caused by the ingress of water and/or chemical at-
 603 tack, such as carbonation. There are differences between properties of C-S-H samples prepared by (a)
 604 C₃S or C₂S hydration; (b) co-precipitation (double-decomposition) methods [76]. C-S-H has a 'defect-
 605 tobermorite' structure with a mean silicate chain length depending on the Ca/Si ratio, pH and the
 606 presence of aluminum [77]. It has variable "non-gel" water content (i.e. structural water and water pre-
 607 sent in the interlayer [78, 79]), also depending on the Ca/Si ratio and the synthesis route, variable par-
 608 ticle morphology, stacking, and "gel" water content, i.e. water present between C-S-H particles. Many
 609 C-S-H experimental solubility data sets available to date have been critically analyzed [80], including C-
 610 S-H type phases with variable aluminum and alkali contents [76, 81-84].

611 C-S-H solubility can be reliably modelled using either solid solution models [11, 80, 85] or (to a limited
 612 extent) using a surface complexation approach [86, 87]. Quantitative knowledge of C-S-H solubility is
 613 needed in essentially all studies of cement hydration and of waste-cement interactions, which explains
 614 why measuring and modeling the C-S-H solubility and water content is a major topic in cement chem-
 615 istry [76].

616 In Table 4, five alternative C-S-H solid solution models are represented, in part for backward compati-
 617 bility with previous versions of Cemdata (Cemdata07 and Cemdata14); they are provided in the
 618 Cemdata18 database. Here we provide a brief overview of those models with some recommendations
 619 for their use.

620

621 Table 4: Solid solution models of C-S-H (provided in separate modules of Cemdata18 database).

622 Phase,	$\Delta_f G^\circ$	$\Delta_f H^\circ$	S°	a_0	a_1	a_2	V°	Ref
623 End member	[kJ/mol]	[kJ/mol]	[J/K/mol]	[J/K/mol]	[J/mol/K ²]	[J K/mol]	[cm ³ /mol]	
624 <u>C-S-H (CSH-II solid solution)</u>								
625 Tob: C _{0.83} SH _{1.3}	-1744.36	-1916	80	85	0.160		59	[1]
627 Jen: C _{1.67} SH _{2.1}	-2480.81	-2723	140	210	0.120	-3.07·10 ⁶	78	[1]
628								
629 <u>C-S-H-K-N (ECSH-1 solid solution)</u>								
630 TobCa-1: C _{0.83} SH _{1.83}	-1863.62	-2059.5	114.6	170.4			68	[85]
632 SH: SH (SiO ₂ H ₂ O)	-1085.45	-1188.6	111.3	119.8			34	[85]
633 NaSH-1: N _{0.5} S _{0.2} H _{0.45}	-433.57	-480.4	41.2	37.9			10.5	[88]
634 KSH-1: K _{0.5} S _{0.2} H _{0.45}	-443.35	-490.0	48.4	40.6			12.4	[88]
635 SrSH-1: SrSH ₂	-2020.89	-2231.6	141.9	174.8			64	[88]
636	(-2017.47 ^b)	(-2228 ^b)						
637								
638 <u>C-S-H-K-N (ECSH-2 solid solution)</u>								
639 TobCa-2: C _{0.83} SH _{1.83}	-1863.62	-2059.5	114.6	170.4			68	[85]
640 JenCa: CS _{0.6} H _{1.1}	-1569.05	-1741.6	73.0	114.5			36	[85]
641 NaSH-2: N _{0.5} S _{0.2} H _{0.45}	-430.72	-477.6	41.2	37.9			10.5	[88]
642 KSH-2: K _{0.5} S _{0.2} H _{0.45}	-440.49	-487.2	48.4	40.6			12.4	[88]
643 SrSH-2: SrSH ₂	-2019.75	-2230.5	141.9	174.8			64	[88]
644	(-2016.33 ^b)	(-2227 ^b)						
645								
646 <u>C-S-H (CSHQ solid solution)</u>								
647								

648	TobH Ca/Si=0.67: C _{2/3} SH _{1.5}	-1668.56	-1841.5	89.9	141.6			55	[11]	
649	TobD Ca/Si =1.25: C _{5/6} S _{2/3} H _{1.83}	-1570.89	-1742.4	121.8	166.9			48	[11]	
650	JenH Ca/Si =1.33: C _{1.33} SH _{2.17}	-2273.99	-2506.3	142.5	207.9			76	[11]	
651	JenD Ca/Si=2.25: C _{1.5} S _{0.67} H _{2.5}	-2169.56	-2400.7	173.4	232.8			81	[11]	
652	NaSH: N _{0.5} S _{0.2} H _{0.45}	-431.20	-478.0	41.2	37.9			10.5	[88, 89]	
653	KSH: K _{0.5} S _{0.2} H _{0.45}	-440.80	-489.6	48.4	40.6			12.4	[88, 89]	
654										
655										
656	<u>C-S-H (CSH3T solid solution)</u>									
657	TobH Ca/Si=0.67: C ₁ S _{3/2} H _{5/2}	-2561.53	-2832.97	152.8	231.2			85	[11]	
658	T5C Ca/Si=1.0: C _{5/4} S _{5/4} H _{5/2}	-2518.66	-2782.03	159.9	234.1			79	[11]	
659	T2C Ca/Si=1.5: C _{3/2} S ₁ H _{5/2}	-2467.08	-2722.40	167.0	237.0			81	[11]	
660										
661										
662	<u>C-(N-)A-S-H (CNASH solid solution)</u>									
663	TobH ^c : C ₁ S _{3/2} H _{5/2}	-2560.00	-2831.4	152.8	231.2	-	-	-	85.0	[90]
664	INFCA: C ₁ A _{5/32} S _{38/32} H _{53/32}	-2342.90	-2551.3	154.5	180.9	-	-	-	59.3	[90]
665	INFCN: C ₁ N _{5/16} S _{3/2} H _{19/16}	-2452.46	-2642.0	185.6	183.7	-	-	-	71.1	[90]
666	INFCA: C ₁ A _{5/32} N _{11/32} S _{38/32} H _{42/32}	-2474.28	-2666.7	198.4	179.7	-	-	-	69.3	[90]
667	T5C ^c : C _{5/4} S _{5/4} H _{5/2}	-2516.90	-2780.3	159.9	234.1	-	-	-	79.3	[90]
668	5CA: C _{5/4} A _{1/8} S ₁ H _{13/8}	-2292.82	-2491.3	163.1	177.1	-	-	-	57.3	[90]
669	5CNA: C _{5/4} N _{1/4} A _{1/8} S ₁ H _{11/8}	-2381.81	-2568.7	195.0	176.2	-	-	-	64.5	[90]
670	T2C ^c : C _{3/2} S ₁ H _{5/2}	-2465.40	-2720.7	167.0	237.0	-	-	-	80.6	[90]
671										

672 a₀, a₁, a₂, are the empirical coefficients of the heat capacity equation: C_p^o = a₀ + a₁T + a₂T⁻²; no value = 0.

673 ^a Only CSH-II solid solution included in Cemdata'07.03 database. ^b for the ACW conditions. ^c Thermodynamic
674 properties were slightly modified relative to the T2C, T5C, and TobH end members of the downscaled CSH3T
675 thermodynamic model [11].

676

677 **CSH-II model.** This simple ideal C-S-H solid solution model [85] has been used for many years, and
678 was included (with a modified stability to better describe the changes in the calcium concentrations
679 with pH and less water to correspond to the composition of C-S-H present in cements) into Cemda-
680 ta07 database [1, 29]. The original model [85] consisted of two binary ideal solutions CSH-I and CSH-II.
681 CSH-I used end-members of amorphous silica (SH; SiO₂) and a tobermorite-like C-S-H gel phase (Tob-
682 I; (Ca(OH)₂)₂(SiO₂)_{2.4}·2H₂O). CSH-II used end-members of tobermorite-like (Tob-II;
683 (Ca(OH)₂)_{0.8333}SiO_{2.0.8333}·H₂O) and jennite-like (Jen; (Ca(OH)₂)_{1.6666}SiO₂·H₂O) C-S-H gel phases. The CSH-II
684 phase co-exists with CH (portlandite) at Ca/Si ratios above 1.5 to 1.7. The CSH-I solid solution has been
685 shown to be unrealistic ([80] and references therein) and amorphous SiO₂ co-exists with C-S-H gel of
686 Ca/Si ratios = 0.4-0.8. The water content in this C-S-H II is lower than in the other models discussed
687 below, but corresponds well to the water present in the interlayer of C-S-H as measured by ¹H-NMR
688 [78, 79]. In Cemdata18, we provide the CSH-II solid solution model only, covering the range of Ca/Si
689 ratios from 0.83 to 1.67, for backward compatibility with the Cemdata07 database and as an alternative
690 to the newer models.

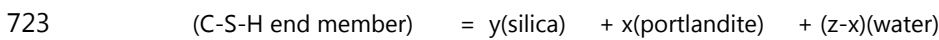
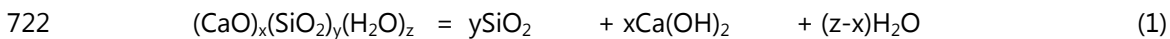
691

692 **ECSH-1 and ECSH-2 models** extend both CSH-I and CSH-II models with Na-, K- and Sr- containing
693 end members. Aimed at pragmatic description of uptake of minor cations, these provisional ideal solid
694 solution models [88] were constructed with help of the statistical dual-thermodynamic method [91]
695 based on GEM-Selektor calculations. With this method, one can retrieve both the unknown stoichiom-

696 etry and the standard molar Gibbs energy $\Delta_f G^\circ_{298}$ of ideal solid solution end members from the exper-
 697 imental bulk compositions of the aqueous solution and co-existing solid solution. In total, 13 possible
 698 end member stoichiometries with the general formula
 699 $[(\text{Ca}(\text{OH})_2)_{n_{\text{Ca}}}(\text{Sr}(\text{OH})_2)_{n_{\text{Sr}}}(\text{KOH})_{n_{\text{K}}}(\text{NaOH})_{n_{\text{Na}}}\text{SiO}_2\text{H}_2\text{O}]_{n_{\text{Si}}}$ were considered for these models. To develop
 700 these models, the n_{Ca} , n_{Sr} , ... coefficients were adjusted in order to minimize the standard deviations
 701 of estimated G°_{298} values for model end members in trial GEM calculations for a number of experi-
 702 mental data points. These trial GEM calculations employed: (1) the Nagra-PSI database [24]; (2) many
 703 experimental data points at different Ca/Si, Sr/Si, Na/Si, K/Si ratios; and (3) varying stoichiometry coef-
 704 ficients of solid solution end members within the ranges of $0.1 < n_{\text{Si}} < 2$, $0 < n_{\text{Ca}} < 1.6$, $0 < n_{\text{Sr}} < 2$, $0 < n_{\text{K}}$
 705 < 2 , and $0 < n_{\text{Na}} < 2$.

706 Followed by ‘forward GEM modelling’ of Sr uptake data in pure water and in artificial cement water
 707 (ACW), this procedure resulted in ideal ECSH-II and ECSH-I solid solution models that provided the op-
 708 timal description of data (over 96 experiments published in [92] and additional in-house Sr uptake da-
 709 ta on C-S-H in water and in ACW). $\Delta_f G^\circ_{298}$ values for Na- and K-containing end members were also fi-
 710 ne-tuned using literature data [81] on Na and K uptake isotherms in C-S-H (Figure 10). The ECSH-1
 711 and ECSH-2 models can realistically describe the uptake of cations and the decrease of (maximum)
 712 Ca/Si ratios in equilibrium with portlandite upon increasing alkali concentration in aqueous solution.
 713 However, it was not possible to use the same $\Delta_f G^\circ_{298}$ of SrSH end member to model isotherms of Sr
 714 uptake in C-S-H prepared in water and in the artificial cement pore water (ACW with pH ≈ 13.3 at 25 °C,
 715 containing 0.18 M KOH, 0.114 M NaOH and 1.2 mM $\text{Ca}(\text{OH})_2$). We believe that the $\Delta_f G^\circ_{298}(\text{SrSH})$ differ-
 716 ence (up to 3.4 kJ mol⁻¹) can probably be explained by different silica polymerization and cation ex-
 717 change capacity of C-S-H due to the presence of alkali. We anticipate that ECSH-1 and ECSH-2 will be
 718 replaced by more accurate C-S-H-K-Na models in the near future.

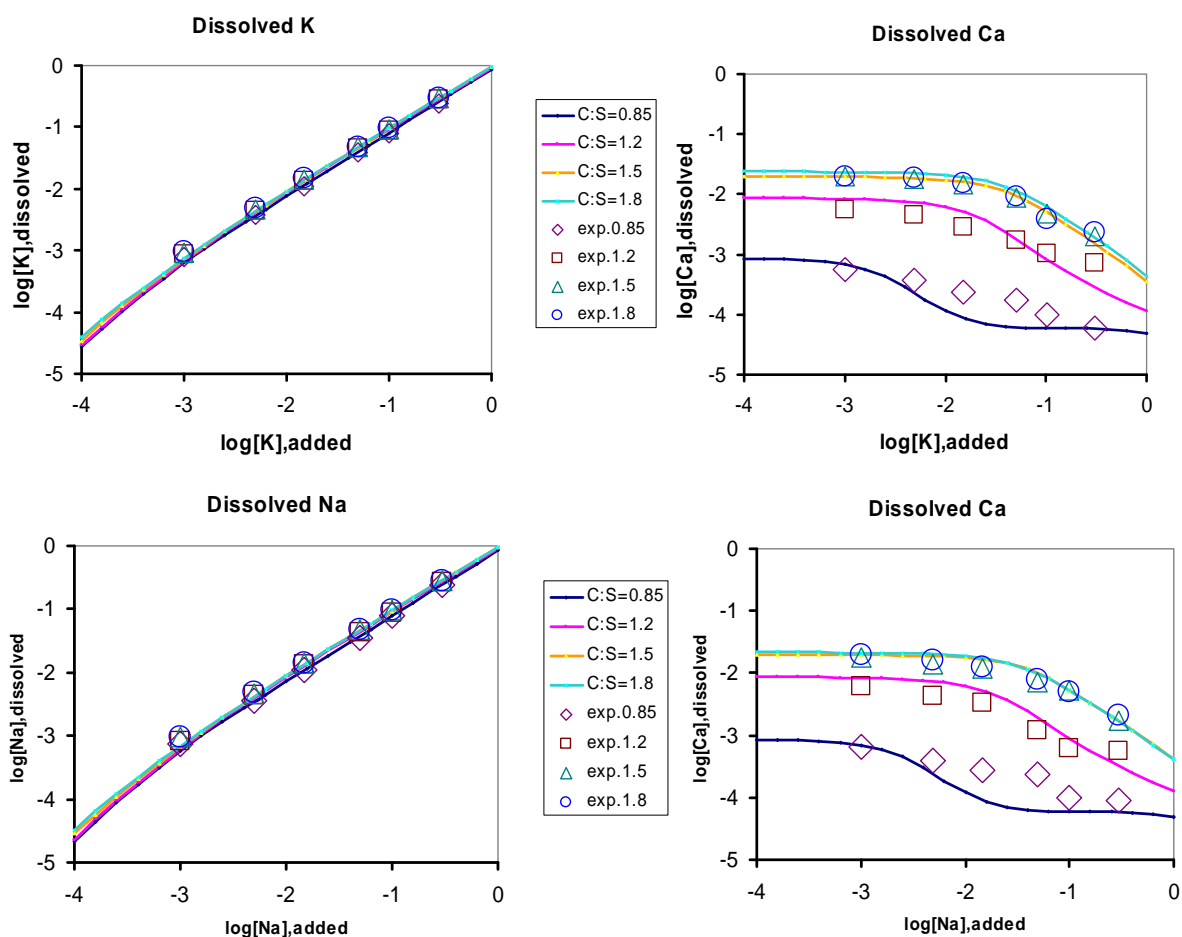
719 With no known thermodynamic properties of structural analogues available, the standard entropy and
 720 heat capacity of the ECSH end members were estimated assuming linear dependencies of entropy and
 721 heat capacity effects of reactions on the Ca/Si ratio in C-S-H [11]:



$$724 \quad \Delta_r S^\circ_{298} = y (61.054 + 5.357 x/y) \quad (2a)$$

$$725 \quad \Delta_r Cp^\circ_{298} = y (31.881 - 11.905 x/y) \quad (2b)$$

726 Using eqs (2a,b), $\Delta_r S^\circ_{298}$ and $\Delta_r Cp^\circ_{298}$ were calculated and rounded off to the nearest whole numbers.
 727 The $\Delta_r H^\circ_{298}$ values were calculated from $\log_{10} K^\circ_{298}$ and $\Delta_r S^\circ_{298}$ values together with the S° , Cp° , $\Delta_f H^\circ$ and
 728 $\Delta_f G^\circ$ values at $T_r = 298.15$ K using the ReacDC module of GEM-Selektor code and thermodynamic
 729 properties of water, portlandite and amorphous silica from the GEMS version of the PSI/Nagra 12/07
 730 TDB [22, 23] and Cemdata18 databases. The resulting thermodynamic properties (Table 4) are ex-
 731 pected to suffice for temperatures between 0 and 90 °C within 0.5 pK units uncertainty.



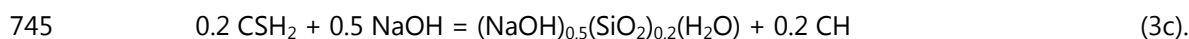
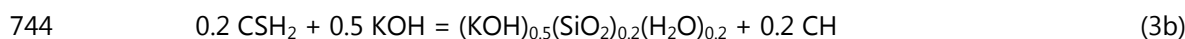
732

733

734 Figure 10: Comparison of sorption isotherms for K or Na calculated using the ECSH-II Aq-SS model
 735 (curves) with the data for K and Na sorption [81] (scattered symbols). Abscissa: \log_{10} moles of added K
 736 or Na per 1 kg H_2O ; ordinate: \log_{10} molar.

737

738 Next, the S_{298}° , Cp_{298}° and values of the SrSH, NaSH and KSH end members of ECSH phases were eval-
 739 uated. This was done by taking the properties of their reference calcium hydroxide counterpart $\text{C}_1\text{S}_1\text{H}_2$
 740 and then either subtracting or adding respective properties of solid portlandite $\text{Ca}(\text{OH})_2$, as well as
 741 solid $\text{Sr}(\text{OH})_2$, solid NaOH or solid KOH from Wagman et al. [93]. This is equivalent to assuming $\Delta_r S_{298}^\circ$
 742 = 0 and $\Delta_r Cp_{298}^\circ = 0$ for the reactions:



746 For these calculations, $\Delta_r S_{298}^\circ$, and $\Delta_r Cp_{298}^\circ$, S_{298}° , Cp_{298}° of the reference compound CSH_2 were com-
 747 puted using Eqs 1, 2a and 2b. Note that the stoichiometries of the K and Na C-S-H end members de-
 748 fined by reactions 3b and 3c correspond to $\text{N}_{0.25}\text{S}_{0.2}\text{H}_{0.45}$ or $\text{K}_{0.25}\text{S}_{0.2}\text{H}_{0.45}$, but not $\text{N}_{0.25}\text{S}_{0.2}\text{H}_{0.3}$ or
 749 $\text{K}_{0.25}\text{S}_{0.2}\text{H}_{0.3}$ as defined in Kulik et al. [88]. The respective values for $\Delta_r G_{298}^\circ$, and $\Delta_r H_{298}^\circ$ are summarised
 750 in Table 4.

751

752 **CSHQ model** [11] was developed in order to address some known shortcomings of earlier CSH-I and
753 CSH-II models [29, 85], namely insufficient connection to the C-S-H structure and the unrealistic as-
754 sumption of ideal mixing between tobermorite-like and amorphous silica end members. It was based
755 on structural data supporting the defect-tobermorite model [94-96], represented as a solid solution
756 model with four different structural sites (sublattices) [11]: $[BTI^{+2}]_1:[TU^-]_2:[CU^0]_2:[IW^0]_5$. The main as-
757 sumption was that in BTI sites, the incorporation of Ca^{2+} ion in the interlayer occurs simultaneously
758 with the removal of a bridging tetrahedron in the silica "dreierketten" chain, and this process is re-
759 versible. Excess calcium can also be incorporated as a $Ca(OH)_2$ moiety, either interstitially in the tober-
760 morite interlayer, or forming domains of jennite-like structure. This was accounted for by an exchange
761 of a vacancy with $Ca(OH)_2$ in CU sites. The occupation of TU and IW sublattices was fixed as $2CaSiO_{3.5}^-$
762 and $4H_2O+vacancy$, respectively. This led to four end members with stoichiometries depending on the
763 assumed Ca^{2+}/H^+ ratio in BTI sites.

764 This solid solution model has a correct built-in dependence of the mean silica chain length (MCL) on
765 Ca/Si ratios. By downscaling the end-member stoichiometries to Si = 1.0 and adjusting the G_{298}^0 values
766 of end members, the CSHQ model could be fine-tuned to various C-S-H solubility data sets [11]. In this
767 Cemdata18 database, two end members for K and Na (similar to those from the ECSH model) were
768 provisionally added to improve predictions of pH and composition of the PC porewater.

769 The downscaled ideal CSHQ model (Table 4) provides a reasonable fit to the variety of C-S-H solubility
770 data in the [Ca]-[Si], [Ca]-C/S and [Si]-Ca/Si spaces as discussed in more detail in [11].

771 An extension to cover the uptake of alkalis by C-S-H was based on an ideal solid solution model be-
772 tween jennite, tobermorite, $[(KOH)_{2.5}SiO_2H_2O]_{0.2}$ and $[(NaOH)_{2.5}SiO_2H_2O]_{0.2}$ as proposed by Kulik et al.
773 [88] and using the thermodynamic data reported in [89]: $\Delta_r G^\circ = -440'800$ J/mol and $-431'200$ J/mol (at
774 20°C) for $[(KOH)_{2.5}SiO_2H_2O]_{0.2}$ and $[(NaOH)_{2.5}SiO_2H_2O]_{0.2}$, respectively.

775

776 **CSH3T model** [11] was aimed at more consistency with the tobermorite-like structure of C-S-H phases
777 at $Ca/Si < 1.5$. The evidence of interlayer ordering in tobermorite-like C-S-H with $0.9 < C/S < 1.25$ [96]
778 has led to setting the CU sites always vacant, and to splitting the BTI sublattice into two
779 $([BTI1^+]_1:[BTI2^+]_1:[TU^-]_2:[IW^0]_4)$ with substitutions of $Si_{0.5}OH^+$ by $HO_{0.5}Ca_{0.5}^+$. This yielded a solid solution
780 model with end members TobH ($C_2S_3H_5$), T5C ($C_{2.5}S_{2.5}H_5$), T2C ($C_3S_2H_5$), connected by an ordering reac-
781 tion $\frac{1}{2}TobH + \frac{1}{2}T2C = T5C$. The model has a built-in dependence of the mean chain length on the
782 composition, consistent with measured values [95] for the co-precipitated tobermorite-like C-S-H. The
783 CSH3T model [11] in its downscaled form (Table 4) can be computed just using a simple ideal mixing
784 model. The CSH3T model has been later extended with U(VI) end members [97] and with Al and Na
785 end members [90]. The ideal CSH3T SS model [11] produces quite realistic curves for solubility of the
786 synthetic C-S-H co-precipitation (double decomposition) data. More accurate C-S-H multi-site solid
787 solution models are in development.

788

789 **CNASH_ss model** [90] includes Al and Na and represents an extension of the CSH3T model that was
790 optimised for alkali activated systems. The calcium (alkali) aluminosilicate hydrate (C-(N-)A-S-H) gel-
791 like phase that precipitates in alkali-activated cements contains significantly less Ca, more Al and alkali

792 and has a more densely packed structure than the C-(A-)S-H which forms in hydrated PC-based mate-
793 rials [98, 99]. However, both phases are based on the same defect-tobermorite structure. In alkali-
794 activated slag cements (an exemplary 'high-Ca' alkali-activated material [100]), the C-(N-)A-S-H phase
795 typically has a $\text{Ca/Si} \approx 1$ and an $\text{Al/Si} \leq 0.25$ [90].

796 Many solubility and chemical composition data for the C-(N-)A-S-H system have been published.
797 Much of this data was used to develop an ideal solid solution thermodynamic model (CNASH_{ss}), in-
798 cluding configurational entropy terms, which explicitly includes mixing of Al and Na [90]. The
799 CNASH_{ss} model enables Al incorporation into C-(N-)A-S-H gel to be explicitly considered in thermo-
800 dynamic modelling simulations. The CNASH_{ss} model has been applied to simulate phase assemblag-
801 es in NaOH, sodium silicate, Na_2CO_3 , and Na_2SO_4 -activated slag systems [74, 101]. This model is also
802 applicable to thermodynamic modelling of PC-based materials; however, it less closely represents the
803 full body of available solubility data for the C-S-H phase [102] at $\text{Ca/Si} > \sim 1.3$ than other C-S-H ther-
804 modynamic models, e.g. [11, 80]. CNASH_{ss} closely represents the full set of solubility data for the C-
805 (N-)A-S-H gel phase down to $\text{Ca/Si} = 0.67$. Therefore, we recommend using CNASH_{ss} for alkali acti-
806 vated systems rather than hydrated PC systems, where we recommend the use of CSHQ or C-S-H-II.

807 Additional solubility data for C-(N-)A-S-H gel not used to validate CNASH_{ss} were recently published,
808 including for C-(N-)A-S-H gels at synthesis temperatures of 7°C, 50°C and 80°C [103, 104] and using K
809 rather than Na [84, 105]. Future refinement to the CNASH_{ss} thermodynamic model should include
810 these data and formally extend the model to different temperatures and alkali type.

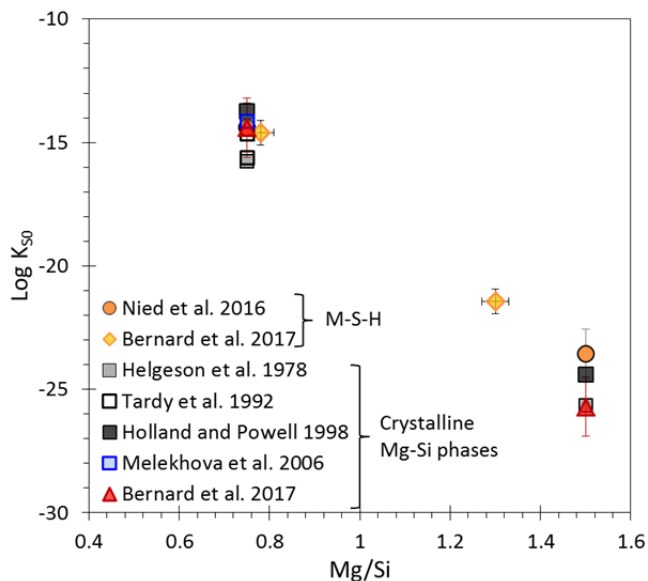
811 During the last 20 years, ideal solid solution models of C-S-H have evolved starting from simple ideal
812 solid solutions using full end-member mixing up to recent truly multi-site mixing models consistent
813 with both solubility data and structural/spectroscopic data. Because end members in multi-site solid
814 solutions are constructed of moieties substituting each other on different sublattices, such models
815 have the best potential for: (1) extension by adding moieties for other elements of interest (e.g. K, Na,
816 Al, U, Sr) in their respective sites; (2) generating all possible end members; and (3) parameterizing end
817 members based on available solubility, element uptake, and spectroscopic data (e.g. using the
818 GEMSFITS code [106]) and are the subjects of ongoing research.

819 For the calcium silicate hydrate complexes, $\text{CaH}_3\text{SiO}_4^+$ ($\text{CaHSiO}_3^+ + 2\text{H}_2\text{O}$) and $\text{CaH}_2\text{SiO}_4^0$ (CaSiO_3^0
820 $+ 2\text{H}_2\text{O}$), the reported complex formation data show a significant scatter. In particular, complex
821 formation constants for $\text{CaH}_2\text{SiO}_4^0$ vary by more than one log unit. While the PSI/Nagra TDB [22, 23]
822 reports a complex formation constant of $10^{4.6}$ for the reaction $\text{Ca}^{2+} + \text{SiO}_3^{2-} \rightarrow \text{CaSiO}_3^0$ (see Table 2),
823 which has a large effect on the silicon concentrations in presence of C-S-H at $\text{Ca/Si} > 1$ [80], no such
824 constant is defined in the PHREEQC database [18]. Walker et al. [80] recommended to use a constant
825 of $10^{4.0}$, making the complex less important, while recently an even lower complex formation constant
826 of $10^{2.9}$ has been derived based on titration experiments [107]. This large scatter of data results in very
827 diverging assessment of the importance of the CaSiO_3^0 complex at $\text{Ca/Si} > 1$ and has a significant
828 impact on the C-S-H solubility as this complex accounts for about 90% of aqueous dissolved silicon in
829 equilibrium with both C-S-H and portlandite. Dedicated investigations not only of calcium silicate
830 hydrate complexes but also of other possible complexes between aluminum, calcium and silicate at
831 high pH values are urgently needed.

832

833 2.8 Magnesium silicate hydrates

834 The formation of magnesium silicates hydrate (M-S-H) has been observed at the interfacial zone of
835 cement paste with clays [67, 108, 109] and/or as secondary products from the degradation of cement
836 pastes by groundwater or seawater [110-112]. The combination of leaching and carbonation of the
837 cement paste decreases pH at the surface of the cement, decalcifies C-S-H and leads the formation of
838 a Mg-enriched phase, M-S-H. M-S-H phases are poorly ordered but have a layered structure with
839 tetrahedral silica arranged in sheets similar to clay minerals, have variable Mg/Si from ≈ 0.8 to Mg/Si
840 ≈ 1.2 and are stable at pH values between 7.5 to 11.5 [40, 113-115]. Given the difference in structure
841 and pH domains, most studies [114-117] observed the precipitation of distinct C-S-H and M-S-H
842 phases and not of a mixed magnesium calcium silicate hydrate phase. Solubility measurements [40,
843 113, 118] indicated an only slightly higher solubility of the poorly ordered M-S-H in comparison to
844 crystalline magnesium-silicates such as talc, antigorite or chrysotile as shown in Figure 11. The ideal
845 solid solution model for M-S-H published by Nied et al. [40] has been selected for the present version
846 of the database. As several groups [113, 114, 118] are currently working on thermodynamic data for
847 M-S-H, we expect that more sophisticated models will be published in the coming years.



848

849 Figure 11: Evolution of the solubility product (K_{s0}) of magnesium silicate hydrates at room temperature
850 as a function of the total Mg/Si; referring to reactions using Mg^{2+} , SiO_2 and H_2O as indicated in Table
851 2. Adapted from [118].

852

853 2.9 Zeolites

854 Interactions of highly alkaline solutions in hydrated PC systems with service environments will likely
855 result in the partial dissolution of aluminosilicate minerals from adjacent rocks and the formation of
856 secondary zeolite minerals [119] in the context of deep underground nuclear waste repositories.

857 Zeolite formation also occurs in alkali activated cement systems. These zeolites are often related to the
858 poorly crystalline N-A-S-H (sodium-aluminium-silicate-hydrate) and K-A-S-H (potassium-aluminium-
859 silicate-hydrate) gels that form in these systems [74, 103]; the type of gel formed depends on the
860 presence of Na^+ or K^+ , cation concentrations, the relative degree of saturation of the liquid phase with
861 respect to silica, pH and temperature [120]. Several papers in recent years estimated solubility data for
862 different zeolites, based mainly on heat capacity and enthalpy measurements [47, 74, 121]. This may
863 lead to considerable bias in the estimated solubility data in the range of several log units due to
864 uncertainties associated with the measurements of enthalpy data. The determination of solubility data
865 for zeolites has been hindered by variability in cation composition (Ca, Na, K), Al/Si ratios, H_2O
866 contents and atomic structure, and also their slow reaction kinetics.

867 In 2017, two independent studies [41, 103] reported very similar solubility products for zeolite Y and X
868 (or for N-A-S-H gel with Al/Si = 0.5 and Al/Si = 0.8) based on experimental data. The data for zeolite
869 X(Na), zeolite Y(Na) and chabazite [41] make it possible to predict zeolite formation in sodium
870 activated cements; data for potassium-based zeolites are still missing in the Cemdata18 database. Also
871 data for natrolite and zeolite P(Ca) have been included [41]. In experiments with high pH values their
872 formation was kinetically hindered (although natrolite and zeolite P(Ca) were more stable than zeolite
873 X(Na), zeolite Y(Na) and chabazite). Thus we recommend that natrolite and zeolite P(Ca) should be
874 considered in modelling the interface between cement and adjacent rocks. However, their formation
875 may be suppressed in models for alkali activated systems, where zeolite X(Na), zeolite Y(Na) and
876 chabazite or their amorphous or nanocrystalline precursors are formed [122].

877

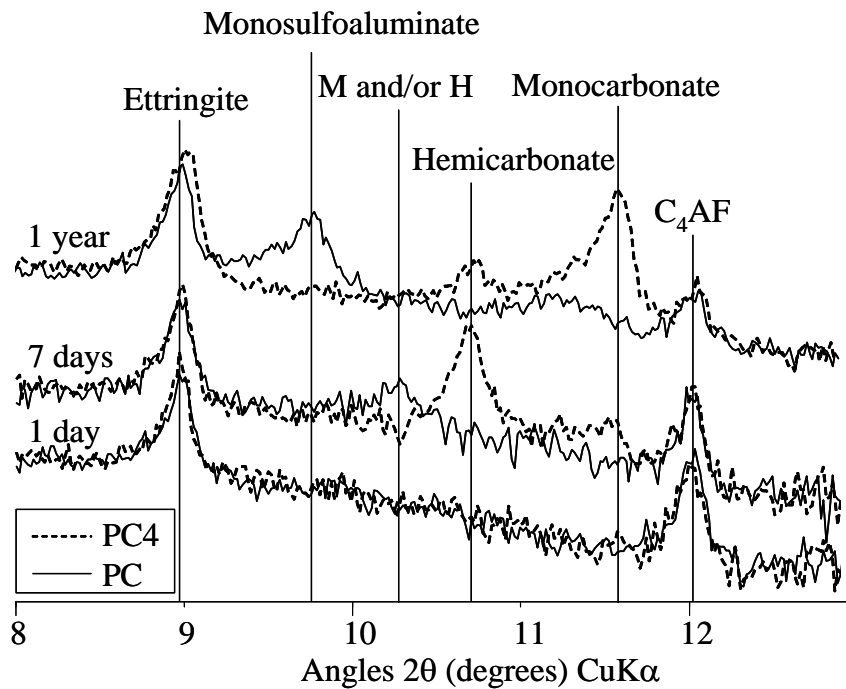
878 **3 Comparison Cemdata07 with Cemdata18**

879 The updates since the first cemdata version, cemdata07 (published in 2008), are significant. In
880 particular, the distribution of iron and aluminium, the volume and Ca/Si in C-S-H as well as the alkali
881 concentrations in the pore solution in PC can significantly affect thermodynamic modelling results. To
882 illustrate these differences, the effect of limestone on the same PC was calculated with Cemdata07 and
883 Cemdata18 and compared below. The effect of relative humidity on calculated hydrates is used below
884 as a second example. These comparisons concentrate on PC, as compiled specific data for alkali
885 activated materials are only now available (in this paper).

886 **3.1 Effect of limestone on solid and liquid phase composition**

887 The influence of limestone on cement hydration has been widely studied and was the subject of
888 several publications by the authors [2, 20, 123]. Experimental investigations showed that the presence
889 of calcium carbonate prevents the destabilisation of ettringite to monosulfate at long hydrations times
890 and stabilises monocarbonate together with ettringite (see e.g. [123-125] and Figure 12).

891



892
893

894 Figure 12: Experimentally observed phase assemblage in a PC without additional limestone (PC) and
895 with 4 wt.% of limestone (PC4); reproduced from [123].

896

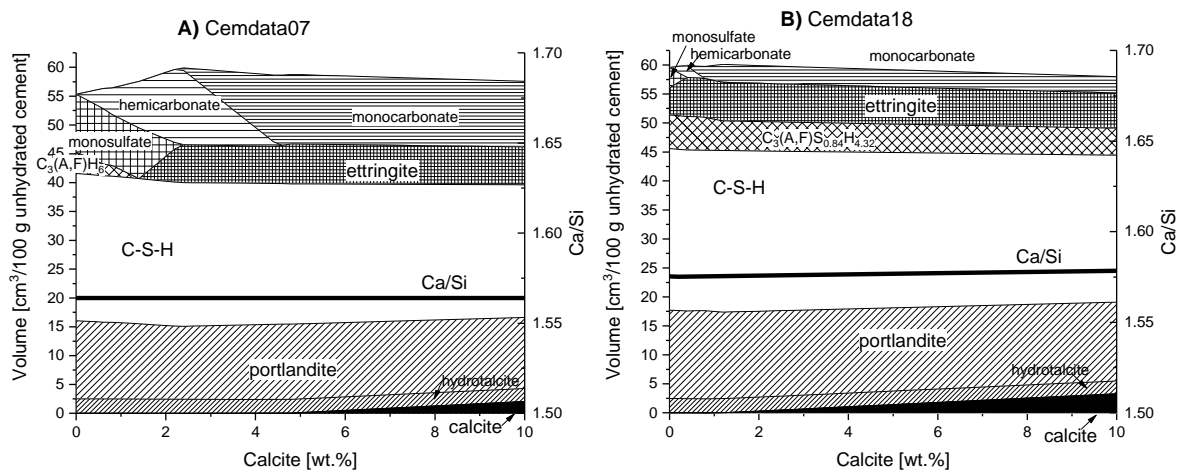
897 Also thermodynamic modelling [2, 20, 123] (mainly using the Cemdata2007 database) showed that the
898 presence of small amounts of limestone significantly impacted the mineralogy of hydrated cements. In
899 the absence of any limestone no ettringite but only monosulfate as well as of a small amount of
900 katoite ($C_3(A,F)H_6$) was predicted as shown in Figure 13A. The presence of a small amount of limestone
901 was calculated to stabilise hemicarbonate and at higher dosages monocarbonate plus ettringite,
902 resulting in an increase of the total volume. The higher volume in the presence of a small amount of
903 limestone due to the stabilization of ettringite has been found to have a positive effect on the
904 mechanical properties of PC and blended cements [20, 124].

905 The stability of siliceous hydrogarnet was a matter of debate during the development of Cemdata07
906 and in most calculations with Cemdata07 the formation of siliceous hydrogarnet $C_3AS_{0.8}H_{4.4}$ had been
907 suppressed assuming kinetic hindrance. Based on the data compiled in Cemdata07, which originated
908 from measurements from [7, 72, 126], ettringite and siliceous hydrogarnet were calculated to be
909 significantly more stable than monosulfate, hemi- or monocarboaluminate thus theoretically
910 preventing their presence. Since monosulfate, hemi- and monocarboaluminate are experimentally
911 observed in hydrated PC, it was assumed that this was due to a kinetic hindrance in the formation of
912 siliceous hydrogarnet and that possibly a later conversion of hemi- and monocarboaluminate to
913 siliceous hydrogarnet could occur.

914

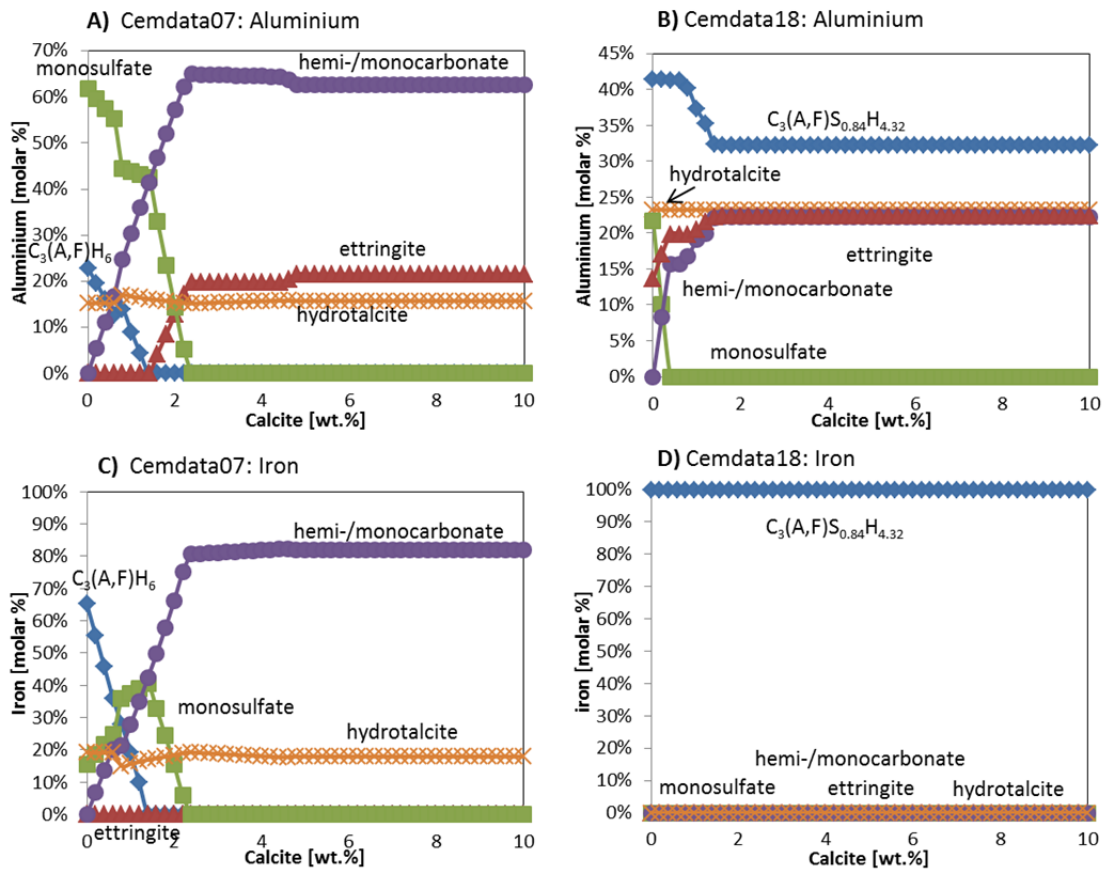
915 The new data for $(C_3A_{0.5}F_{0.5}S_{0.84}H_{4.32})$ by Dilnesa et al. [9], included in Cemdata18, suggest that mixed
916 Al- and Fe-containing siliceous hydrogarnet can coexist with monosulfate, hemi- and
917 monocarboaluminate at ambient conditions, which is in better agreement with the observed

918 experimental data presented in Figure 12 and elsewhere [123-125]. Figure 13B displays the predicted
 919 phase assemblage of a hydrated PC with limestone using Cemdata18 as given in Table 1- Table 4; em-
 920 ploying CSHQ and M_4AH_{10} . The formation of hemi- and monocarboaluminate accompanied by a stabi-
 921 lisation of ettringite instead of monosulfoaluminate was correctly predicted by both datasets. As
 922 shown in Figure 13 the biggest difference between the two datasets is the prediction of a katoite-type
 923 siliceous hydrogarnet phase ($C_3A_{0.5}F_{0.5}S_{0.84}H_{4.32}$), modelled as solid solution with a varying alumina and
 924 iron by using Cemdata18, together with hemi- and monocarboaluminate and ettringite throughout the
 925 modelled composition range independently of the $CaCO_3$ content.
 926



927
 928 Figure 13: Comparison of calculated solid phase assemblage using A) Cemdata07 and B) Cemdata18
 929 assuming complete hydration of PC using the composition reported in [123].

930
 931 The consideration of the siliceous hydrogarnet solid solution in Cemdata18 led to a quite significant
 932 redistribution of alumina and iron within the phase assemblage. Whereas with Cemdata07 around 70%
 933 of the available alumina was bound in AFm phases (see Figure 14A) the predictions based on Cemda-
 934 ta18 suggest that only about 25% of alumina is bound in AFm phases and ~30% in the hydrogarnet
 935 phase (Figure 14B). For iron, the difference is even more drastic. The predictions with Cemdata18 sug-
 936 gest that close to 100% of the iron is bound by the siliceous hydrogarnet solid solution (Figure 14D)
 937 which is also in agreement with experimental observations [64-66], where predominantly the formation
 938 of mixed aluminum and iron containing hydrogarnet phases in close proximity to the original ferrite
 939 phases was observed in hydrated cements.



940

941

942 Figure 14: Effect of the amount of limestone on the phase assemblage and the distribution of
 943 aluminium and iron in hydrated PC calculated using Cemdata07 (A, C) and Cemdata18 (B, D).

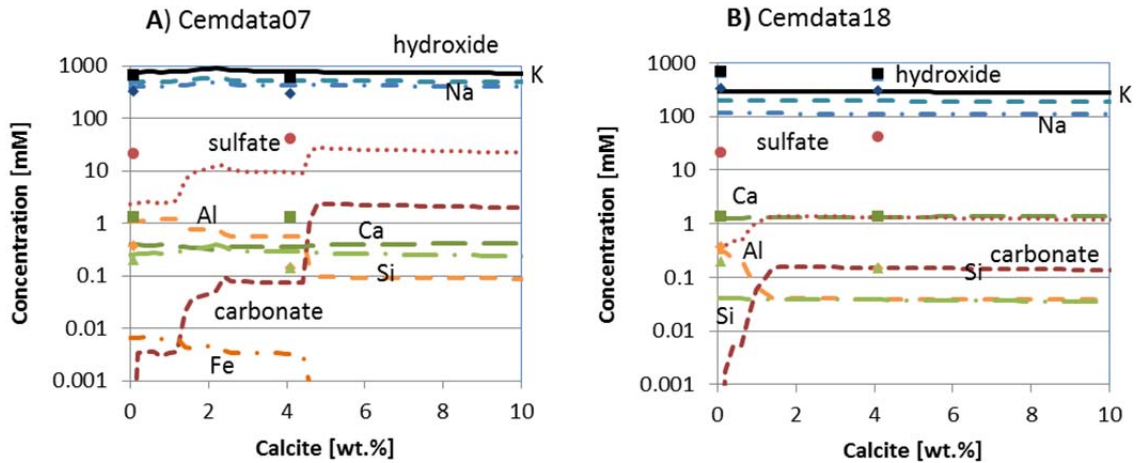
944

945 The binding of alkalis in C-S-H lowers the alkali and hydroxide concentrations [81, 84, 88] in the pore
 946 solution of hydrated PC and thus the pH values from above 14 to ~13 to 13.5 [1, 29, 123, 127]. The
 947 disregard of alkali binding by C-S-H would result in very high predicted pH values of 14 and above,
 948 which does not agree with measurements of the pore solution composition [5, 29]. As in 2007 no
 949 thermodynamic models to describe the uptake of alkali in C-S-H were available, distribution
 950 coefficients (K_d values) were used together with Cemdata07 in most calculations of hydrated cements
 951 as described in details e.g. in [1, 29, 123]. The use of distribution coefficient allowed predicting the
 952 alkali concentrations in PC relatively well as shown in Figure 15A, but the approach was not adequate
 953 to predict alkali uptake in low Ca/Si C-S-H present in blended cements. K_d values do not account for
 954 competitive sorption on specific sites as would be expected for the C-S-H gel, and also tend to be
 955 experiment-specific and so cannot generally be applied to other systems under different conditions. In
 956 the Cemdata18, the uptake of alkalis by C-S-H is modelled by introducing additional Na- and K-
 957 endmembers ($[(NaOH)_{2.5}SiO_2H_2O]_{0.2}$ and $[(KOH)_{2.5}SiO_2H_2O]_{0.2}$) in the CSHQ model, as described above
 958 (section 2.7). The introduction of these provisional data simplify the modelling, as no additional K_d
 959 values have to be introduced in the models, and allows the calculation of alkali uptake over the whole
 960 range of Ca/Si ratios, although the agreement between measured and calculated alkali concentrations
 961 is only satisfactorily, as shown in Figure 15B. Due to the lack of appropriate models for sodium and po-

962 tassium uptake in C-S-H valid over the complete range of Ca/Si, the modelling of alkali and hydroxide
963 concentrations in the pore solution remains a challenge.

964 The trends in the concentrations of calcium, sulfate, silicon and aluminium are generally correctly
965 reproduced by both models (see e.g. [1, 29, 123, 127], Figure 15) although there are differences be-
966 tween measured and calculated values, in particular for Ca and Al for Cemdata07 and for sulfate and
967 silicon for Cemdata18.

968



969

970 Figure 15: Effect of the amount of limestone on the phase assemblage and the distribution of
971 aluminium and iron in hydrated PC calculated using A) Cemdata07 and B) Cemdata18.

972

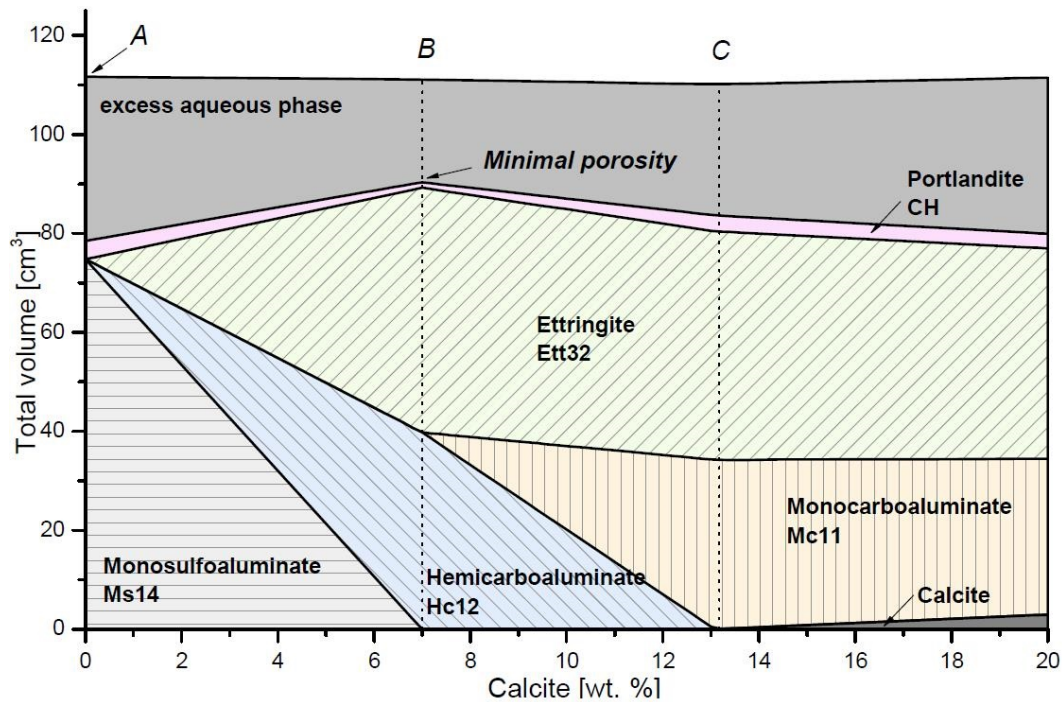
973

974 3.2 Effect of relative humidity on hydrated cements

975 Using the thermodynamic properties of phases with different water contents described in Section 2.5
976 and Table 1 it was possible to predict the drying behaviour of hydrated systems.

977 Drying of the $\text{CaO-Al}_2\text{O}_3\text{-SO}_3\text{-CO}_2\text{-H}_2\text{O}$ was simulated because it is directly relevant to PC and
978 limestone blended cements. The initial model mixture contained C_3A , portlandite (CH), calcium sulfate
979 ($\text{SO}_3/\text{Al}_2\text{O}_3=1$ molar bulk ratio), and varying amounts of calcite at 25°C. The amount of solids was kept
980 constant at 100 g and reacted with 90 g water. A diagram of the specific volume changes of the
981 hydrated mixture with respect to calcite content is shown in Figure 16.

982



983

984 Figure 16 Calculated specific volume changes of a hydrated model mixture consisting of C_3A ,
 985 portlandite and with fixed sulfate ratio ($SO_3/Al_2O_3=1$, molar bulk ratio) in dependence of changing
 986 calcite content at 25°C.

987

988 Due to their differing AFm-AFt mineralogy hydrate phase assemblages A, B and C in Figure 16, with
 989 0%, 7% and 13.2% of calcite respectively, were selected as initial hydrated systems for the drying
 990 modeling. Drying was simulated by continuously removing water from the assemblages until a RH of
 991 zero was reached. The investigated systems were:

992

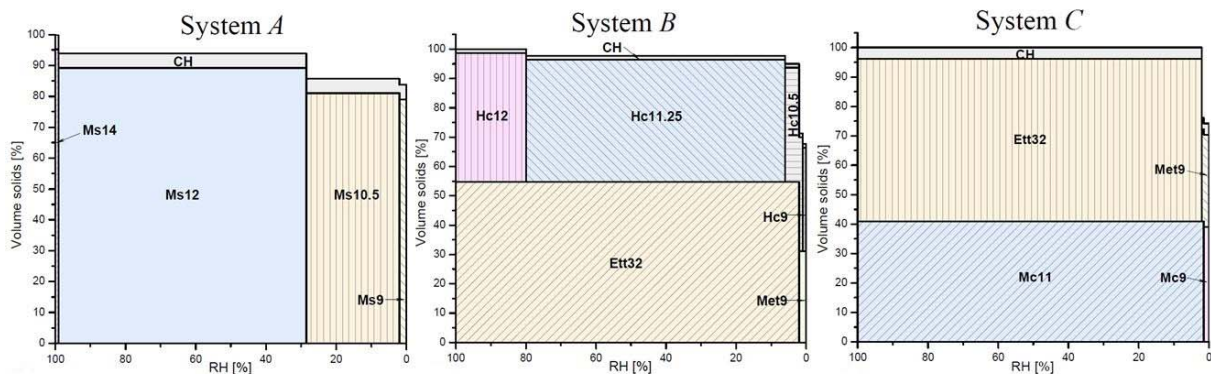
- System A: monosulfoaluminate (Ms14) and portlandite (CH)
- System B: ettringite (Ett32), hemicarboaluminate (Hc12) and portlandite (CH)
- System C: ettringite (Ett32), monocarboaluminate (Mc11) and portlandite (CH)

995

996 Figure 17 a, b and c present the evolution of specific solid volume as a function of RH. We can see that
 997 dehydration happens stepwise at critical RH stability limits of the phase assemblages, representing
 998 invariant points where the RH is fixed due to phase rule restrictions. At this critical RH two hydration
 999 states of the same cement hydrate coexist and buffer the humidity in a similar manner as conventional
 1000 drying agents. Another important finding is that the addition of calcite and the formation of
 1001 carboaluminates and ettringite will enhance the dimensional stability of hydrated cement paste and
 1002 makes it less sensitive to humidity fluctuations, which appears to be relevant for limestone blended
 1003 cements. Due to the presence of monocarboaluminate and ettringite system C is the most stable
 1004 phase assemblage, which only decomposes at very low humidities (below 2% RH) whereas
 1005 monosulfoaluminate quickly loses part of its interlayer water at <99% RH.

1006

1007 Something important to keep in mind is that, although experimentally we observe the changes shown
 1008 in Figure 17, several of these dehydration processes are metastable with respect to other phase as-
 1009 semblages. This has to be considered when predicting the drying behaviour of cementitious systems.



1010
 1011 Figure 17: Calculated specific volume changes of a hydrated model mixture consisting of C_3A ,
 1012 portlandite and with fixed sulfate ratio ($SO_3/Al_2O_3=1$, molar bulk ratio) in dependence of changing
 1013 calcite content at 25°C. , as shown in Figure 16 for the Systems A, B and C.

1014
 1015
 1016

1017 4 Conclusions

1018 The Cemdata18 database summarised in this paper can reliably calculate the type, composition,
 1019 amount and volume of hydrates formed and the pH and composition of the pore solution during
 1020 hydration and degradation of cementitious systems. The Cemdata18 database, as compiled in Table 1
 1021 to Table 4, includes carefully selected thermodynamic data published in the literature based on critical
 1022 reviews supplemented with new experimental data. Data for solids commonly encountered in cement
 1023 systems in the temperature range 0-100°C, including C-S-H, M-S-H, hydrogarnet, hydrocalcite-like
 1024 phases, some zeolite, AFm and AFt phases and their respective solid solutions has been compiled. The
 1025 Cemdata18 database is an update of the Cemdata07 and Cemdata14 databases, and is compatible
 1026 with the GEMS version of the PSI/Nagra 12/07 TDB [22, 23]. Cemdata18 TDB is freely downloadable
 1027 (<http://www.empa.ch/cemdata>) in formats supporting the computer programs GEM-Selektor [13, 14]
 1028 and PHREEQC [18]. Further details are available in Appendix A and B.

1029

1030 The most important additions to the Cemdata18 TDB include:

- 1031 • C-S-H:
 - 1032 ○ CSHQ model for Portland and blended cements, the uptake of alkalis by C-S-H is
 - 1033 modelled by additional Na- and K-containing end members
 - 1034 ○ CSH3T model that corresponds to pure defect-tobermorite structure with ordering at
 - 1035 Ca/Si ratio close to 1.0, and forms the basis for CNASH-ss model

- 1036 o C-(N-)A-S-H model for alkali activated materials (CNASH-ss), which calculates the uptake
- 1037 of aluminium and sodium in low Ca/Si C-S-H
- 1038 • iron-containing hydrates, in particular for the mixed Fe-Al-hydrogarnet solid solution, $C_3FS_{0.84}H_{4.32}$ -
- 1039 $C_3A_{0.5}F_{0.5}S_{0.84}H_{4.32}$, which takes up iron and a part of the aluminium in hydrated cements
- 1040 • AFm and AFt-phases with different water contents to describe the effect of water activity and
- 1041 drying on hydrates
- 1042 • amorphous, microcrystalline AH_3 and for gibbsite to study the effect of AH_3 solubility on the
- 1043 hydrates in calcium aluminate and calcium sulfoaluminate cements
- 1044 • chloride, nitrate and nitrate-containing AFm phases
- 1045 • thaumasite and for the uptake of carbonates in SO_4 -ettringite.
- 1046 • description of the variation in Mg/Al in layered double hydroxides (hydrotalcite-like phases)
- 1047 observed in alkali activated materials
- 1048 • data for M-S-H and some Na- and Ca-based zeolites, which can form at the interaction zone of
- 1049 cement with clays, rocks or seawater and in alkali activated materials.

1050 These additions improve the reliability of thermodynamic modelling of cement systems, in particular
 1051 for alkali activated materials and for processes at cement/environment interfaces, where hydrates such
 1052 as thaumasite, Friedel's salt, M-S-H, and zeolites may form.

1053 The consideration of siliceous hydrogarnet solid solution in Cemdata18 leads to a quite significant
 1054 redistribution of alumina and iron within the phase assemblage in PC; the predictions based on
 1055 Cemdata18 suggest that alumina is bound not only in AFt, AFm phases and hydrotalcite but also in
 1056 siliceous hydrogarnet phase while all hydrated iron is present in siliceous hydrogarnet.

1057

1058 Several C-S-H solubility models as well two models for hydroxide-hydrotalcite are available (Table 4,
 1059 Appendix A and B). The CSHQ and the OH-hydrotalcite with Mg/Al = 2 are well adapted for PC
 1060 systems. Although CSHQ is able to describe the entire range of Ca/Si ratios encountered, it is best
 1061 used for high Ca/Si C-S-H as it lacks the ability to predict aluminium uptake, however, this is less
 1062 important in PC where the aluminium content is relatively low. For alkali activated binders, the CNASH
 1063 model has been developed for C-S-H type calcium (alkali) aluminosilicate hydrate gels with lower
 1064 calcium but higher aluminium and alkali content. An Mg-Al layered double hydroxide model with
 1065 variable Mg/Al ratio is also available for use in alkali activated cement systems.

1066

1067 Despite significant additions to the Cemdata18 TDB, several important gaps still exist in the database.
 1068 In particular, reliable thermodynamic data for alkali, aluminium and water uptake in C-S-H applicable
 1069 to high and low Ca/Si C-S-H and M-S-H, data for hydrotalcite-like phases of variable composition and
 1070 for different interlayer ions, data for further zeolites derived from experimental solubility
 1071 measurements, data for aqueous complexes which possibly form at high pH values as well as data for
 1072 the reaction products of alkali silica reaction are needed. However, these data gaps should be viewed
 1073 as possible future improvements rather than barriers to use thermodynamic modelling: Cemdata18
 1074 database has already been successfully applied to model hydrated PC, calcium aluminate, calcium
 1075 sulfoaluminate and blended cements, and also alkali activated materials. Cemdata18, therefore,

1076 enables improved characterisation and understanding of the chemistry and related in-service perfor-
1077 mance properties of a wide range of cement systems, including the most common types.

1078

1079 **Acknowledgements**

1080 The partial financial support from the NANOCEM consortium (www.nanocem.org), the Swiss National
1081 Foundation (SNF grants No. 117605, 132559, 130419 and 200021_169014), from Nagra, Wettingen,
1082 Switzerland, and from the BMBF ThermAc3 Verbundprojekt (Germany) are gratefully acknowledged.

1083 The authors thank also Tres Thoenen, Ravi Patel and Andres Idiart for their support on the PHREEQC
1084 version.

1085

1086

1087 **References**

- 1088 [1] B. Lothenbach, T. Matschei, G. Möschner, F.P. Glasser, Thermodynamic modelling of the effect of
 1089 temperature on the hydration and porosity of Portland cement, *Cem Concr Res*, 38 (2008) 1-18.
- 1090 [2] T. Matschei, B. Lothenbach, F.P. Glasser, The role of calcium carbonate in cement hydration, *Cem*
 1091 *Concr Res*, 37 (2007) 551-558.
- 1092 [3] M. Moesgaard, D. Herfort, M. Steenberg, L.F. Kirkegaard, Y. Yue, Physical performance of blended
 1093 cements containing calcium aluminosilicate glass powder and limestone, *Cem Concr Res*, 41 (2011)
 1094 359-364.
- 1095 [4] T. Matschei, F.P. Glasser, Temperature dependence, 0 to 40 °C, of the mineralogy of Portland
 1096 cement paste in the presence of calcium carbonate, *Cem Concr Res*, 40 (2010) 763-777.
- 1097 [5] B. Lothenbach, F. Winnefeld, C. Alder, E. Wieland, P. Lunk, Effect of temperature on the pore
 1098 solution, microstructure and hydration products of Portland cement pastes, *Cem Concr Res*, 37 (2007)
 1099 483-491.
- 1100 [6] F. Deschner, B. Lothenbach, F. Winnefeld, J. Neubauer, Effect of temperature on the hydration
 1101 Portland cement blended with siliceous fly ash, *Cem Concr Res*, 52 (2013) 169-181.
- 1102 [7] T. Matschei, B. Lothenbach, F.P. Glasser, Thermodynamic properties of Portland cement hydrates in
 1103 the system $\text{CaO-Al}_2\text{O}_3\text{-SiO}_2\text{-CaSO}_4\text{-CaCO}_3\text{-H}_2\text{O}$, *Cem Concr Res*, 37 (2007) 1379-1410.
- 1104 [8] B.Z. Dilnesa, B. Lothenbach, G. Le Saout, G. Renaudin, A. Mesbah, Y. Filinchuk, A. Wichser, E.
 1105 Wieland, Iron in carbonate containing AFm phases, *Cem Concr Res*, 41 (2011) 311-323.
- 1106 [9] B.Z. Dilnesa, B. Lothenbach, G. Renaudin, A. Wichser, D. Kulik, Synthesis and characterization of
 1107 hydrogarnet $\text{Ca}_3(\text{Al}_x\text{Fe}_{1-x})_2(\text{SiO}_4)_y(\text{OH})_{4(3-y)}$, *Cem Concr Res*, 59 (2014) 96-111.
- 1108 [10] B.Z. Dilnesa, B. Lothenbach, G. Renaudin, A. Wichser, E. Wieland, Stability of monosulfate in the
 1109 presence of iron, *J Am Ceram Soc*, 95 (2012) 3305-3316.
- 1110 [11] D.A. Kulik, Improving the structural consistency of C-S-H solid solution thermodynamic models,
 1111 *Cem Concr Res*, 41 (2011) 477-495.
- 1112 [12] B. Lothenbach, L. Pelletier-Chaignat, F. Winnefeld, Stability in the system $\text{CaO-Al}_2\text{O}_3\text{-H}_2\text{O}$, *Cem*
 1113 *Concr Res*, 42 (2012) 1621-1634.
- 1114 [13] D. Kulik, T. Wagner, S. Dmytrieva, G. Kosakowski, F. Hingerl, K. Chudnenko, U. Berner, GEM-
 1115 Selektor geochemical modeling package: revised algorithm and GEMS3K numerical kernel for coupled
 1116 simulation codes, *Computational Geosciences*, 17 (2013) 1-24.
- 1117 [14] T. Wagner, D.A. Kulik, F.F. Hingerl, S.V. Dmytrieva, GEM-Selektor geochemical modeling package:
 1118 TSolMod library and data interface for multicomponent phase models, *Canadian Mineralogist*, 50
 1119 (2012) 1173-1195.
- 1120 [15] P. Blanc, X. Bourbon, A. Lassin, E. Gaucher, Chemical model for cement-based materials:
 1121 Temperature dependence of thermodynamic functions for nanocrystalline and crystalline C-S-H
 1122 phases, *Cem Concr Res*, 40 (2010) 851-866.
- 1123 [16] P. Blanc, X. Bourbon, A. Lassin, E. Gaucher, Chemical model for cement-based materials:
 1124 Thermodynamic data assessment for phases other than CSH, *Cem Concr Res*, 40 (2010) 1360-1374.
- 1125 [17] C.M. Bethke, *Geochemical and Biogeochemical Reaction Modeling*, (2nd Ed.), Cambridge
 1126 University Press, New York, NY, USA, 2008.
- 1127 [18] D.J. Parkhurst, C.A.J. Appelo, Description of input and examples for PHREEQC version 3 - A
 1128 computer program for speciation, batch-reaction, one-dimensional transport, and inverse geochemical
 1129 calculations, 6, USGS, Denver, CO, USA., 2013.
- 1130 [19] J.E. Cross, F.T. Ewart, HATCHES - A thermodynamic database and management system, *Radiochim*
 1131 *Acta*, 52/53 (1991) 421-422.
- 1132 [20] D. Damidot, B. Lothenbach, D. Herfort, F.P. Glasser, Thermodynamics and cement science, *Cem*
 1133 *Concr Res*, 41 (2011) 679-695.

- 1134 [21] G. Möschner, B. Lothenbach, J. Rose, A. Ulrich, R. Figi, R. Kretzschmar, Solubility of Fe-ettringite
1135 ($\text{Ca}_6[\text{Fe}(\text{OH})_6]_2(\text{SO}_4)_3 \cdot 26\text{H}_2\text{O}$), *Geochim Cosmochim Acta*, 72 (2008) 1-18.
- 1136 [22] T. Thoenen, W. Hummel, U. Berner, E. Curti, The PSI/Nagra Chemical Thermodynamic Data Base
1137 12/07, PSI report 14-04, Villigen PSI, Switzerland, 2014.
- 1138 [23] T. Thoenen, D.A. Kulik, Nagra/PSI Chemical Thermodynamic Data Base 01/01 for the GEM-Selektor
1139 (V.2- PSI) Geochemical Modeling Code: Release 28-02-03. Internal Report TM-44-03-04, available from
1140 <http://gems.web.psi.ch/TDB/doc/pdf/TM-44-03-04-web.pdf> (checked 2018-04-19), (2003).
- 1141 [24] W. Hummel, U. Berner, E. Curti, F.J. Pearson, T. Thoenen, Nagra/PSI Chemical Thermodynamic Data
1142 Base 01/01, Universal Publishers/uPUBLISH.com, USA, also published as Nagra Technical Report NTB
1143 02-16, Wettingen, Switzerland, 2002.
- 1144 [25] E. Shock, D. Sassani, M. Willis, D. Sverjensky, Inorganic species in geologic fluids: Correlations
1145 among standard molal thermodynamic properties of aqueous ions and hydroxide complexes, *Geochim*
1146 *Cosmochim Acta*, 61 (1997) 907-950.
- 1147 [26] D. Sverjensky, E. Shock, H. Helgeson, Prediction of the thermodynamic properties of aqueous
1148 metal complexes to 1000 C and 5 kb, *Geochim Cosmochim Acta*, 61 (1997) 1359-1412.
- 1149 [27] M. Balonis, B. Lothenbach, G. Le Saout, F.P. Glasser, Impact of chloride on the mineralogy of
1150 hydrated Portland cement systems, *Cem Concr Res*, 40 (2010) 1009-1022.
- 1151 [28] T. Matschei, F.P. Glasser, The thermal stability of thaumasite, *Mater Struct*, 48 (2015) 2277–2289.
- 1152 [29] B. Lothenbach, F. Winnefeld, Thermodynamic modelling of the hydration of Portland cement, *Cem*
1153 *Concr Res*, 36 (2006) 209-226.
- 1154 [30] L.G. Baquerizo, T. Matschei, K.L. Scrivener, Impact of water activity on the stability of ettringite,
1155 *Cem Concr Res*, 76 (2016) 31-44.
- 1156 [31] L.G. Baquerizo, T. Matschei, K.L. Scrivener, Hydration states of AFm cement phases, *Cem Concr Res*,
1157 73 (2015) 143-157.
- 1158 [32] L.G. Baquerizo, T. Matschei, K.L. Scrivener, M. Saeidpour, A. Thorell, L. Wadsö, Methods to
1159 determine hydration states of minerals and cement hydrates, *Cem Concr Res*, 65 (2014) 85-95.
- 1160 [33] M. Balonis, F.P. Glasser, The density of cement phases, *Cem Concr Res*, 39 (2009) 733-739.
- 1161 [34] M. Balonis, The influence of inorganic chemical accelerators and corrosion inhibitors on the
1162 mineralogy of hydrated Portland cement systems, Thesis, University of Aberdeen, Aberdeen, UK, 2010.
- 1163 [35] M. Balonis, M. Medala, F.P. Glasser, Influence of calcium nitrate and nitrite on the constitution of
1164 AFm and AFt cement hydrates, *Adv Cem Res*, 23 (2011) 129-143.
- 1165 [36] M. Balonis, F.P. Glasser, Calcium nitrite corrosion inhibitor in portland cement: influence of nitrite
1166 on chloride binding and mineralogy, *J Am Ceram Soc*, 94 (2011) 2230-2241.
- 1167 [37] B.Z. Dilnesa, Fe-containing hydrates and their fate during cement hydration: thermodynamic data
1168 and experimental study, Thesis, EPFL, Lausanne, 2012.
- 1169 [38] D. Garvin, V.B. Parker, H.J. White, CODATA thermodynamic tables. Selections for some compounds
1170 of calcium and related mixtures: a prototype set of tables, Springer Verlag, Berlin, 1987.
- 1171 [39] K.B. Rozov, U. Berner, D.A. Kulik, L.W. Diamond, Solubility and thermodynamic properties of
1172 carbonate-bearing hydrotalcite-pyroaurite solid solutions with a 3:1 Mg/(Al+Fe) mole ratio, *Clay Clay*
1173 *Miner*, 59 (2011) 215-232.
- 1174 [40] D. Nied, K. Enemark-Rasmussen, E. L'Hôpital, J. Skibsted, B. Lothenbach, Properties of magnesium
1175 silicate hydrates (M-S-H), *Cem Concr Res*, 79 (2016) 323-332.
- 1176 [41] B. Lothenbach, E. Bernard, U. Mäder, Zeolite formation in the presence of cement hydrates and
1177 albite, *Phys Chem Earth*, 99 (2017) 77-94.
- 1178 [42] V.J. Babushkin, G.M. Matveyev, O.P. Mchedlov-Petrosyan, Thermodynamics of Silicates. Springer-
1179 Verlag, Berlin, H, (1985).
- 1180 [43] H.C. Helgeson, J.M. Delany, H.W. Nesbitt, D.K. Bird, Summary and critique of the thermodynamic
1181 properties of rock-forming minerals, *Am J Sci*, 278-A (1978) 1-229.

- 1182 [44] R.A. Robie, B.S. Hemingway, Thermodynamic properties of minerals and related substances at
 1183 298.15 K and 1 bar (105 Pascals) pressures and at higher temperatures, US Geol Surv Bull, 2131 (1995)
 1184 1-461.
- 1185 [45] G. Möschner, B. Lothenbach, A. Ulrich, R. Figi, R. Kretschmar, Solid solution between Al-ettringite
 1186 and Fe-ettringite ($\text{Ca}_6[\text{Al}_{1-x}\text{Fe}_x(\text{OH})_6]_2(\text{SO}_4)_3 \cdot 26\text{H}_2\text{O}$), *Cem Concr Res*, 39 (2009) 482-489.
- 1187 [46] E. Corazza, C. Sabelli, The crystal structure of syngenite, $\text{K}_2\text{Ca}(\text{SO}_4)_2 \cdot \text{H}_2\text{O}$, *Z Kristallog*, 124 (1967)
 1188 398-408.
- 1189 [47] P. Blanc, P. Vieillard, H. Gailhanou, S. Gaboreau, N. Marty, F. Claret, B. Made, E. Giffaut,
 1190 ThermoChimie database developments in the framework of cement/clay interactions, *Appl Geochem*,
 1191 55 (2015) 95-107.
- 1192 [48] R.M. Milton, Molecular sieve adsorbents, US Patent No (1959) 2,882,244.
- 1193 [49] G. Gottardi, E. Galli, Natural Zeolites, *Mineral and Rocks*, 18 (1985).
- 1194 [50] H. Boysen, M. Lerch, A. Stys, A. Senyshyn, Structure and oxygen mobility in mayenite ($\text{Ca}_{12}\text{Al}_{14}\text{O}_{33}$):
 1195 a high-temperature neutron powder diffraction study, *Acta Crystallogr*, B63 (2007) 675-682.
- 1196 [51] W. Hörkner, H. Müller-Buschbaum, Zur Kristallstruktur von CaAl_2O_4 , *J Inorg Nucl Chem*, 38 (1976)
 1197 983-984.
- 1198 [52] D.W. Goodwin, A.J. Lindop, The crystal structure of $\text{CaO} \cdot 2\text{Al}_2\text{O}_3$, *Acta Crystallogr B*, 26 (1970) 1230-
 1199 1235.
- 1200 [53] F. Winnefeld, B. Lothenbach, Phase equilibria in the system $\text{Ca}_4\text{Al}_6\text{O}_{12}\text{SO}_4 - \text{Ca}_2\text{SiO}_4 - \text{CaSO}_4 - \text{H}_2\text{O}$
 1201 referring to the hydration of calcium sulfoaluminate cements, *RILEM Technical Letters*, 1 (2016) 10-16.
- 1202 [54] D. Damidot, S.J. Barnett, F.P. Glasser, D.E. Macphee, Investigation of the $\text{CaO}-\text{Al}_2\text{O}_3-\text{SiO}_2-\text{CaSO}_4-$
 1203 $\text{CaCO}_3-\text{H}_2\text{O}$ system at 25°C by thermodynamic calculation, *Adv Cem Res*, 16 (2004) 69-76.
- 1204 [55] T. Schmidt, B. Lothenbach, M. Romer, K.L. Scrivener, D. Rentsch, R. Figi, A thermodynamic and
 1205 experimental study of the conditions of thaumasite formation, *Cem Concr Res*, 38 (2008) 337-349.
- 1206 [56] D.E. Macphee, S.J. Barnett, Solution properties of solids in the ettringite-thaumasite solid solution
 1207 series, *Cem Concr Res*, 34 (2004) 1591-1598.
- 1208 [57] F. Bellmann, On the formation of thaumasite $\text{CaSiO}_3 \cdot \text{CaSO}_4 \cdot \text{CaCO}_3 \cdot 15\text{H}_2\text{O}$: Part I, *Adv Cem Res*, 16
 1209 (2004) 55-60.
- 1210 [58] U.A. Birnin-Yauri, F.P. Glasser, Friedel's salt, $\text{Ca}_2\text{Al}(\text{OH})_6(\text{Cl},\text{OH}) \cdot 2\text{H}_2\text{O}$: its solid solutions and their
 1211 role in chloride binding, *Cem Concr Res*, 28 (1998) 1713-1723.
- 1212 [59] M.Y. Hobbs, Solubilities and ion exchange properties of solid solutions between OH, Cl and CO_3
 1213 end members of the monocalcium aluminate hydrates, Thesis, University of Waterloo, Ontario, Canada,
 1214 2001.
- 1215 [60] J.V. Bothe Jr, P.W. Brown, PhreeqC modeling of Friedel's salt equilibria at 23 ± 1 °C, *Cem Concr*
 1216 *Res*, 34 (2004) 1057-1063.
- 1217 [61] R.O. Grishchenko, A.L. Emelina, P.Y. Makarov, Thermodynamic properties and thermal behavior of
 1218 Friedel's salt, *Thermochim Acta*, 570 (2013) 74-79.
- 1219 [62] F.P. Glasser, A. Kindness, S.A. Stronach, Stability and solubility relationships in AFm phases. Part I.
 1220 Chloride, sulfate and hydroxide, *Cem Concr Res*, 29 (1999) 861-866.
- 1221 [63] G. Falzone, M. Balonis, G. Sant, X-AFm stabilization as a mechanism of bypassing conversion
 1222 phenomena in calcium aluminate cements, *Cem Concr Res*, 72 (2015) 54-68.
- 1223 [64] B.Z. Dilnesa, E. Wieland, B. Lothenbach, R. Dähn, K. Scrivener, Fe-containing phases in hydrated
 1224 cements, *Cem Concr Res*, 58 (2014) 45-55.
- 1225 [65] M. Vespa, E. Wieland, R. Dähn, B. Lothenbach, Identification of the thermodynamically stable Fe-
 1226 containing phase in aged cement pastes, *J Am Ceram Soc*, 98 (2015) 2286-2294.
- 1227 [66] H.F.W. Taylor, D.E. Newbury, An electron microprobe study of a mature cement paste, *Cem Concr*
 1228 *Res*, 14 (1984) 565-573.

- 1229 [67] U. Mäder, A. Jenni, C. Lerouge, S. Gaboreau, S. Miyoshi, Y. Kimura, V. Cloet, M. Fukaya, F. Claret, T.
1230 Otake, M. Shibata, B. Lothenbach, 5-year chemico-physical evolution of concrete–claystone interfaces,
1231 Mont Terri rock laboratory (Switzerland), *Swiss J Geosci*, 110 (2017) 307-327.
- 1232 [68] S.A. Bernal, R. San Nicols, R.J. Myers, R. Mejia de Gutierrez, F. Puertas, J.S.J. Van Deventer, J.L.
1233 Provis, MgO content of slag controls phase evolution and structural changes induced by accelerated
1234 carbonation in alkali-activated binders, *Cem Concr Res*, 57 (2014) 33-43.
- 1235 [69] I.G. Richardson, A.R. Brough, G.W. Groves, C.M. Dobson, The characterization of hardened alkali-
1236 activated blast-furnace slag pastes and the nature of the calcium silicate hydrate (C-S-H) phase, *Cem*
1237 *Concr Res*, 24 (1994) 813-829.
- 1238 [70] H. Taylor, Crystal structures of some double hydroxide minerals, *Mineral Mag*, 39 (1973) 377-389.
- 1239 [71] I. Richardson, Clarification of possible ordered distributions of trivalent cations in layered double
1240 hydroxides and an explanation for the observed variation in the lower solid-solution limit, *Acta*
1241 *Crystallogr B*, 69 (2013) 629-633.
- 1242 [72] D.G. Bennett, D. Read, M. Atkins, F.P. Glasser, A thermodynamic model for blended cements. II:
1243 Cement hydrate phases; thermodynamic values and modelling studies, *J Nucl Mater*, 190 (1992) 315-
1244 325.
- 1245 [73] W. Gao, Z. Li, Solubility and K SP of $Mg_4Al_2(OH)_{14} \cdot 3H_2O$ at the various ionic strengths,
1246 *Hydrometallurgy*, 117-118 (2012) 36-46.
- 1247 [74] R.J. Myers, B. Lothenbach, S. Bernal, J.L. Provis, Thermodynamic modelling of alkali-activated slag-
1248 based cements, *Appl Geochem*, 61 (2015) 233-247.
- 1249 [75] M. Zajac, S.K. Bremseth, M. Whitehead, M. Ben Haha, Effect of $CaMg(CO_3)_2$ on hydrate
1250 assemblages and mechanical properties of hydrated cement pastes at 40°C and 60°C, *Cem Concr Res*,
1251 65 (2014) 21-29.
- 1252 [76] B. Lothenbach, A. Nonat, Calcium silicate hydrates: solid and liquid phase composition, *Cem Concr*
1253 *Res*, 78 (2015) 57-70.
- 1254 [77] I. Richardson, Tobermorite/jennite-and tobermorite/calcium hydroxide-based models for the
1255 structure of CSH: applicability to hardened pastes of tricalcium silicate, β -dicalcium silicate, Portland
1256 cement, and blends of Portland cement with blast-furnace slag, metakaolin, or silica fume, *Cem Concr*
1257 *Res*, 34 (2004) 1733-1777.
- 1258 [78] A. Muller, K. Scrivener, A. Gajewicz, P. McDonald, Use of bench-top NMR to measure the density,
1259 composition and desorption isotherm of C–S–H in cement paste, *Microporous and Mesoporous*
1260 *Materials*, 178 (2013) 99-103.
- 1261 [79] A. Muller, K. Scrivener, J. Skibsted, A. Gajewicz, P. McDonald, Influence of silica fume on the
1262 microstructure of cement pastes: New insights from 1H NMR relaxometry, *Cem Concr Res*, 74 (2015)
1263 116-125.
- 1264 [80] C.S. Walker, S. Sutou, C. Oda, M. Mihara, A. Honda, Calcium silicate hydrate (C-S-H) gel solubility
1265 data and a discrete solid phase model at 25 °C based on two binary non-ideal solid solutions, *Cem*
1266 *Concr Res*, 79 (2016) 1-30.
- 1267 [81] S.-Y. Hong, F.P. Glasser, Alkali binding in cement pastes: Part I. The C-S-H phase, *Cem Concr Res*,
1268 29 (1999) 1893-1903.
- 1269 [82] E. L'Hôpital, B. Lothenbach, D. Kulik, K. Scrivener, Influence of calcium to silica ratio on aluminium
1270 uptake in calcium silicate hydrate, *Cem Concr Res*, 85 (2016) 111-121.
- 1271 [83] E. L'Hôpital, B. Lothenbach, G. Le Saout, D.A. Kulik, K. Scrivener, Incorporation of aluminium in
1272 calcium-silicate hydrate, *Cem Concr Res*, 75 (2015) 91-103.
- 1273 [84] E. L'Hôpital, B. Lothenbach, K. Scrivener, D.A. Kulik, Alkali uptake in calcium alumina silicate
1274 hydrate (C-A-S-H), *Cem Concr Res*, 85 (2016) 122-136.
- 1275 [85] D.A. Kulik, M. Kersten, Aqueous solubility diagrams for cementitious waste stabilization systems: II,
1276 End-member stoichiometries of ideal calcium silicates hydrate solid solutions, *J Am Ceram Soc*, 84
1277 (2001) 3017-3026.

1278 [86] J. Haas, A. Nonat, From C–S–H to C–A–S–H: Experimental study and thermodynamic modelling,
1279 *Cem Concr Res*, 68 (2015) 124-138.

1280 [87] S.V. Churakov, C. Labbez, Thermodynamics and molecular mechanism of Al incorporation in
1281 calcium silicate hydrates, *J Phys Chem C*, 121 (2017) 4412-4419.

1282 [88] D. Kulik, J. Tits, E. Wieland, Aqueous-solid solution model of strontium uptake in C-S-H phases,
1283 *Geochim Cosmochim Acta*, 71 (2007) A530.

1284 [89] B. Lothenbach, G. Le Saout, M. Ben Haha, R. Figi, E. Wieland, Hydration of a low-alkali CEM III/B-
1285 SiO₂ cement (LAC), *Cem Concr Res*, 42 (2012) 410-423.

1286 [90] R. Myers, S.A. Bernal, J.L. Provis, A thermodynamic model for C-(N-)A-S-H gel: CNASH_ss.
1287 Derivation and validation, *Cem Concr Res*, 66 (2014) 27-47.

1288 [91] D. Kulik, Dual-thermodynamic estimation of stoichiometry and stability of solid solution end
1289 members in aqueous-solid solution systems, *Chem Geol*, 225 (2006) 189-212.

1290 [92] J. Tits, E. Wieland, C.J. Müller, C. Landesman, M.H. Bradbury, Strontium binding by calcium silicate
1291 hydrates, *J Colloid Interface Sci*, 300 (2006) 78-87.

1292 [93] D.D. Wagman, E.H. Evans, V.B. Parker, R.H. Schumm, I. Halow, Bailey S.M, Churney K.L., N.R. L., The
1293 NBS tables of chemical thermodynamic properties. Selected values for inorganic and C1 and C2
1294 organic substances in SI units, *J Phys Chem Ref Data*, 11, Suppl. 2 (1982) 1-392.

1295 [94] I.G. Richardson, The calcium silicate hydrates, *Cem Concr Res*, 38 (2008) 137-158.

1296 [95] J.J. Chen, J.J. Thomas, H.F.W. Taylor, H.M. Jennings, Solubility and structure of calcium silicate
1297 hydrate, *Cem Concr Res*, 34 (2004) 1499-1519.

1298 [96] K. Garbev, M. Bornefeld, G. Beuchle, P. Stemmermann, Cell dimensions and composition of
1299 nanocrystalline calcium silicate hydrate solid solutions. part 2: X-Ray and thermogravimetry study, *J Am
1300 Ceram Soc*, 91 (2008) 3015-3023.

1301 [97] X. Gaona, D.A. Kulik, N. Macé, E. Wieland, Aqueous–solid solution thermodynamic model of U(VI)
1302 uptake in C–S–H phases, *Appl Geochem*, 27 (2012) 81-95.

1303 [98] A.J. Allen, J.J. Thomas, H.M. Jennings, Composition and density of nanoscale calcium–silicate–
1304 hydrate in cement, *Nat Mater*, 6 (2007) 311-316.

1305 [99] J.J. Thomas, A.J. Allen, H.M. Jennings, Density and water content of nanoscale solid C–S–H formed
1306 in alkali-activated slag (AAS) paste and implications for chemical shrinkage, *Cem Concr Res*, 42 (2012)
1307 377-383.

1308 [100] J.L. Provis, S.A. Bernal, Geopolymers and related alkali-activated materials, *Annu Rev Mater Res*,
1309 44 (2014) 299-327.

1310 [101] R.J. Myers, S.A. Bernal, J.L. Provis, Phase diagrams for alkali-activated slag binders, *Cem Concr
1311 Res*, 95 (2017) 30-38.

1312 [102] C.S. Walker, D. Savage, M. Tyrer, K.V. Ragnarsdottir, Non-ideal solid solution aqueous solution
1313 modeling of synthetic calcium silicate hydrate, *Cem Concr Res*, 37 (2007) 502-511.

1314 [103] L. Gomez-Zamorano, M. Balonis, B. Erdemli, N. Neithalath, G. Sant, C–(N)–S–H and N–A–S–H gels:
1315 Compositions and solubility data at 25°C and 50°C, *J Am Ceram Soc*, 100 (2017) 2700-2711.

1316 [104] R.J. Myers, E. L'Hôpital, J.L. Provis, B. Lothenbach, Effect of temperature and aluminium on
1317 calcium (alumino)silicate hydrate chemistry under equilibrium conditions, *Cem Concr Res*, 68 (2015)
1318 83-93.

1319 [105] R.J. Myers, E. L'Hôpital, J.L. Provis, B. Lothenbach, Composition-solubility-structure relationships
1320 in calcium (alkali) aluminosilicate hydrate (C-(N,K)-A-S-H), *Dalton Trans*, 44 (2015) 13530-13544.

1321 [106] G.D. Miron, D.A. Kulik, S.V. Dmytrieva, T. Wagner, GEMSFITS: Code package for optimization of
1322 geochemical model parameters and inverse modeling., *Appl Geochem*, 55 (2015) 28-45.

1323 [107] L. Nicoleau, E. Schreiner, Determination of Ca²⁺ complexation constants by monomeric silicate
1324 species at 25°C with a Ca²⁺ ion selective electrode, *Cem Concr Res*, 98 (2017) 36-43.

- 1325 [108] A. Jenni, U. Mäder, C. Lerouge, S. Gaboreau, B. Schwyn, In situ interaction between different
1326 concretes and Opalinus clay, *Phys Chem Earth*, 70-71 (2014) 71-83.
- 1327 [109] A. Dauzères, G. Achiedo, D. Nied, E. Bernard, S. Alahrache, B. Lothenbach, Magnesium
1328 perturbation in low-pH concretes placed in clayey environment—solid characterizations and modeling,
1329 *Cem Concr Res*, 79 (2016) 137-150.
- 1330 [110] D. Bonen, M.D. Cohen, Magnesium sulfate attack on portland cement paste—II. Chemical and
1331 mineralogical analyses, *Cem Concr Res*, 22 (1992) 707-718.
- 1332 [111] M. Santhanam, M.D. Cohen, J. Olek, Mechanism of sulfate attack: a fresh look: part 1: summary of
1333 experimental results, *Cem Concr Res*, 32 (2002) 915-921.
- 1334 [112] U.H. Jakobsen, K. De Weerd, M.R. Geiker, Elemental zonation in marine concrete, *Cem Concr Res*,
1335 85 (2016) 12-27.
- 1336 [113] C. Roosz, S. Grangeon, P. Blanc, V. Montouillout, B. Lothenbach, P. Henocq, E. Giffaut, P. Vieillard,
1337 S. Gaboreau, Crystal structure of magnesium silicate hydrates (M S H): the relation with 2:1 Mg–Si
1338 phyllosilicates, *Cem Concr Res*, 73 (2015) 228-237.
- 1339 [114] E. Bernard, B. Lothenbach, F. Le Goff, I. Pochard, A. Dauzères, Effect of magnesium on calcium
1340 silicate hydrates (C-S-H), *Cem Concr Res*, 97 (2017) 61-72.
- 1341 [115] D.R.M. Brew, F.P. Glasser, Synthesis and characterisation of magnesium silicate hydrate gels, *Cem
1342 Concr Res*, 35 (2005) 85-98.
- 1343 [116] B. Lothenbach, D. Nied, E. L'Hôpital, G. Achiedo, A. Dauzères, Magnesium and calcium silicate
1344 hydrates *Cem Concr Res*, 77 (2015) 60-68.
- 1345 [117] W.-S. Chiang, G. Ferraro, E. Fratini, F. Ridi, Y.-Q. Yeh, U. Jeng, S.-H. Chen, P. Baglioni, Multiscale
1346 structure of calcium-and magnesium-silicate-hydrate gels, *J Mater Chem A*, 2 (2014) 12991-12998.
- 1347 [118] E. Bernard, B. Lothenbach, D. Rentsch, I. Pochard, A. Dauzères, Formation of magnesium silicate
1348 hydrates (M-S-H), *Phys Chem Earth*, 99 (2017) 142-157.
- 1349 [119] J.A.T. Smellie, Maqarin Natural Analogue Study: Phase III, SKB, SKB Technical Report 98-04,
1350 Stockholm, Sweden, 1998.
- 1351 [120] S.J. Chipera, J.A. Apps, Geochemical stability of natural zeolites, *Reviews in Mineralogy and
1352 Geochemistry*, 45 (2001) 117-161.
- 1353 [121] R. Arthur, H. Sasamoto, C. Walker, M. Yui, Polymer model of zeolite thermochemical stability, *Clay
1354 Clay Miner*, 59 (2011) 626-639.
- 1355 [122] J.L. Provis, G.C. Lukey, J.S. van Deventer, Do geopolymers actually contain nanocrystalline
1356 zeolites? A reexamination of existing results, *Chem Mater*, 17 (2005) 3075-3085.
- 1357 [123] B. Lothenbach, G. Le Saout, E. Gallucci, K. Scrivener, Influence of limestone on the hydration of
1358 Portland cements, *Cem Concr Res*, 38 (2008) 848-860.
- 1359 [124] K. De Weerd, M. Ben Haha, G. Le Saout, K.O. Kjellsen, H. Justnes, B. Lothenbach, Hydration
1360 mechanisms of ternary Portland cements containing limestone powder and fly ash, *Cem Concr Res*, 41
1361 (2011) 279-291.
- 1362 [125] F. Deschner, F. Winnefeld, B. Lothenbach, S. Seufert, P. Schwesig, S. Dittrich, F. Goetz-
1363 Neunhoeffler, J. Neubauer, Hydration of a Portland cement with high replacement by siliceous fly ash
1364 *Cem Concr Res*, 42 (2012) 1389-1400.
- 1365 [126] T.G. Jappy, F.P. Glasser, Synthesis and stability of silica-substituted hydrogarnet $\text{Ca}_3\text{Al}_2\text{Si}_{3-x}\text{O}_{12-4x}(\text{OH})_{4x}$,
1366 *Adv Cem Res*, 4 (1991) 1-8.
- 1367 [127] A. Vollpracht, B. Lothenbach, R. Snellings, J. Haufe, The pore solution of blended cements: a
1368 review, *Mater Struct*, 49 (2016) 3341-3367.
- 1369 [128] W.R. Smith, R.W. Missen, *Chemical Reaction Equilibrium Analysis: Theory and Algorithms*, Wiley-
1370 Interscience, New York 1982. reprinted with corrections, Krieger, Malabar, FL., 1991.
- 1371 [129] T. Matschei, F.P. Glasser, New approaches to quantification of cement hydration, in: J. Stark (Ed.)
1372 16 Internationale Baustofftagung (ibautil), Weimar, Germany, 2006, pp. 390-400.

1373 [130] B.J. Merkel, B. Planer-Friederich, Groundwater Geochemistry. A Practical Guide to Modeling of
1374 Natural and Contaminated Aquatic Systems, Springer Berlin, 2008.

1375 [131] G.M. Anderson, D.A. Crerar, Thermodynamics in Geochemistry: the Equilibrium Model, Oxford
1376 University Press, Oxford, 1993.

1377 [132] D. Kulik, Minimising uncertainty induced by temperature extrapolations of thermodynamic data:
1378 a pragmatic view on the integration of thermodynamic databases into geochemical computer codes,
1379 in: The use of thermodynamic databases in performance assessment, OECD, Barcelona, 2002, pp. 125-
1380 137.

1381 [133] J.W. Johnson, E.H. Oelkers, H.C. Helgeson, SUPCRT92: A software package for calculating the
1382 standard molal thermodynamic properties of minerals, gases, aqueous species, and reactions from 1 to
1383 5000 bar and 0 to 1000°C, Comput Geosci, 18 (1992) 899-947.

1384

1385

1386 **Appendix: Cemdata18 thermodynamic dataset**

1387 **A Cemdata18 dataset in GEMS format**

1388 Cemdata18 database in GEM-Selektor v.3 format can be freely downloaded
1389 (<http://www.empa.ch/cemdata>) and is fully compatible with the GEMS version of the PSI/Nagra 12/07
1390 TDB [22, 23] (<http://gems.web.psi.ch>). As several alternative C-S-H models, as well as two models for
1391 hydroxide-hydrotalcite are available, the user needs to select the appropriate models during the
1392 generation of new projects, as illustrated in Figure A.1. The CSHQ and the OH-hydrotalcite with Mg/Al
1393 = 2 are well adapted for Portland cement systems (select cemdata, pc, ht and cshq as indicated at the
1394 left hand side of Figure A.1).

1395 For alkali activated binders, the CNASH model has been developed for C-S-H type calcium (alkali)
1396 aluminosilicate hydrate gels with lower calcium but higher aluminium and alkali content. An Mg-Al
1397 layered double hydroxide model with variable Mg/Al ratio is also available for use in alkali activated
1398 cement systems. For alkali activated binders, the selection of cemdata and aam and deselection of pc
1399 is recommended as illustrated at the right hand side of Figure A.1.

1400

Built-in Database	Version	Built-in Database	Version
<input checked="" type="checkbox"/> support		<input checked="" type="checkbox"/> support	
<input checked="" type="checkbox"/> template		<input checked="" type="checkbox"/> template	
<input type="checkbox"/> supcrt		<input type="checkbox"/> supcrt	
<input checked="" type="checkbox"/> psi-nagra		<input checked="" type="checkbox"/> psi-nagra	
<input checked="" type="checkbox"/> 3rdparty		<input checked="" type="checkbox"/> 3rdparty	
<input checked="" type="checkbox"/> cemdata	18.01	<input checked="" type="checkbox"/> cemdata	18.01
<input checked="" type="checkbox"/> .		<input checked="" type="checkbox"/> .	
<input checked="" type="checkbox"/> pc	18.01	<input type="checkbox"/> pc	18.01
<input checked="" type="checkbox"/> .		<input type="checkbox"/> .	
<input checked="" type="checkbox"/> ht	18.01	<input type="checkbox"/> ht	18.01
<input checked="" type="checkbox"/> csh		<input type="checkbox"/> csh	
<input checked="" type="checkbox"/> cshq	18.01	<input type="checkbox"/> cshq	18.01
<input type="checkbox"/> cshkn	18.01	<input type="checkbox"/> cshkn	18.01
<input type="checkbox"/> csh3t	18.01	<input type="checkbox"/> csh3t	18.01
<input type="checkbox"/> csh2o	18.01	<input type="checkbox"/> csh2o	18.01
<input type="checkbox"/> aam	18.01	<input checked="" type="checkbox"/> aam	18.01
<input type="checkbox"/> .		<input checked="" type="checkbox"/> .	
<input type="checkbox"/> csh+ht	18.01	<input checked="" type="checkbox"/> csh+ht	18.01
<input checked="" type="checkbox"/> ss	18.01	<input checked="" type="checkbox"/> ss	18.01
<input checked="" type="checkbox"/> ss-fe3	18.01	<input checked="" type="checkbox"/> ss-fe3	18.01

1401

1402 Figure A.1: Selection of modules of Cemdata18 and related databases in GEM-Selektor to model PC
 1403 (Portland-cement) systems (left) and to model AAM (alkali-activated materials). For PC systems, one of
 1404 four alternative solid solution models of C-S-H should be selected (see Section 2.7); selection of Fe-
 1405 containing solid solutions ("ss-fe3" module) is also optional.

1406

1407 B Cemdata18 dataset in PHREEQC format

1408 To enable users to model cementitious systems using the Cemdata18 dataset with the popular
 1409 PHREEQC geochemical speciation code [18], a PHREEQC ".dat" format database of the Cemdata18
 1410 dataset (CEMDATA18-09-10-2017.dat) is provided for download from <http://www.empa.ch/cemdata>.
 1411 This LMA (Law of Mass Action) type dataset has been generated using the reaction generator module
 1412 of the ThermoMatch code (Miron et al. in preparation) and exported into the PHREEQC format ".dat"
 1413 file using the ThermoMatch database export module. The reaction generator algorithm is based on the
 1414 matrix "row reduce" method described by Smith and Missen [128]. In this process, all aqueous and
 1415 solid species from the Cemdata18 GEM-Selektor database were considered. The supplementary data
 1416 for aqueous, gaseous and solid species corresponding to the list of elements covered by Cemdata18
 1417 were selected from the GEMS version of the PSI/Nagra TDB [22, 23]. The latter and the Cemdata18
 1418 GEM database are mutually consistent, and should be used together in GEMS codes for modelling
 1419 cementitious systems.

1420 To generate PHREEQC-style reactions for product species, firstly the following master species were
 1421 selected based on their generic predominance: Ca^{+2} , Mg^{+2} , Sr^{+2} , Na^+ , K^+ , H^+ , CO_3^{-2} , SO_4^{-2} , Cl^- , NO_3^- ,
 1422 AlO_2^- , FeO_2^- , SiO_2^0 , H_2O^0 . Using selected master species, the reactions were automatically generated for
 1423 the remaining (product) species, and their properties at 25°C and 1 bar were calculated. Formation
 1424 reactions were generated for aqueous product species, and dissolution reactions - for gaseous and
 1425 solid product species. The LMA dataset of reactions was then exported into a PHREEQC "dat" file
 1426 (CEMDATA18-09-10-2017.dat) using the ThermoMatch database export module. Parameters for the

1427 $\log K^\circ = f(T)$ analytical expressions were calculated for the 3-term extrapolation method that assumes
 1428 the $\Delta_r C_p^\circ$ to be not zero and independent of temperature. These reported parameters are used by
 1429 PHREEQC for calculating the $\log_{10} K^\circ$ as a function of temperature. Such temperature extrapolations of
 1430 $\log_{10} K^\circ$ should be valid at least up to 100°C.

1431 Table B.1 contains the generated formation reactions for the aqueous product species, together with
 1432 the values for reaction standard effects at 25°C and 1 bar. Table B.2 contains the generated dissolution
 1433 reactions for gaseous and solid product species, together with the reaction standard effects at 25°C
 1434 and 1 bar. Table B.2 contains, in addition to the Cemdata18 database as detailed in Table 1 to Table 4,
 1435 also the thermodynamic data of all solids composed of Al, C, Ca, Cl, Fe, H, K, Mg, N, Na, S, Si or Sr
 1436 compiled in the GEMS version of the PSI/Nagra 12/07 TDB [22, 23], needed to allow the generation of
 1437 a compatible dataset in PHREEQC. Figures B.1, B.2, and B.3 show comparisons of cement-related mod-
 1438 elling problems between GEM-Selektor (using GEM-type Cemdata18) and PHREEQC (using LMA-type
 1439 Cemdata18 CEMDATA18-09-10-2017.dat). For the PHREEQC calculations, PHREEQC for Windows ver-
 1440 sion 2.18.00 (uses PHREEQC-2 source version 2.18.3-5570) was used. In all three cases, the considered
 1441 solid solutions were modelled in PHREEQC using the simple ideal mixing model.

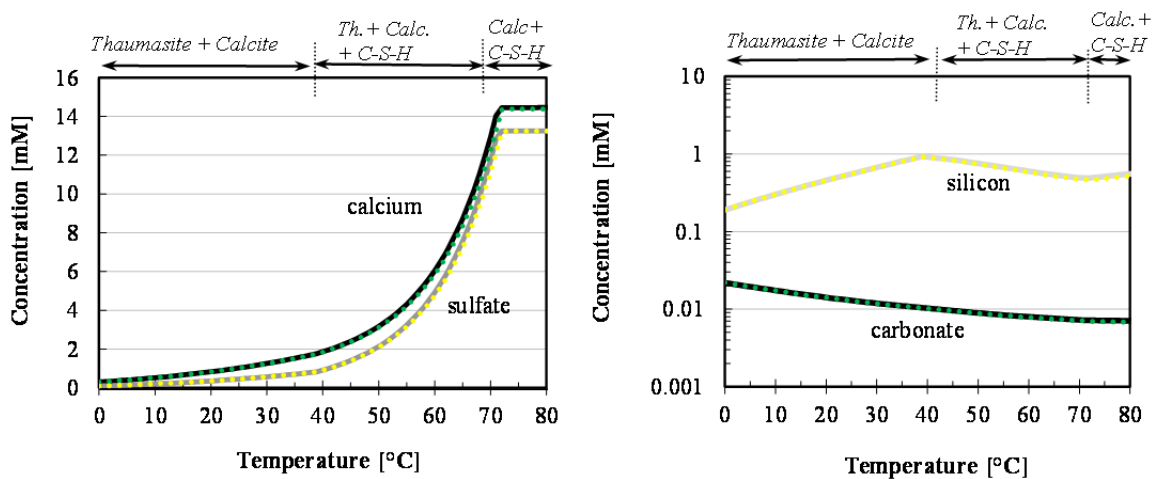
1442

1443 Table B.1 (in separate file)

1444

1445 Table B.2 (in separate file)

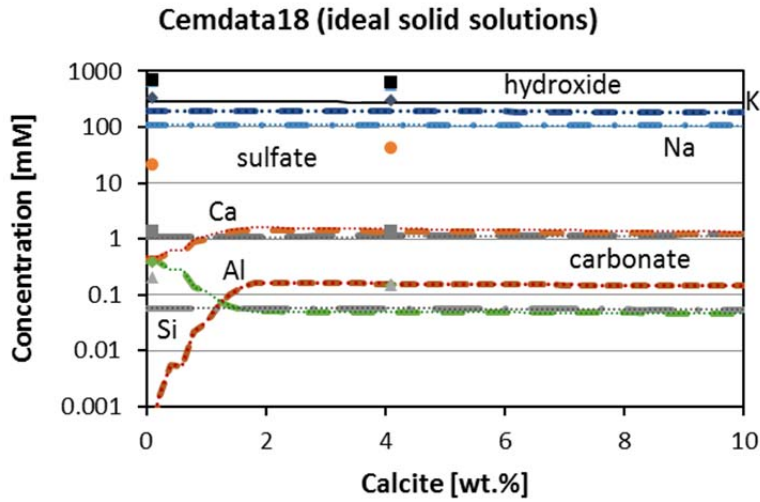
1446



1447

1448 **Figure B1.** Calculated (curves) solubility data for thaumasite, based on the new thermodynamic data
 1449 for thaumasite complemented with the CSHQ data from Cemdata18 [1, 7] in GEM format; Calculated
 1450 (dotted lines) solubility data for thaumasite, based on data Cemdata18 [1, 7] in PHREEQC format.

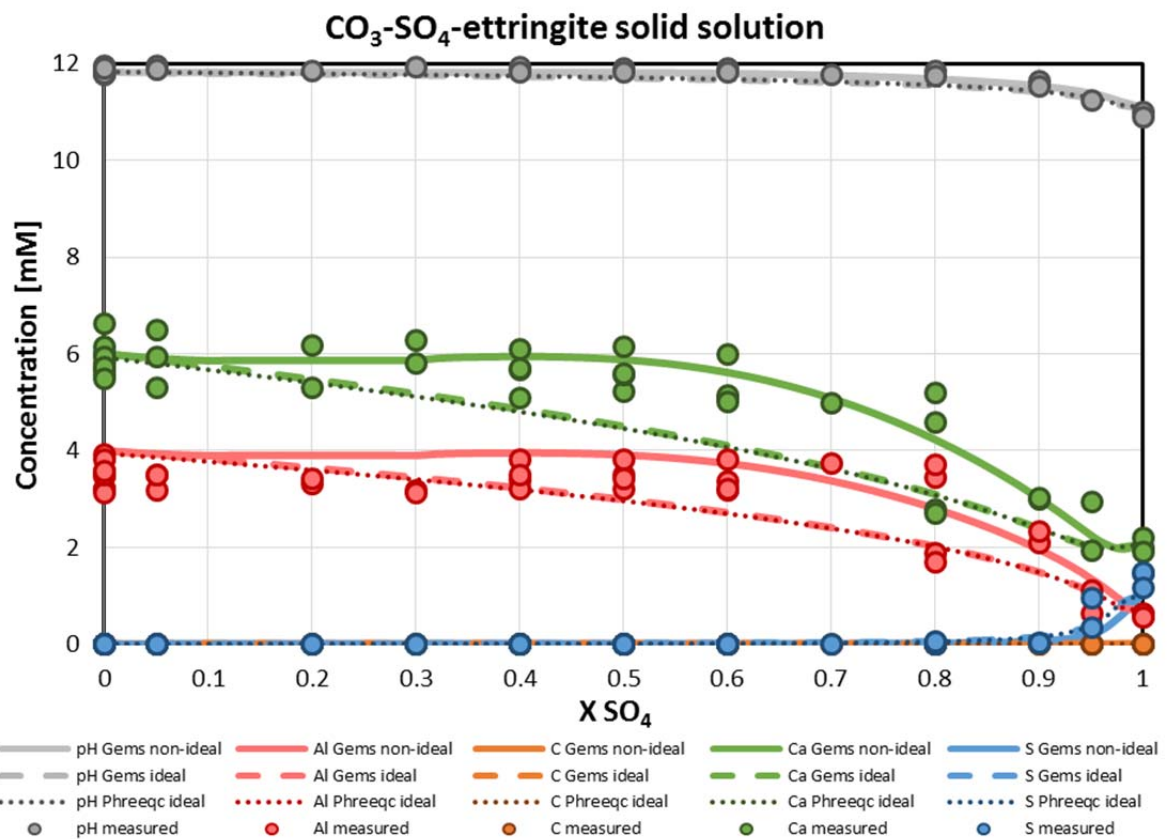
1451



1452

1453 **Figure B2:** Effect of the amount of limestone on the phase assemblage and the distribution of alumin-
 1454 ium and iron in hydrated Portland cement calculated using Cemdata18 GEM format (dashed lines) and
 1455 Cemdata18 PHREEQC format (dotted lines), in both cases using ideal solid solutions.

1456



1457

1458 **Figure B3.** Calculated aqueous composition in equilibrium with $\text{CO}_3\text{-SO}_4\text{-ettringite}$ solid solution as a
 1459 function of SO_4 in the solid. Solid lines calculated using the Cemdata18 GEM format using non ideal
 1460 solid solution; Dashed lines calculated using the Cemdata18 GEM format using ideal solid solution;
 1461 Dotted lines calculated using the Cemdata18 PHREEQC format using ideal solid solution; Circles: ex-
 1462 perimental data [7, 129]

1463 **C Thermodynamic equations and assumptions**

1464 The solubility products compiled in Cemdata18 have generally been derived from solutions composi-
 1465 tion measured at different temperatures, as documented in detail in [1, 7-10, 12, 27, 28, 30, 31, 34-37,
 1466 39-41]. The activity of a species i , a_i , has been calculated with GEMS from the measured concentrations
 1467 considering the formation of aqueous complexes. By definition $a_i = \gamma_i \cdot m_i$ where γ_i is the activity coeffi-
 1468 cient and m_i the concentration in mol/kg H₂O. Activity coefficients of aqueous species γ_i were comput-
 1469 ed using the built-in extended Debye-Hückel equation with the common ion-size parameter a_i of 3.67
 1470 Å for KOH and 3.31 Å for NaOH solutions and the common third parameter b_y according to the equa-
 1471 tion (C.1):

$$1472 \log \gamma_i = \frac{-A_y z_i^2 \sqrt{I}}{1 + B_y a_i \sqrt{I}} + b_y I \quad (C.1)$$

1473 where z_i denotes the charge of species i , I is the effective molal ionic strength, b_y is a semi-empirical
 1474 parameter (~ 0.123 for KOH and ~ 0.098 for NaOH electrolyte at 25°C), and A_y and B_y are P, T -
 1475 dependent coefficients. For uncharged species, equation (C.1) reduces to $\log \gamma_i = b_y I$. This extended
 1476 Debye-Hückel activity correction is applicable up to approx. 1 m ionic strength [130].

1477 From the solubility products K of solids calculated at different temperatures T , the Gibbs free energy of
 1478 reaction, $\Delta_r G^\circ$, the Gibbs free energy of formation, $\Delta_f G^\circ$, and the absolute entropy, S° , at $T_0=298.15$ K
 1479 were obtained according to equations (C.2) and (C.3):

$$1480 \Delta_r G^\circ = \sum_i \nu_i \Delta_f G^\circ = -RT \ln K \quad (C.2)$$

$$1481 \Delta_a G_T^\circ = \Delta_f G_{T_0}^\circ - S_{T_0}^\circ (T - T_0) + \int_{T_0}^T C_p^0 dT - \int_{T_0}^T \frac{C_p^o}{T} dT \quad (C.3)$$

1482 Using $C_p^o = a_0 + a_1 T + a_2 T^2 + a_3 T^{0.5}$ [131], where a_{0-3} are the empirical parameters defined for each
 1483 mineral, the two integral terms of equation (C.3) can be solved to give equation (C.4):

$$1484 \Delta_a G_T^\circ = \Delta_f G_{T_0}^\circ - S_{T_0}^\circ (T - T_0) - a_0 \left(T \ln \frac{T}{T_0} - T + T_0 \right) - 0.5 a_1 (T - T_0)^2 - a_2 \frac{(T - T_0)^2}{2T \cdot T_0^2} - a_3 \frac{2(\sqrt{T} - \sqrt{T_0})^2}{\sqrt{T_0}} \quad (C.4)$$

1486 where ν_i are the stoichiometric reaction coefficients, $R = 8.31451$ J/mol/K, T is the temperature in K,
 1487 and C_p^o is the heat capacity at constant pressure. The apparent Gibbs free energy of formation, $\Delta_a G_T^\circ$,
 1488 refers to standard Gibbs energies of elements at 298.15 K. A more detailed description of the deriva-
 1489 tion of the dependence of the Gibbs free energy on temperature is available in [131, 132].

1490

1491 Dependence of the solubility product on temperature, consistent to Eq C.4 can be expressed as:

$$1492 \log K_T = A_0 + A_1 T + \frac{A_2}{T} + A_3 \ln T + \frac{A_4}{T^2} + A_5 T^2 + A_6 \sqrt{T} \quad (C.5)$$

1493 [131], where A_0, \dots, A_6 are empirical coefficients. If the entropy (S°), the enthalpy ($\Delta_f H^\circ$), and the coeffi-
 1494 cients (a_0, a_1, \dots) of the heat capacity equation ($C_p^\circ = a_0 + a_1 T + a_2 T^2 + a_3 T^{0.5} + a_4 T^2$) of the species are
 1495 available, the coefficients A_0, \dots, A_6 can be calculated directly (see [131]). These calculations involving
 1496 Eqs C.4 and C.5 are all implemented in the GEM-Selektor.

1497 The heat capacity function, $C_p = f(T)$ is usually obtained from calorimetry experiments. In many cases,
 1498 the heat capacity has to be estimated by using a reference reaction with a solid having a known heat
 1499 capacity and similar structure, as described in publications [1, 7-10, 12, 27, 28, 30, 31, 34-37, 39-41].
 1500 Helgeson et al. [43] applied this principle successfully to estimate heat capacities of silicate minerals by
 1501 formulating reactions involving structurally-related minerals with known heat capacity functions. This
 1502 method has limitations due to the differing thermodynamic properties of "water" varieties, bound
 1503 loosely as a hydration water, or structurally as OH-groups. To minimize errors associated with the vary-
 1504 ing strengths of bonding for "water", reference reactions had been formulated to involve no "free" wa-
 1505 ter as a substituent in reactions, wherever appropriate.

1506 The value of $\Delta_r C_p^0$ has little influence on the calculated log K value in the temperature range 0-100°C
 1507 and is thus often assumed to be constant in a narrow temperature range: $\Delta_r C_p^0_T = \Delta_r C_p^0_{T_0} = \Delta a_0$. This
 1508 simplifies Eq. C.5 to the so called 3-term approximation of the temperature dependence, see Eq. C.6,
 1509 which can be used to compute the standard thermodynamic properties of each solid [132] to obtain a
 1510 temperature-dependent "log K" function using equations C.6-C.12 (implemented in GEMS).

$$1511 \quad \log K_T = A_0 + A_2 T^{-1} + A_3 \ln T \quad (\text{C.6})$$

$$1512 \quad \text{and} \quad A_0 = \frac{0.4343}{R} \cdot \left[\Delta_r S_{T_0}^0 - \Delta_r C_p^0_{T_0} (1 + \ln T_0) \right] \quad (\text{C.7})$$

$$1513 \quad A_2 = \frac{0.4343}{R} \cdot (\Delta_r H_{T_0}^0 - \Delta_r C_p^0_{T_0} T_0) \quad (\text{C.8})$$

$$1514 \quad A_3 = \frac{0.4343}{R} \cdot \Delta_r C_p^0_{T_0} \quad (\text{C.9})$$

$$1515 \quad \Delta_r S_T^0 = \Delta_r S_{T_0}^0 + \Delta_r C_p^0_{T_0} \ln \frac{T}{T_0} \quad (\text{C.10})$$

$$1516 \quad \Delta_r H_T^0 = \Delta_r H_{T_0}^0 + \Delta_r C_p^0_{T_0} (T - T_0) \quad (\text{C.11})$$

$$1517 \quad \Delta_r G_T^0 = \Delta_r H_T^0 + T \Delta_r S_T^0 \quad (\text{C.12})$$

1518 Within the relatively narrow temperature range of 0 to 100°C, where the Cemdata18 database is valid,
 1519 this simplification has a negligible influence on the resulting solubility products, also for non-
 1520 isoelectric reactions as exemplified for ettringite in [20].

1521

1522 **D Thermodynamic data for aqueous and gaseous species**

1523 The thermodynamic data for aqueous and gaseous species compatible with Cemdata18 are summa-
 1524 rized in Table D.1 and D.2.

1525

1526 **Table D.1** Standard (partial molal) thermodynamic properties and equation of state parameters of
 1527 aqueous species at 25°C, 1 bar used in GEM calculations, as detailed in the GEMS version of the
 1528 PSI/Nagra 12/07 TDB [22, 23]. Numbers referring to the charge of aqueous species are written after the
 1529 plus or minus signs to avoid any ambiguity; "@" is used to represent a neutral aqueous species.

Species	ΔG^0	ΔH^0	S^0	C_p^0	V^0	$a_1 \cdot 10^*$	$a_2 \cdot 10^{-2^*}$	a_3	$a_4 \cdot 10^{-4}$	c_1	$c_2 \cdot 10^{-4}$	$\omega_0 \cdot 10^{-5}$
	(kJ/mol)	(kJ/mol)	(J/mol-K)	(J/mol-K)	(J/bar)	(cal/mol/ba	(cal/mol)	(cal-K/mol/bar)	(cal-K/mol)	(cal/mol/K)	(cal-K/mol)	(cal/mol)
Al(SO ₄) ⁺	-1250.43	-1422.67	-172.38	-204.01	-6.02	1.3869	-4.3920	7.4693	-2.5974	-11.6742	-12.9914	1.1729
Al(SO ₄) ²⁻	-2006.30	-2338.40	-135.50	-268.37	31.11	6.8275	8.8925	2.2479	-3.1466	-12.0220	-16.1447	2.1199
Al ⁺³	-483.71	-530.63	-325.10	-128.70	-45.24	-3.3802	-17.0071	14.5185	-2.0758	10.7000	-8.0600	2.7530
AlO ⁺	-660.42	-713.64	-112.97	-125.11	0.31	2.1705	-2.4811	6.7241	-2.6763	-2.5983	-9.1455	0.9570
AlO ₂ ⁻	-827.48	-925.57	-30.21	-49.04	9.47	3.7221	3.9954	-1.5879	-2.9441	15.2391	-5.4585	1.7418
AlO ₂ H [⊙]	-864.28	-947.13	20.92	-209.21	13.01	3.5338	0.8485	5.4132	-2.8140	-23.4129	-13.2195	-0.0300
AlOH ⁺²	-692.60	-767.27	-184.93	55.97	-2.73	2.0469	-2.7813	6.8376	-2.6639	29.7923	-0.3457	1.7247
Ca(CO ₃) [⊙]	-1099.18	-1201.92	10.46	-123.86	-15.65	-0.3907	-8.7325	9.1753	-2.4179	-11.5309	-9.0641	-0.0380
Ca(HCO ₃)	-1146.04	-1231.94	66.94	233.70	13.33	3.7060	1.2670	5.2520	-2.8310	41.7220	8.3360	0.3080
Ca(HSiO ₃)	-1574.24	-1686.48	-8.33	137.80	-6.74	1.0647	-5.1787	7.7785	-2.5649	30.8048	3.6619	0.5831
Ca(SO ₄) [⊙]	-1310.38	-1448.43	20.92	-104.60	4.70	2.4079	-1.8992	6.4895	-2.7004	-8.4942	-8.1271	-0.0010
Ca ⁺²	-552.79	-543.07	-56.48	-30.92	-18.44	-0.1947	-7.2520	5.2966	-2.4792	9.0000	-2.5220	1.2366
CaOH ⁺	-717.02	-751.65	28.03	6.05	5.76	2.7243	-1.1303	6.1958	-2.7322	11.1286	-2.7493	0.4496
CH ₄ [⊙]	-34.35	-87.81	87.82	277.26	37.40	6.7617	8.7279	2.3212	-3.1397	42.0941	10.4707	-0.3179
Cl ⁻	-131.29	-167.11	56.74	-122.49	17.34	4.0320	4.8010	5.5630	-2.8470	-4.4000	-5.7140	1.4560
ClO ₄ ⁻	-8.54	-129.33	182.00	-24.00	43.90	8.1411	15.5654	-7.8077	-3.4224	16.4500	-6.5700	0.9699
CO ₂ [⊙]	-386.02	-413.84	117.57	243.08	32.81	6.2466	7.4711	2.8136	-3.0879	40.0325	8.8004	-0.0200
CO ₃ ⁻²	-527.98	-675.31	-50.00	-289.33	-6.06	2.8524	-3.9844	6.4142	-2.6143	-3.3206	-17.1917	3.3914
e ⁻	0	0	65.34	14.42	0	0	0	0	0	0	0	0
Fe(CO ₃) [⊙]	-644.49	-763.51	-58.45	-123.03	-17.23	-0.6069	-9.2604	9.3828	-2.3961	-11.4137	-9.0233	-0.0380
Fe(HCO ₃) ⁺	-689.86	-794.10	-8.87	231.41	8.18	3.1064	-0.1934	5.8191	-2.7710	43.9175	8.2195	0.5831
Fe(HSO ₄) ⁺	-853.48	-990.45	10.21	338.23	18.81	4.5330	3.2897	4.4500	-2.9149	58.2305	13.4217	0.5121
Fe(HSO ₄) ⁺	-787.15	-981.91	-248.95	426.71	2.32	2.8251	-0.8804	6.0891	-2.7426	83.8315	17.6994	1.9551
Fe(SO ₄) [⊙]	-848.81	-993.86	-16.86	-101.60	1.67	1.9794	-2.9454	6.9007	-2.6572	-8.4131	-7.9804	-0.0380
Fe(SO ₄) ⁺	-784.71	-942.42	-124.68	-145.93	-2.64	1.7837	-3.4232	7.0885	-2.6374	-5.1341	-10.1600	0.9986
Fe(SO ₄) ₂ ⁻	-1536.81	-1854.38	-87.78	-210.37	30.49	6.6756	8.5215	2.3937	-3.1312	-5.4923	-13.3173	1.9457
Fe ⁺²	-91.50	-92.24	-105.86	-32.44	-22.64	-0.7867	-9.6969	9.5479	-2.3780	14.7860	-4.6437	1.4382
Fe ⁺³	-17.19	-49.58	-277.40	-76.71	-37.79	-2.4256	-13.6961	11.1141	-2.2127	19.0459	-6.8233	2.5812
FeCl ⁺	-223.59	-258.05	-42.09	86.49	0.85	2.1468	-2.5367	6.7401	-2.6741	24.6912	1.1617	0.7003
FeCl ⁺²	-156.92	-212.67	-178.82	14.83	-22.86	-0.7164	-9.5277	9.4878	-2.3851	23.8149	-2.3482	1.7013
FeCl ₂ ⁺	-291.92	-385.75	-129.66	300.72	10.27	3.5610	0.9165	5.3828	-2.8168	57.6940	11.5846	1.0276

FeCl ₃ [⊗]	-417.51	-564.39	-131.06	368.22	35.94	6.6686	8.5038	2.4024	-3.1304	57.3959	14.8930	-0.0380
FeO ⁺	-222.00	-255.09	-46.44	-200.94	-42.02	-3.7118	-16.8408	12.3595	-2.0827	-15.3982	-12.8325	0.7191
FeO ₂ ⁻	-368.26	-443.82	44.35	-234.93	0.45	2.3837	-1.9602	6.5182	-2.6979	-13.3207	-14.5028	1.4662
FeO ₂ H [⊗]	-419.86	-480.95	92.88	-312.14	7.21	2.7401	-1.0905	6.1776	-2.7338	-37.8300	-18.2305	-0.0300
FeOH ⁺	-274.46	-325.65	-41.84	63.06	-16.71	-0.2561	-8.4029	9.0457	-2.4315	21.4093	0.0209	0.7003
FeOH ⁺²	-241.87	-292.79	-106.27	-33.69	-25.34	-1.1562	-10.6009	9.9077	-2.3407	14.6102	-4.7048	1.4382
H ⁺	0	0	0	0	0	0	0	0	0	0	0	0
H ₂ [⊗]	17.73	-4.02	57.74	166.85	25.26	5.1427	4.7758	3.8729	-2.9764	27.6251	5.0930	-0.2090
H ₂ O [⊗]	-237.18	-285.88	69.92	75.36	18.07	0	0	0	0	0	0	0
H ₂ S [⊗]	-27.93	-39.03	125.52	179.17	34.95	6.5097	6.7724	5.9646	-3.0590	32.3000	4.7300	-0.1000
HCN [⊗]	114.37	103.75	131.30	0	0	0	0	0	0	0	0	0
HCO ₃ ⁻	-586.94	-690.01	98.45	-34.85	24.21	7.5621	1.1505	1.2346	-2.8266	12.9395	-4.7579	1.2733
HS ⁻	11.97	-16.22	68.20	-93.93	20.21	5.0119	4.9799	3.4765	-2.9849	3.4200	-6.2700	1.4410
HSiO ₃ ⁻	-1014.60	-1144.68	20.92	-87.20	4.53	2.9735	-0.5181	5.9467	-2.7575	8.1489	-7.3123	1.5511
HSO ₃ ⁻	-529.10	-627.70	139.75	-5.38	32.96	6.7014	8.5816	2.3771	-3.1338	15.6949	-3.3198	1.1233
HSO ₄ ⁻	-755.81	-889.23	125.52	22.68	34.84	6.9788	9.2590	2.1108	-3.1618	20.0961	-1.9550	1.1748
K(SO ₄) ⁻	-1031.77	-1158.77	146.44	-45.13	27.46	5.9408	6.7274	3.0989	-3.0571	9.9089	-5.2549	1.0996
K ⁺	-282.46	-252.14	101.04	8.39	9.01	3.5590	-1.4730	5.4350	-2.7120	7.4000	-1.7910	0.1927
KOH [⊗]	-437.11	-474.15	108.37	-85.02	14.96	3.7938	1.4839	5.1619	-2.8402	-6.1240	-7.2104	-0.0500
Mg(CO ₃) [⊗]	-998.98	-1132.12	-100.42	-116.50	-16.78	-0.5450	-9.1130	9.3320	-2.4020	-10.4990	-8.7060	-0.0380
Mg(HCO ₃)	-1047.02	-1153.97	-12.55	254.42	9.34	3.2710	0.2060	5.6690	-2.7880	47.2840	9.3400	0.5990
Mg(HSiO ₃)	-1477.15	-1613.91	-99.50	158.65	-10.85	0.6289	-6.2428	8.1967	-2.5209	36.7882	4.6702	0.9177
Mg ⁺²	-453.99	-465.93	-138.07	-21.66	-22.01	-0.8217	-8.5990	8.3900	-2.3900	20.8000	-5.8920	1.5372
MgOH ⁺	-625.87	-690.02	-79.91	129.23	1.64	2.3105	-2.1365	6.5827	-2.6906	32.0008	3.2394	0.8449
MgSO ₄ [⊗]	-1211.97	-1368.77	-50.88	-90.31	1.81	1.9985	-2.8987	6.8823	-2.6591	-6.8307	-7.4304	-0.0380
N ₂ [⊗]	18.19	-10.37	95.81	234.16	33.41	6.2046	7.3685	2.8539	-3.0836	35.7911	8.3726	-0.3468
Na(CO ₃) ⁻	-797.11	-938.56	-44.31	-51.28	-0.42	2.3862	-1.9521	6.5103	-2.6982	15.3395	-5.5686	1.7870
Na(HCO ₃)	-847.39	-929.50	154.72	200.33	32.32	6.1730	7.2943	2.8760	-3.0805	33.8790	6.7193	-0.0380
Na(SO ₄) ⁻	-1010.34	-1146.66	101.75	-30.09	18.64	4.7945	3.9284	4.1990	-2.9414	13.4899	-4.5256	1.2606
Na ⁺	-261.88	-240.28	58.41	38.12	-1.21	1.8390	-2.2850	3.2560	-2.7260	18.1800	-2.9810	0.3306
NaOH [⊗]	-418.12	-470.14	44.77	-13.40	3.51	2.2338	-2.3287	6.6683	-2.6826	4.0146	-3.6863	-0.0300
NH ₃ [⊗]	-26.67	-81.53	107.82	76.89	24.45	5.0911	2.7970	8.6248	-2.8946	20.3000	-1.1700	-0.0500
NH ₄ ⁺	-79.40	-133.26	111.17	67.11	18.08	3.8763	2.3448	8.5605	-2.8759	17.4500	-0.0210	0.1502
NO ₃ ⁻	-110.91	-206.89	146.94	-66.80	28.66	7.3161	6.7824	-4.6838	-3.0594	7.7000	-6.7250	1.0977
O ₂ [⊗]	16.45	-12.24	108.95	234.13	30.50	5.7889	6.3536	3.2528	-3.0417	35.3530	8.3726	-0.3943
OH ⁻	-157.27	-230.01	-10.71	-136.34	-4.71	1.2527	0.0738	1.8423	-2.7821	4.1500	-10.3460	1.7246
S ₂ O ₃ ⁻²	-519.99	-649.86	66.94	-238.47	27.59	6.6685	12.4951	-7.7281	-3.2955	-0.0577	-14.7066	2.9694
SCN ⁻	92.70	76.40	144.01	-39.69	35.36	7.0244	9.3687	2.0708	-3.1662	10.7414	-4.9900	1.1073
SO ₃ ⁻²	-487.89	-636.89	-29.29	-280.99	-4.12	2.4632	-1.7691	6.4494	-2.7058	-2.7967	-16.7843	3.3210
SO ₄ ⁻²	-744.46	-909.70	18.83	-266.09	12.92	8.3014	-1.9846	-6.2122	-2.6970	1.6400	-17.9980	3.1463
Sr(CO ₃) [⊗]	-1107.83	-1207.29	35.56	-134.32	-15.23	-0.3332	-8.5922	9.1201	-2.4237	-12.9961	-9.5733	-0.0380
Sr(HCO ₃) ⁺	-1157.54	-1239.00	95.94	210.07	14.08	3.7702	1.4274	5.1820	-2.8380	37.4746	7.1883	0.2058
Sr(SO ₄) [⊗]	-1321.37	-1451.50	61.59	-110.60	5.02	2.4382	-1.8251	6.4604	-2.7035	-9.6731	-8.4183	-0.0380
Sr ⁺²	-563.84	-550.87	-31.51	-41.56	-17.76	0.7071	-10.1508	7.0027	-2.3594	10.7452	-5.0818	1.1363
SrOH ⁺	-725.16	-754.14	61.09	-31.66	7.10	2.8620	-0.7922	6.0586	-2.7462	4.7576	-4.5826	0.3306

Temperature correction using Cp(T) integration						a ₀	a ₁	a ₂	(Cp ⁰ = a ₀ + a ₁ T + a ₂ T ²)
SiO ₂ ^{@**}	-833.41	-887.86 [*]	41.34	44.47	1.61	46.94	0.034	-1.13E+06	
Temperature correction using logK(T)						A ₀	A ₁	A ₂	(logK _T = A ₀ + A ₁ T + A ₂ T ⁻¹)
SiO ₃ ^{-2**}	-938.51	-1098.74	-80.20	119.83	0	-10.0006	0	-3917.5	
Si ₄ O ₁₀ ^{-4***}	-3600.81	-3915.99	305.20	328.58	0	0	0	-10822.8	
CaSiO ₃ ^{@**}	-1517.56	-1668.06	-136.68	88.90	0	0	0	1371.49	
MgSiO ₃ [@]	-1425.03	-1554.54	-75.17	-264.79	0	5.7	0	0	
AlSiO ₅ ^{-3***}	-1769.01	-2027.33	-110.41	70.78	-3.41	0	0	158.02	
AlHSiO ₃ ⁺²	-1540.55	-1634.31	-24.99	-215.896	0	14.5828	0	-2141.57	
FeHSiO ₃ ⁺²	-1087.15	-1194.26	-70.77	-163.91	0	9.7	0	0	
Fe ₂ (OH) ₂ ⁺⁴	-491.9	-614.44	-281.97	-2.71	0	6.94586	0	-2950.45	
Fe ₃ (OH) ₄ ⁺⁵	-964.33	-1232.44	-472.43	71.30	0	4.1824	0	-3125.33	
SrSiO ₃ ^{@***}	-1527.29	-1617.43	79.92	78.39	1.64	0	0	1302.92	
S ⁻²	120.42	-16.22	-295.55	-93.93	0	-19	0	0	

1530 * parameters of the HKF-equation of state; given in original calorimetric units (see [25, 26, 133]) as used in GEM.

1531 ** calculated in Matschei et al. [7] assuming Δ_rS° = Δ_rC_p° = 0 using S° and C_p° from SiO₂ (quartz) for the reactions: SiO₂⁰ ->
1532 SiO₂(quartz) Δ_rG° = Δ_rH° = -21.386; SiO₃²⁻ + 2H⁺ -> SiO₂⁰ + H₂O Δ_rG° = 132.08, Δ_rH° = 75, Δ_rS° = -191.46, Δ_rC_p° = 0; SiO₃²⁻ + Ca²⁺ -> Ca-
1533 SiO₃⁰ Δ_rG° = Δ_rH° = -26.257, Δ_rS° = 0, Δ_rC_p° = 0;

1534 *** calculated in this paper assuming Δ_rS° = Δ_rC_p° = 0 using S° and C_p° from SiO₂ (quartz) for the reactions: SiO₃²⁻ + AlO₂⁻ -> AlSiO₃³⁻
1535 Δ_rG° = Δ_rH° = -3.025, Δ_rS° = 0, Δ_rC_p° = 0; Si₄O₁₀⁴⁻ + 4H⁺ -> 4SiO₂⁰ + 2H₂O Δ_rG° = Δ_rH° = 207.2, Δ_rS° = 0, Δ_rC_p° = 0; SiO₃²⁻ + Mg²⁺ ->
1536 MgSiO₃⁰ Δ_rG° = -32.54, Δ_rH° = 0, Δ_rS° = 109.126, Δ_rC_p° = 0; SiO₃²⁻ + Sr²⁺ -> SrSiO₃⁰ Δ_rG° = Δ_rH° = -29.944, Δ_rS° = 0, Δ_rC_p° = 0;

1537 ^{iv} From the GEMS version of the PSI/Nagra 12/07 TDB [22, 23]: Al³⁺ + HSiO₃⁻ -> AlHSiO₃⁺² Δ_rG° = -42.24, Δ_rH° = 41, Δ_rS° = 279.19,
1538 Δ_rC_p° = 0; Fe⁺³ + HSiO₃⁻ -> FeHSiO₃⁺² Δ_rG° = -55.37, Δ_rH° = 0, Δ_rS° = 185.7, Δ_rC_p° = 0; 2Fe⁺³ + 2H₂O -> Fe₂(OH)₂⁺⁴ + 2H⁺ Δ_rG° =
1539 16.84, Δ_rH° = 56.486, Δ_rS° = 132.98, Δ_rC_p° = 0; 3Fe⁺³ + 4H₂O -> Fe₃(OH)₄⁺⁵ + 4H⁺ Δ_rG° = 35.96, Δ_rH° = 59.834, Δ_rS° = 80.07, Δ_rC_p° = 0;

1540

1541

1542 **Table D.2** Standard (partial molal) thermodynamic properties and heat capacity coefficients
1543 (Cp⁰ = a₀ + a₁T + a₂T²) of gaseous species at 25°C, 1 bar used in GEM calculations, as used in
1544 the GEMS version of the PSI/Nagra 12/07 TDB [22, 23].

Species	ΔG ⁰ (kJ/mol)	ΔH ⁰ (kJ/mol)	S ⁰ (J/mol·K)	Cp ⁰ (J/mol·K)	V ⁰ (J/bar)	a ₀ (J/mol·K)	a ₁ (J/mol·K ²)	a ₂ (J·K/mol)
CH ₄	-50.66	-74.81	186.26	35.75	2479	23.64	0.0479	-192464
CO ₂	-394.39	-393.51	213.74	37.15	2479	44.22	0.0088	-861904
H ₂	0	0	130.68	28.82	2479	27.28	0.0033	50208
H ₂ O	-228.68	-242.40	187.25	40.07	2479	52.99	-0.0435	5472
H ₂ S	-33.75	-20.63	205.79	34.20	2479	32.68	0.0124	-192464
N ₂	0	0	191.61	29.13	2479	28.58	0.0038	-50208
O ₂	0	0	205.14	29.32	2479	29.96	0.0042	-167360

1545

1546